

**NATIONAL CENTER FOR EARTHQUAKE
ENGINEERING RESEARCH**

State University of New York at Buffalo

Hybrid Control of Seismic-Excited Nonlinear and Inelastic Structural Systems

by

J. N. Yang, Z. Li and A. Danielians

Department of Civil Engineering
University of California at Irvine
Irvine, California 92717-0002

REPRODUCED BY
U.S. DEPARTMENT OF COMMERCE
NATIONAL TECHNICAL
INFORMATION SERVICE
SPRINGFIELD, VA 22161

Technical Report NCEER-91-0020

August 1, 1991

This research was conducted at the University of California at Irvine and was partially supported by the National Science Foundation under Grant No. ECE 86-07591.

NOTICE

This report was prepared by the University of California at Irvine as a result of research sponsored by the National Center for Earthquake Engineering Research (NCEER) and the National Science Foundation. Neither NCEER, associates of NCEER, its sponsors, the University of California at Irvine, nor any person acting on their behalf:

- a. makes any warranty, express or implied, with respect to the use of any information, apparatus, method, or process disclosed in this report or that such use may not infringe upon privately owned rights; or
- b. assumes any liabilities of whatsoever kind with respect to the use of, or the damage resulting from the use of, any information, apparatus, method or process disclosed in this report.



**Hybrid Control of Seismic-Excited Nonlinear
and Inelastic Structural Systems**

by

J.N. Yang¹, Z. Li² and A. Danielians³

August 1, 1991

Technical Report NCEER-91-0020

NCEER Project Number 90-2202

and

NSF Grant Numbers NSF-BCS-89-04524 and BCS-91-96089

NSF Master Contract Number ECE 86-07591

- 1 Professor, Department of Civil Engineering, University of California at Irvine
- 2 Post Doctoral Research Associate, Department of Civil Engineering, University of California at Irvine
- 3 Former Graduate Student, Department of Civil Engineering, University of California at Irvine

NATIONAL CENTER FOR EARTHQUAKE ENGINEERING RESEARCH
State University of New York at Buffalo
Red Jacket Quadrangle, Buffalo, NY 14261

PREFACE

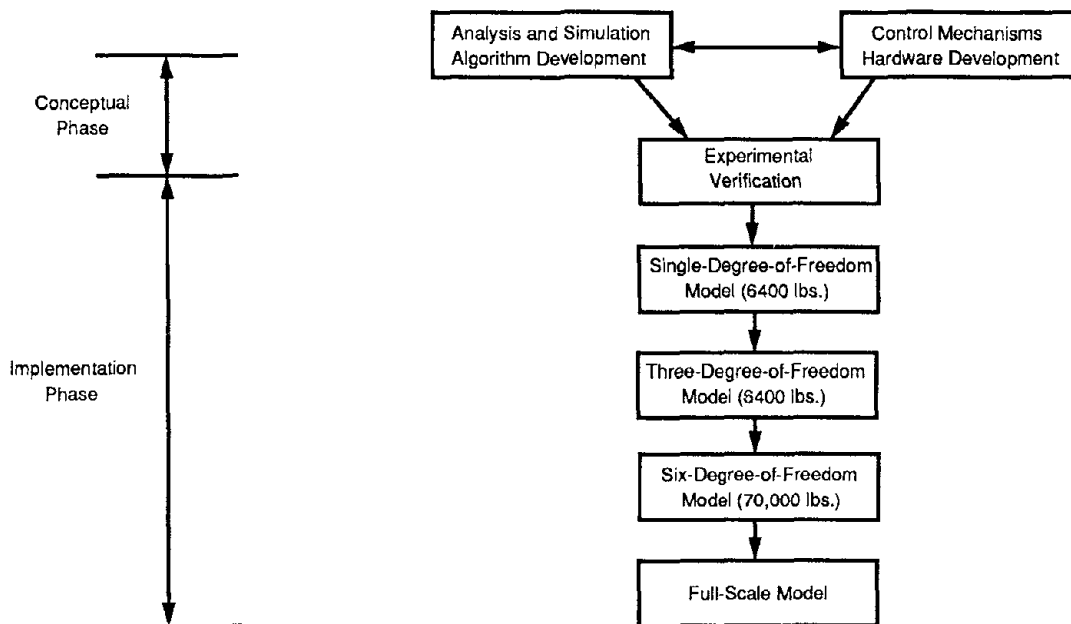
The National Center for Earthquake Engineering Research (NCEER) is devoted to the expansion and dissemination of knowledge about earthquakes, the improvement of earthquake-resistant design, and the implementation of seismic hazard mitigation procedures to minimize loss of lives and property. The emphasis is on structures and lifelines that are found in zones of moderate to high seismicity throughout the United States.

NCEER's research is being carried out in an integrated and coordinated manner following a structured program. The current research program comprises four main areas:

- Existing and New Structures
- Secondary and Protective Systems
- Lifeline Systems
- Disaster Research and Planning

This technical report pertains to Program 2, Secondary and Protective Systems, and more specifically, to protective systems. Protective Systems are devices or systems which, when incorporated into a structure, help to improve the structure's ability to withstand seismic or other environmental loads. These systems can be passive, such as base isolators or viscoelastic dampers; or active, such as active tendons or active mass dampers; or combined passive-active systems.

In the area of active systems, research has progressed from the conceptual phase to the implementation phase with emphasis on experimental verification. As the accompanying figure shows, the experimental verification process began with a small single-degree-of-freedom structure model, moving to larger and more complex models, and finally, to full-scale models.



The theory of hybrid control, a combined active/passive control mechanism, is further developed in this report, which includes a refined version of the instantaneous optimal control algorithm. The potential applicability of such a control strategy is illustrated through several examples involving a combination of sliding isolators or lead-core rubber bearings with active devices such as actuators or active mass dampers.

ABSTRACT

It has been shown recently that a combined use of active and passive control systems, referred to as the hybrid control system, is more effective, beneficial and practical, in some cases, for reducing the building response under strong earthquakes. However, the use of hybrid control systems involves active control of nonlinear or inelastic structural systems. In Part I, a refined version of the instantaneous optimal control algorithms for nonlinear or inelastic structural systems is proposed. The main advantage of the proposed control algorithms is that the control vector is determined directly from the measured response state vector without a necessity of tracking a time-dependent system matrix as proposed previously [30-31]. The optimal algorithm is simplified considerably for the time-variant linear system, which is a special case of the nonlinear system. A method of simulating the controlled response of the hysteretic system using the present control algorithm is presented. Likewise, a variation of the proposed control algorithms, utilizing the measured acceleration and velocity responses as feedbacks for the determination of the optimal control vector, is also presented. Applications of the proposed algorithm to various types of aseismic hybrid control systems are demonstrated. These include a combination of sliding isolators or lead-core rubber bearing isolators and active devices, such as actuators, active mass dampers, etc. The performances of various control systems are evaluated and compared numerically and the advantages of the aseismic hybrid control systems are demonstrated. It is shown that the proposed optimal control algorithm is simple and reliable for on-line operations and it is effective for practical applications.

In Part II, instantaneous optimal control for nonlinear and inelastic systems is formulated incorporating the specific hysteretic model of the system. The resulting optimal control vector is obtained as a function of the total deformation, velocity and the hysteretic component of the structural response. The hysteretic component of the structural response can be estimated from the measured structural response and the hysteretic model used. It is shown that the optimal control vector satisfies not only the necessary conditions but also the sufficient condition of optimality. Specific applications

of the optimal algorithm to two types of hybrid control systems are demonstrated. These include (i) active control of base-isolated buildings using frictional-type sliding base isolators, and (ii) active control of base-isolated buildings using lead-core rubber bearings. Numerical examples are worked out to demonstrate the applications of the proposed control algorithm. It is shown that the performance of such an optimal algorithm improves over that of the algorithm without considering the hysteretic components in the determination of the control vector.

ACKNOWLEDGEMENTS

This research is partially supported by the National Science Foundation Grant Nos. NSF-BCS-89-04524 and BCS-91-96089 and National Center for Earthquake Engineering Research Grant No. NCEER-90-2202. Partial support by the University of California, Irvine through an allocation of computer time is acknowledged.

PART I
TABLE OF CONTENTS

SECTION	TITLE	PAGE
1.	INTRODUCTION	I-1
2.	FORMULATION	I-4
2.1	General Nonlinear or Hysteretic Structures	I-4
2.2	Instantaneous Optimal Control	I-7
2.3	Time-Variant Linear Systems	I-9
2.4	Instantaneous Optimal Control with Acceleration and Velocity Feedback	I-11
2.5	Simulation of Controlled Response for Hysteretic Structural System	I-12
3.	NUMERICAL EXAMPLE	I-16
4.	CONCLUSION	I-54
5.	REFERENCES	I-55
APPENDIX A	FOURTH-ORDER RUNGE-KUTTA METHOD	I-59
APPENDIX B	INSTANTANEOUS OPTIMAL CONTROL ALGORITHMS	I-61

PART I
LIST OF FIGURES

FIGURE	TITLE	PAGE
2.1	Structural Model of a Multi-Story Building with Active Control Systems: (a) Active Tendon Control System; (b) Active Mass Damper	I-5
3.1	Structural Model of a Multi-Story Building with Active Control Systems: (a) Active Tendon Control System; (b) Active Mass Damper	I-17
3.2	A Simulated Earthquake Ground Acceleration	I-18
3.3	Deformation of First Story Unit Using Passive Control Systems: (a) Without Control; (b) With Active Mass Damper; (c) With Base Isolation System alone; (d) With Base Isolation System and Passive Mass Damper ($m_d=50\%m_i$); (e) With Base Sliding System	I-21
3.4	Hysteresis Loops for Shear Force in i th Story-Unit: (a) Without Control; (b) With Active Mass Damper; (c) With Base Sliding System	I-22
3.5	Required Active Control Force (Active Mass Damper Alone)	I-24
3.6	Structure Model of a Multi-Story Building: (a) With Base Isolation System; (b) With Base Isolation System and Actuator	I-25
3.7	Structure Model of a Multi-Story Building: (a) With Base Isolation System and Passive Mass Damper; (b) With Base Isolation System and Active Mass Damper	I-27
3.8	Hysteretic Characteristics of Base Isolation System: (a) Lead-core Rubber Bearing System; (b) Frictional-type Sliding System	I-28
3.9	Deformation of Rubber Bearing Base Isolation System: (a) Without Control; (b) With Passive Mass Damper ($m_d=50\%m_i$); (c) With Actuator; (d) With Actuator (Limited No. of Sensors); (e) With Active Mass Damper; (f) With Active Mass Damper (Limited No. of Sensors)	I-29

PART I

LIST OF FIGURES

FIGURE	TITLE	PAGE
3.10	Hysteresis Loop for Shear Force in Rubber Bearing Base Isolation System: (a) Without Control; (b) With Passive Mass Damper; (c) With Active Mass Damper; (d) With Active Mass Damper (Limited No. of Sensors); (e) With Actuator; (f) With Actuator (Limited No. of Sensors)	I-30
3.11	Maximum Deformation of First Story Unit and Base Isolation System as Function of Mass Ratio of Passive Mass Damper	I-33
3.12	Deformation of First Story Unit: (a) Without Control; (b) With Base Isolation System and Active Mass Damper; (c) With Base Isolation System and Active Mass Damper (Limited No. of Sensors); (d) With Base Isolation System and Actuator; (e) With Base Isolation System and Actuator (Limited No. of Sensors); (f) With Base Sliding System and Actuator	I-35
3.13	Required Active Control Force for Building With Base Isolation System and Active Mass Damper	I-36
3.14	Required Active Control Force for Building With Base Isolation System and Actuator	I-39
3.15	Structure Model of a Multi-Story Building: (a) With Base Sliding System; (b) With Base Sliding System and Actuator	I-41
3.16	Relative Displacement of Base Sliding System: (a) Without Control; (b) With Actuator	I-44
3.17	Hysteresis Loop for Frictional Force in Base Sliding System: (a) Without Control; (b) With Actuator	I-45
3.18	Required Active Control Force for Building With Base Sliding System and Actuator	I-48

PART I

LIST OF TABLES

TABLE	TITLE	PAGE
3.1	Maximum Response Quantities of Building Equipped with Active Mass Damper: \bar{x}_d =maximum relative displacement of the mass damper; x_{mi} =maximum deformation of ith story unit; a_i =maximum absolute acceleration of ith floor; U_m =maximum active control force	I-20
3.2	Maximum Response Quantities of Building Equipped with Base Isolation System and Passive Mass Damper: \bar{x}_d =maximum relative displacement of the mass damper; x_{mi} =maximum deformation of ith floor; a_i =maximum absolute acceleration of ith floor	I-31
3.3	Maximum Response Quantities of Building Equipped with Base Isolation System and Active Mass Damper: \bar{x}_d =maximum relative displacement of the mass damper; x_{mi} =maximum deformation of ith story unit; a_i =maximum absolute acceleration of ith floor; U_m =maximum active control force; \dot{U}_m =maximum active control force rate	I-37
3.4	Maximum Response Quantities of Building Equipped with Sliding-type Isolation System and Actuator \bar{x}_d =maximum relative displacement of the mass damper; x_{mi} =maximum deformation of ith story unit; a_i =maximum absolute acceleration of ith floor; U_m =maximum active control force	I-46
3.5	Maximum Response Quantities of Building Equipped with Base Isolation System and Actuator Using \dot{Z} feedback: x_{mi} =maximum deformation of ith story unit; a_i =maximum absolute acceleration of ith floor; U_m =maximum active control force	I-50
3.6	Maximum Response Quantities of Building Equipped with Base Isolation System and Active Mass Damper Using \dot{Z} feedback x_{mi} =maximum deformation of ith story unit; a_i =maximum absolute acceleration of ith floor; U_m =maximum active control force; I=full Sensors; II=Limited No. of Sensors; (A)=without \dot{Z} feedback; (B)=with \dot{Z} feedback	I-52

PART II
TABLE OF CONTENTS

SECTION	TITLE	PAGE
1.	INTRODUCTION	II-1
2.	OPTIMAL CONTROL OF INELASTIC STRUCTURAL SYSTEMS	II-3
2.1	Nonlinear Hysteretic Model for Inelastic Systems	II-3
2.2	Equations of Motion	II-3
2.3	Instantaneous Optimal Control	II-8
2.4	Sufficient Condition for Optimal Control	II-10
2.5	Estimation of Hysteretic Component Vector \underline{V}	II-10
3.	NUMERICAL EXAMPLE	II-12
4.	CONCLUSIONS	II-28
5.	REFERENCES	II-29

PART II
LIST OF FIGURES

FIGURE	TITLE	PAGE
2.1	Structural Model of a Multi-Story Building Equipped with Aseismic Hybrid Control Systems: (a) Rubber Bearing Isolation System and Active Mass Damper; (b) Base Sliding Isolation System and Actuator	II-5
3.1	A Simulated Earthquake Ground Acceleration	II-13
3.2	Structural Model of a Multi-Story Building Equipped with Aseismic Hybrid Control Systems: (a) Rubber Bearing Isolation System and Active Mass Damper; (b) Base Sliding Isolation System and Actuator	II-16
3.3	Hysteretic Characteristics of Base Isolation System: (a) Lead-core Rubber Bearing System; (b) Frictional-type Sliding System	II-17
3.4	Deformation of First-Story Unit: (a) Without Control; (b) With Sliding Isolation System; (c) With Sliding Isolation System and Actuator with \underline{V} feedback; (d) With Sliding Isolation System and Actuator with \underline{V} feedback	II-24

PART II

LIST OF TABLES

TABLE	TITLE	PAGE
3.1	Maximum Response Quantities of Building Equipped with Base Isolation System and Active Mass Damper (BIS & AMD): \bar{x}_d =maximum relative displacement of the mass damper; x_{mi} =maximum deformation of ith story unit; a_i =maximum absolute acceleration of ith floor; U_m =maximum active control force	II-14
3.2	Maximum Response Quantities of Building Equipped with Base Isolation System and Actuator (Limited No. of Sensors): x_{mi} =maximum deformation of ith story unit; a_i =maximum absolute acceleration of ith floor; U_m =maximum active control force	II-22
3.3	Maximum Response Quantities of Building Equipped with Sliding Isolation System and Actuator (SIS & AF): x_{mi} =maximum deformation of ith story unit; a_i =maximum absolute acceleration of ith floor; U_m =maximum active control force	II-25

HYBRID CONTROL OF SEISMIC-EXCITED STRUCTURAL SYSTEMS

PART I

SECTION 1 INTRODUCTION

In recent years, intensive research efforts have been made in the application of passive and/or active control systems to reduce the response and damage of civil engineering structures caused by earthquakes and strong winds [e.g., 3-14, 16-18, 20-24, 26-41]. The active control system differs from the passive one in that it requires the supply of external energy. In the area of passive control systems, much progress has been accomplished in base isolation systems [e.g., 5-8, 11, 17-18, 24], such as elastomeric bearings, sliding systems, etc., and different types of mechanical energy dissipators, such as viscoelastic dampers, friction dampers and other devices. In the area of active control systems, active mass dampers, active tendon systems, variable stiffness bracings and others have been developed and tested in the laboratory [e.g., 3, 9, 20, 23, 29] and in a few cases installed in prototype full-scale buildings [e.g., 9,12-14].

More recently, it has been shown that a combined use of active and passive control systems, referred to as the hybrid control system, is more effective, beneficial and practical in some cases [e.g., 3, 9, 10, 21-22, 34-36, 39-41]. The idea of hybrid control systems is to utilize the advantages of both the passive and active control systems to extend the range of applicability of both control systems to protect the integrity of the structure. In particular, under extreme environments, such as strong earthquakes, hybrid control systems are superior.

It is well known that most passive control systems behave either nonlinearly, such as sliding isolation systems, or inelastically (hysteretically), such as lead-core rubber bearing isolation systems. As a result, active control of nonlinear or inelastic (hysteretic) structural systems is the major issue of hybrid control. Unfortunately, control theories for nonlinear or hysteretic systems are very limited [e.g., 10, 16, 21, 30, 31]. Recently, instantaneous optimal control algorithms proposed by Yang, et al for linear structures [26-28] have been extended to nonlinear and hysteretic structures [30-31]. In the development of the optimal algorithms for nonlinear structures, the Wilson- θ numerical procedures were used in Refs. 30-31, and the resulting optimal control vector $\underline{U}(t)$

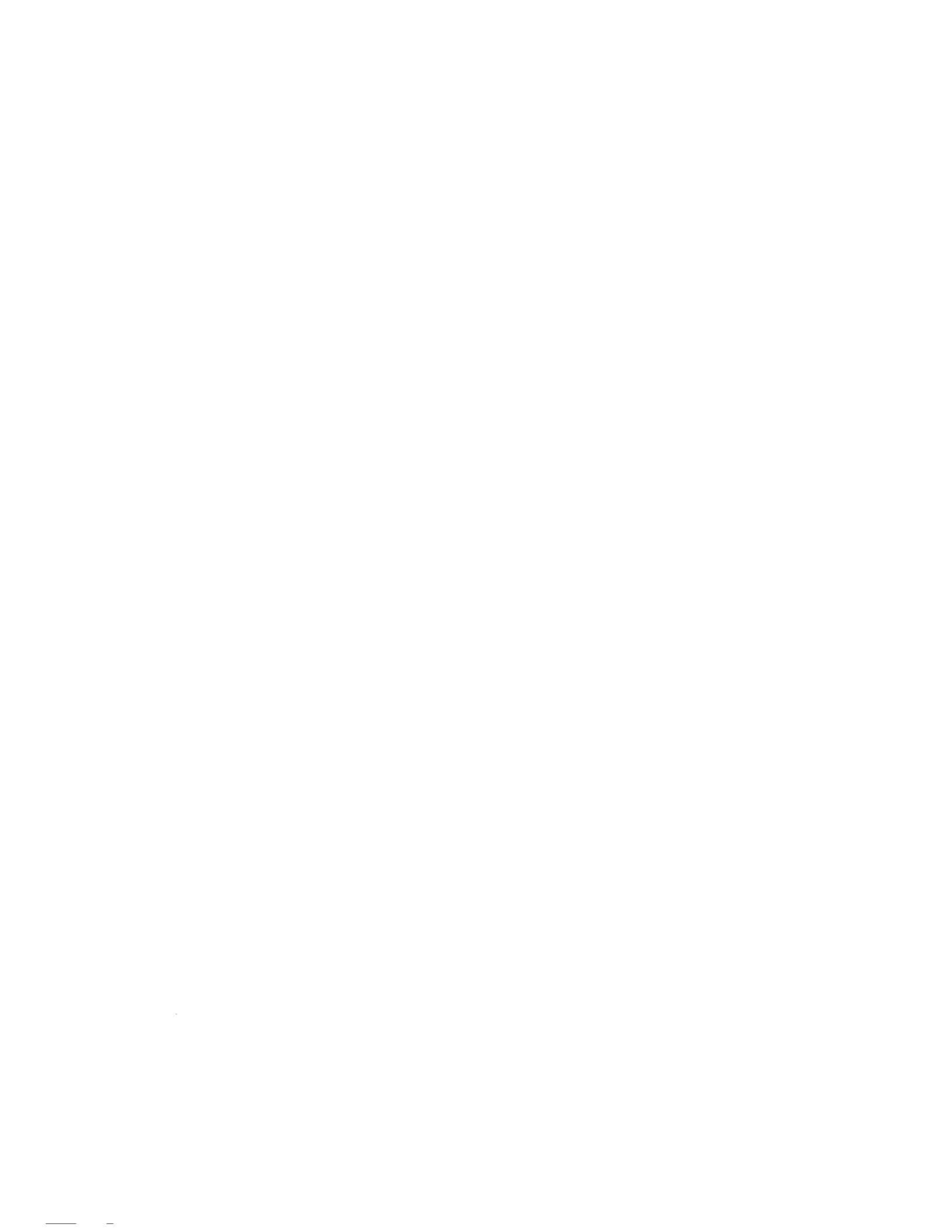
depends on the feedback response and the estimation or tracking of a system matrix. For elastic nonlinear structures, this does not present any problem. For hysteretic systems whose responses are history-dependent, however, the tracking of the system matrix \underline{A}_2 may be subjected to limitations.

The purpose of this report is to propose a refined version of instantaneous optimal control algorithms, which is simple and reliable for on-line operations, for nonlinear or hysteretic structural systems. Emphasis is placed on applications to aseismic hybrid control systems. In the present approach, the Fourth-Order Runge-Kutta numerical method is used to obtain the transition matrix equation, i.e., the system response at time t is expressed in terms of the system response at the previous times $t-\Delta t$ and $t-2\Delta t$. The resulting optimal control vector, $\underline{U}(t)$, at time t depends only on the measured response at time t , thus eliminating the necessity of tracking a history-dependent system matrix. The optimal algorithm is simplified considerably for a time-variant linear system, that is a special case of hysteretic systems. A method of simulating the controlled response of the hysteretic structural system using the proposed control algorithm is also presented.

Recent laboratory experiments indicated some difficulties in measuring the displacement response of the structure subjected to earthquake ground motions. This is because both the ground and the structure are moving during earthquakes, so that there is no absolute reference for the determination of the displacement response. Further, the displacement response obtained by numerically integrating the measured velocity response is not satisfactory due to serious error accumulations and noise pollution. On the other hand, however, the acceleration response can easily be measured by installing acceleration sensors. In this report, an alternate version of the instantaneous optimal control algorithms for nonlinear or inelastic structures, utilizing the acceleration response rather than the displacement response, is proposed following the approach presented by Yang, et al [37-38] for linear structures.

Finally, applications of the proposed algorithms to various types of aseismic hybrid control systems are demonstrated. These include various combinations of active control systems, such as actuators, active mass dampers, etc., and passive base isolation systems, such as sliding isolators and lead-core rubber bearing isolators. The performances of

various hybrid control systems are evaluated and compared numerically, and the advantages of aseismic hybrid control systems are demonstrated. It is shown that the proposed optimal control algorithm is effective and simple for practical applications.



SECTION 2 FORMULATION

2.1 General Nonlinear or Hysteretic Structures

For simplicity of presentation, consider a shear-beam lumped-mass nonlinear or hysteretic building structure implemented by an active control system as shown in Fig. 2.1. The structure is idealized by an n-degree-of-freedom system and subjected to a one-dimensional earthquake ground acceleration $\ddot{X}_o(t)$. The matrix equation of motion of the entire structural system can be expressed as

$$\underline{M}\ddot{\underline{X}}(t) + \underline{F}_D[\dot{\underline{X}}(t)] + \underline{F}_s[\underline{X}(t)] = -\underline{M}\underline{\xi}\ddot{X}_o(t) + \underline{H}\underline{U}(t) \quad (2.1)$$

in which $\underline{X}(t) = [x_1, x_2, \dots, x_n]'$ = an n vector denoting the deformation of each story unit, \underline{M} = an (nxn) mass matrix, $\underline{\xi} = [1, 1, \dots, 1]'$ = an n vector, $\underline{U}(t)$ = a r-dimensional control vector and \underline{H} = an (nxr) location matrix denoting the location of r controllers. For the notations above, an under bar denotes a vector or matrix and a prime indicates the transpose of a vector or matrix. In Eq. (2.1), $\underline{F}_D[\dot{\underline{X}}(t)]$ is an n vector denoting the nonlinear damping force that is assumed to be a function of $\dot{\underline{X}}(t)$ and $\underline{F}_s[\underline{X}(t)]$ is an n vector denoting the nonlinear (or hysteretic) stiffness restoring force that is assumed to be a function of $\underline{X}(t)$.

Introducing the 2n state vector $\underline{Z}(t)$,

$$\underline{Z}(t) = \begin{bmatrix} \underline{X}(t) \\ \dot{\underline{X}}(t) \end{bmatrix} \quad (2.2)$$

one can convert the second-order nonlinear matrix equation, Eq. (2.1), into a first order nonlinear matrix equation as follows:

$$\dot{\underline{Z}}(t) = \underline{g}[\underline{Z}(t)] + \underline{B}\underline{U}(t) + \underline{W}_1\ddot{X}_o(t) \quad (2.3)$$

where $\underline{g}[\underline{Z}(t)]$ is a 2n vector which is a nonlinear function of the state vector $\underline{Z}(t)$

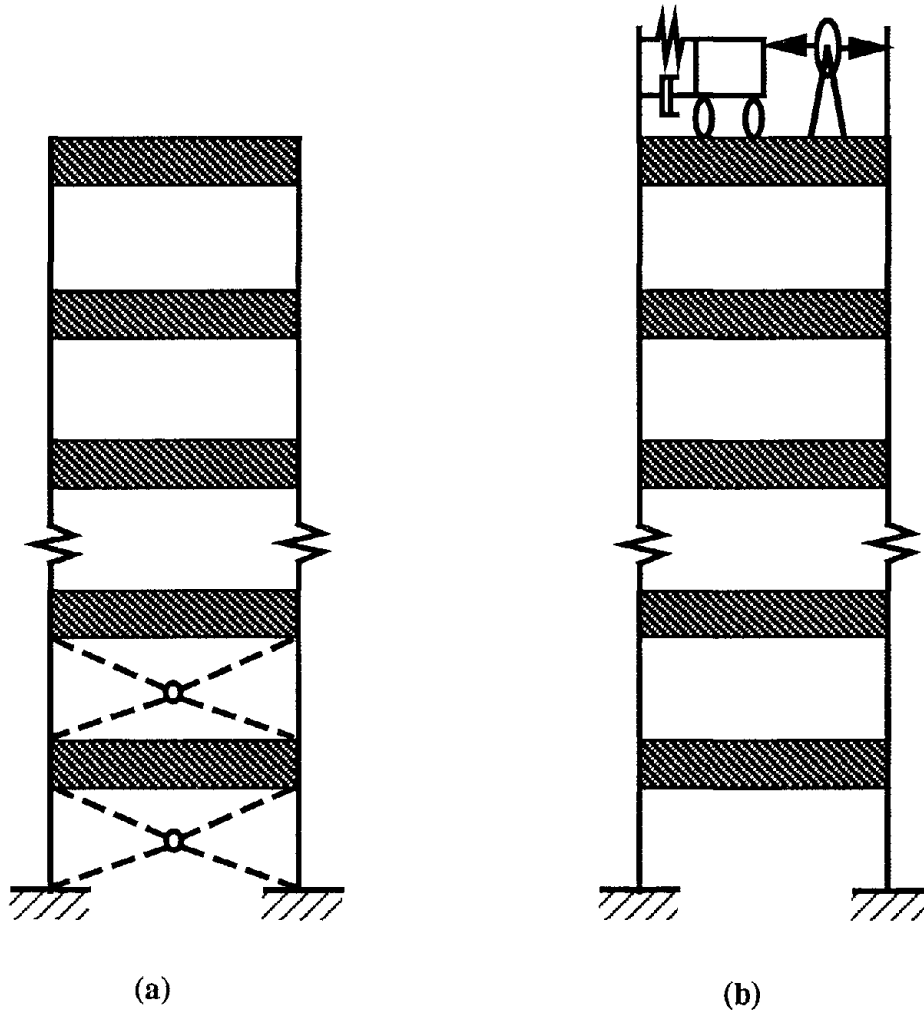


FIGURE 2.1 Structural Model of a Multi-Story Building with Active Control Systems:
(a) Active Tendon Control System; (b) Active Mass Damper

$$\mathbf{g}[\mathbf{Z}(t)] = \begin{bmatrix} \dot{\mathbf{X}}(t) \\ -\mathbf{M}^{-1}(\mathbf{F}_D[\dot{\mathbf{X}}(t)] + \mathbf{F}_s[\mathbf{X}(t)]) \end{bmatrix} \quad (2.4)$$

and $\underline{\mathbf{B}}$ and $\underline{\mathbf{W}}_1$ are $2n$ vectors

$$\underline{\mathbf{B}} = \begin{bmatrix} \mathbf{0} \\ -\mathbf{M}^{-1}\mathbf{H} \end{bmatrix} ; \quad \underline{\mathbf{W}}_1 = \begin{bmatrix} \mathbf{0} \\ -\underline{\xi} \end{bmatrix} \quad (2.5)$$

The first-order nonlinear matrix equation, Eq. (2.3), can be solved step-by-step numerically using the Fourth-Order Runge-Kutta method as follows (see Appendix I):

$$\mathbf{Z}(t) = \mathbf{Z}(t - 2\Delta t) + \frac{1}{6} [\mathbf{A}_0 + 2\mathbf{A}_1 + 2\mathbf{A}_2 + \mathbf{A}_3] \quad (2.6)$$

in which Δt is the integration time step, and $\underline{\mathbf{A}}_0$, $\underline{\mathbf{A}}_1$, $\underline{\mathbf{A}}_2$, and $\underline{\mathbf{A}}_3$ are $2n$ vectors

$$\begin{aligned} \underline{\mathbf{A}}_0 &= 2\Delta t \{ \mathbf{g}[\mathbf{Z}(t - 2\Delta t)] + \underline{\mathbf{B}} \underline{\mathbf{U}}(t - 2\Delta t) + \underline{\mathbf{W}}_1 \ddot{\mathbf{X}}_0(t - 2\Delta t) \} \\ \underline{\mathbf{A}}_1 &= 2\Delta t \{ \mathbf{g}[\mathbf{Z}(t - 2\Delta t) + 0.5\underline{\mathbf{A}}_0] + \underline{\mathbf{B}} \underline{\mathbf{U}}(t - \Delta t) + \underline{\mathbf{W}}_1 \ddot{\mathbf{X}}_0(t - \Delta t) \} \\ \underline{\mathbf{A}}_2 &= 2\Delta t \{ \mathbf{g}[\mathbf{Z}(t - 2\Delta t) + 0.5\underline{\mathbf{A}}_1] + \underline{\mathbf{B}} \underline{\mathbf{U}}(t - \Delta t) + \underline{\mathbf{W}}_1 \ddot{\mathbf{X}}_0(t - \Delta t) \} \\ \underline{\mathbf{A}}_3 &= 2\Delta t \{ \mathbf{g}[\mathbf{Z}(t - 2\Delta t) + \underline{\mathbf{A}}_2] + \underline{\mathbf{B}} \underline{\mathbf{U}}(t) + \underline{\mathbf{W}}_1 \ddot{\mathbf{X}}_0(t) \} \end{aligned} \quad (2.7)$$

As observed from Eq. (2.7), $\underline{\mathbf{A}}_0$, $\underline{\mathbf{A}}_1$, $\underline{\mathbf{A}}_2$, and $\underline{\mathbf{A}}_3$ are functions of $t-2\Delta t$, $t-\Delta t$ and t . For simplicity of presentation, the arguments, $t-2\Delta t$, $t-\Delta t$ and t , have been omitted.

To simplify the mathematical operation, all the vectors in Eq. (2.6) which are functions of $\tau < t$ are grouped into one term, denoted by $\underline{\mathbf{D}}(t-2\Delta t, t-\Delta t)$, as follows:

$$\begin{aligned} \underline{\mathbf{D}}(t - 2\Delta t, t - \Delta t) &= \mathbf{Z}(t - 2\Delta t) + \frac{1}{3} \Delta t \{ \mathbf{g}[\mathbf{Z}(t - 2\Delta t)] + \underline{\mathbf{B}} \underline{\mathbf{U}}(t - 2\Delta t) \\ &\quad + \underline{\mathbf{W}}_1 \ddot{\mathbf{X}}_0(t - 2\Delta t) + 2\mathbf{g}[\mathbf{Z}(t - 2\Delta t) + 0.5\underline{\mathbf{A}}_0] + 4\underline{\mathbf{B}} \underline{\mathbf{U}}(t - \Delta t) \\ &\quad + 4\underline{\mathbf{W}}_1 \ddot{\mathbf{X}}_0(t - \Delta t) + 2\mathbf{g}[\mathbf{Z}(t - 2\Delta t) + 0.5\underline{\mathbf{A}}_1] + \mathbf{g}[\mathbf{Z}(t - 2\Delta t) + \underline{\mathbf{A}}_2] \} \end{aligned} \quad (2.8)$$

Then, Eq. (2.6) can be expressed as

$$\underline{Z}(t) = \underline{D}(t - 2\Delta t, t - \Delta t) + \frac{\Delta t}{3} [\underline{B} \underline{U}(t) + \underline{W}_1 \ddot{\underline{X}}_0(t)] \quad (2.9)$$

It should be mentioned that for the regular Fourth-Order Runge-Kutta method, the integration time step is $\Delta\tau$ that is twice of Δt used in Eqs. (2.6)-(2.9), i.e., $\Delta\tau = 2\Delta t$ or $\Delta t = \Delta\tau/2$. In other words, the integration step size Δt used in the current numerical scheme is one-half of that used in the regular Fourth-Order Runge-Kutta method [Appendix I]. Because the required control vector $\underline{U}(t)$ is computed from the measurement of the response vector, a smaller time step Δt is used for the numerical solution.

As observed from Eqs. (2.2) and (2.4), the $2n$ vector $\underline{g}(\underline{Z})$ is a function of \underline{X} and $\dot{\underline{X}}$ which are elements of the vector \underline{Z} . Thus, the \underline{g} vector can be expressed as a function of the response state vector \underline{Z} , i.e., $\underline{g} = \underline{g}(\underline{Z})$. To evaluate $\underline{g}(\underline{Z})$, the argument vector $\underline{Z} = [\underline{X}', \dot{\underline{X}}']'$, Eq. (2.2), is computed first and then its components, \underline{X} and $\dot{\underline{X}}$, are substituted into the right hand side of Eq. (2.4). For the $\underline{g}[\underline{Z}(t-2\Delta t) + 0.5 \underline{A}_1]$ vector appearing in Eq. (2.8), the argument vector ($2n$ -dimensional), denoted by \underline{S} ,

$$\underline{S} = \underline{Z}(t - 2\Delta t) + 0.5 \underline{A}_1 \quad (2.10)$$

is computed first from Eq. (2.10). Then, \underline{S} is partitioned in the same form as the vector \underline{Z} , i.e., $\underline{S} = [\underline{S}_1', \underline{S}_2']'$, where \underline{S}_1 and \underline{S}_2 are n -dimensional vectors. Finally, the $\underline{g}[\underline{Z}(t-2\Delta t) + 0.5 \underline{A}_1]$ vector is obtained from Eq. (2.4) by replacing \underline{X} and $\dot{\underline{X}}$, respectively, by \underline{S}_1 and \underline{S}_2 . Likewise, the other two vectors $\underline{g}[\underline{Z}(t-2\Delta t) + 0.5 \underline{A}_0]$ and $\underline{g}[\underline{Z}(t-2\Delta t) + \underline{A}_2]$ appearing in Eq. (2.8) are similarly defined.

2.2 Instantaneous Optimal Control

The instantaneous optimal control algorithms proposed by Yang, et al for linear structures [26-28] was extended later to nonlinear structures [30-31]. Instantaneous optimal control is formulated as follows.

The time dependent quadratic objective function $J(t)$ proposed in Refs. 26-28 is given by

$$J(t) = \underline{Z}'(t) \underline{Q} \underline{Z}(t) + \underline{U}'(t) \underline{R} \underline{U}(t) \quad (2.11)$$

in which \underline{Q} is a (2nx2n) positive semi-definite matrix and \underline{R} is a (rxr) positive definite matrix, respectively, representing the relative importance of the response vector $\underline{Z}(t)$ and the control vector $\underline{U}(t)$. The implication of minimizing the objective function given by Eq. (2.11) is that the performance index $J(t)$ is minimized at every time instant t [26-28]. The optimal control vector obtained by minimizing $J(t)$, subjected to the constraint of the equations of motion, is called the instantaneous optimal control algorithm by Yang, et al [Refs. 26-28, 30-31].

To minimize the objective function, $J(t)$, the Hamiltonian H is obtained by introducing a 2n-dimensional Lagrangian multiplier vector $\underline{\lambda}(t)$

$$H = \underline{Z}'(t) \underline{Q} \underline{Z}(t) + \underline{U}'(t) \underline{R} \underline{U}(t) + \underline{\lambda}'(t) \{ \underline{Z}(t) - \underline{D}(t - 2\Delta t, t - \Delta t) - \frac{\Delta t}{3} [\underline{B} \underline{U}(t) + \underline{W}_1 \ddot{\underline{X}}_0(t)] \} \quad (2.12)$$

The necessary conditions for minimizing $J(t)$, subjected to the constraint of Eq. (2.9), are

$$\frac{\partial H}{\partial \underline{Z}} = 0, \quad \frac{\partial H}{\partial \underline{U}} = 0, \quad \frac{\partial H}{\partial \underline{\lambda}} = 0 \quad (2.13)$$

Substituting Eq. (2.12) into Eq. (2.13), one obtains the optimal control vector $\underline{U}(t)$ in the following manner (see Appendix II): (i) when the control vector $\underline{U}(t)$ is assumed to be regulated by the response state vector $\underline{Z}(t)$, the instantaneous optimal closed-loop (feedback) control algorithm is obtained as

$$\underline{U}(t) = - \frac{\Delta t}{3} \underline{R}^{-1} \underline{B}' \underline{Q} \underline{Z}(t) \quad (2.14)$$

(ii) when the control vector $\underline{U}(t)$ is regulated by the measurement of the earthquake ground acceleration $\ddot{\underline{X}}_0(t)$ without a feedback response state vector $\underline{Z}(t)$, the instantaneous optimal open-loop (feedforward) control algorithm is obtained, and (iii) the instantaneous optimal closed-open-loop (feedforward and feedback) control algorithm is obtained by assuming that the control vector $\underline{U}(t)$ is regulated by the measurements of both the

response state vector $\underline{Z}(t)$ and the earthquake ground acceleration $\ddot{X}_0(t)$ (see Appendix B). Although the control operations for the three optimal algorithms are different, the resulting state vector $\underline{Z}(t)$ and control vector $\underline{U}(t)$ remain identical under ideal control environments.

With the optimal control vector given by Eq. (2.14), the response state vector $\underline{Z}(t)$ is obtained by substituting Eq. (2.14) into Eq. (2.9) as follows

$$\underline{Z}(t) = \left[\underline{I} + \left(\frac{\Delta t}{3} \right)^2 \underline{B} \underline{R}^{-1} \underline{B}' \underline{Q} \right]^{-1} \left[\underline{D}(t - 2\Delta t, t - \Delta t) + \frac{\Delta t}{3} \underline{W}_1 \ddot{X}_0(t) \right] \quad (2.15)$$

in which \underline{I} is a $(2n \times 2n)$ identity matrix.

Although the optimal control vector $\underline{U}(t)$, Eq. (14), is derived from the necessary conditions, it was shown in Ref. 41 that Eq. (14) also satisfies the sufficient condition of optimality.

2.3 Time-Variant Linear Systems

The instantaneous optimal control algorithm developed previously for the general nonlinear or hysteretic structural systems is directly applicable to time-variant linear systems. In fact, the time-variant linear system is a special case of the general nonlinear system presented above and the instantaneous optimal control algorithm for such a system is presented in this section.

The matrix equation of motion for a time-variant structural system can be written as

$$\underline{M} \ddot{\underline{X}}(t) + \underline{C}(t) \dot{\underline{X}}(t) + \underline{K}(t) \underline{X}(t) = - \underline{M} \ddot{\underline{X}}_0(t) + \underline{H} \underline{U}(t) \quad (2.16)$$

in which $\underline{C}(t)$ and $\underline{K}(t)$ are time dependent $(n \times n)$ damping and stiffness matrices. With the introduction of the state vector $\underline{Z}(t)$ given by Eq. (2.2), the second order matrix equation of motion given by Eq. (2.16) can be converted into a first order matrix equation of motion as follows

$$\dot{\underline{Z}}(t) = \underline{A}(t) \underline{Z}(t) + \underline{B} \underline{U}(t) + \underline{W}_1 \ddot{\underline{X}}_0(t) \quad (2.17)$$

in which \underline{B} and \underline{W}_1 are given by Eq. (2.5) and

$$\underline{A}(t) = \begin{bmatrix} \underline{0} & \underline{I} \\ -\underline{M}^{-1} \underline{K}(t) & -\underline{M}^{-1} \underline{C}(t) \end{bmatrix} \quad (2.18)$$

Again, using the Fourth-Order Runge-Kutta method, Eq. (2.17) can be solved numerically as follows:

$$\underline{Z}(t) = \underline{Z}(t - 2\Delta t) + \frac{1}{6} [\underline{A}_0 + 2\underline{A}_1 + 2\underline{A}_2 + \underline{A}_3] \quad (2.19)$$

in which

$$\begin{aligned} \underline{A}_0 &= 2\Delta t \{ \underline{A}(t) \underline{Z}(t - 2\Delta t) + \underline{B} \underline{U}(t - 2\Delta t) + \underline{W}_1 \ddot{\underline{X}}_0(t - 2\Delta t) \} \\ \underline{A}_1 &= 2\Delta t \{ \underline{A}(t) [\underline{Z}(t - 2\Delta t) + 0.5\underline{A}_0] + \underline{B} \underline{U}(t - \Delta t) + \underline{W}_1 \ddot{\underline{X}}_0(t - \Delta t) \} \\ \underline{A}_2 &= 2\Delta t \{ \underline{A}(t) [\underline{Z}(t - 2\Delta t) + 0.5\underline{A}_1] + \underline{B} \underline{U}(t - \Delta t) + \underline{W}_1 \ddot{\underline{X}}_0(t - \Delta t) \} \\ \underline{A}_3 &= 2\Delta t \{ \underline{A}(t) [\underline{Z}(t - 2\Delta t) + \underline{A}_2] + \underline{B} \underline{U}(t) + \underline{W}_1 \ddot{\underline{X}}_0(t) \} \end{aligned} \quad (2.20)$$

A comparison between Eqs. (2.6)-(2.7) and Eqs. (2.19)-(2.20) indicates that Eqs. (2.19)-(2.20) can be obtained from Eqs. (2.6)-(2.7) by replacing $\underline{g}[\underline{Z}(t)]$ by $\underline{A}(t) \underline{Z}(t)$. Thus, the instantaneous optimal control vector $\underline{U}(t)$ is identical to Eq. (2.14).

$$\underline{U}(t) = - \frac{\Delta t}{3} \underline{R}^{-1} \underline{B}' \underline{Q} \underline{Z}(t) \quad (2.21)$$

and the response state vector $\underline{Z}(t)$ with instantaneous optimal control is given by Eq. (2.15) in which $\underline{D}(t-2\Delta t, t-\Delta t)$ is as follows

$$\begin{aligned} \underline{D}(t-2\Delta t, t-\Delta t) &= \underline{Z}(t-2\Delta t) + \frac{1}{3} \Delta t \{ 6\underline{A}(t) \underline{Z}(t-2\Delta t) + \underline{A}(t) [\underline{A}_0 + \underline{A}_1 + \underline{A}_2] \\ &\quad + \underline{B} \underline{U}(t-2\Delta t) + 4\underline{B} \underline{U}(t-\Delta t) + \underline{W}_1 \ddot{\underline{X}}_0(t-2\Delta t) + 4\underline{W}_1 \ddot{\underline{X}}_0(t-\Delta t) \} \end{aligned} \quad (2.22)$$

2.4 Instantaneous Optimal Control with Acceleration and Velocity Feedback

The optimal control vector derived above depends on the feedback response state vector $\underline{Z}(t)$ that consists of the displacement response $\underline{X}(t)$ and the velocity response $\dot{\underline{X}}(t)$. For seismic-excited structural systems, the displacement response may not be easy to measure. This is because during strong earthquakes, both the ground and the structure are moving so that there is no absolute reference to measure the displacement. Consequently, it may not be desirable to measure the displacement vector $\underline{X}(t)$. On the other hand, the acceleration responses can easily be measured by installing acceleration sensors.

In this section, an optimal control algorithm is presented so that the control vector $\underline{U}(t)$ is computed from the measurements of the acceleration and velocity responses. We follow the approach proposed by Yang, et al [37-39] for linear structures. In this approach, an alternate time-dependent performance index is given by

$$J^*(t) = \dot{\underline{Z}}'(t) \underline{Q}^* \dot{\underline{Z}}(t) + \underline{U}'(t) \underline{R} \underline{U}(t) \quad (2.23)$$

in which \underline{Q}^* is a $(2n \times 2n)$ positive semi-definite matrix and \underline{R} is a $(r \times r)$ positive definite matrix. It is mentioned that although the displacement response vector $\underline{X}(t)$ does not appear in the performance index $J^*(t)$, Eq. (2.23), it is expected that a minimization of $J^*(t)$ will also reduce $\underline{X}(t)$.

To solve the general nonlinear equation of motion given by Eq. (2.3), the state vector $\underline{Z}(t)$ is expressed by a backward finite difference form, i.e., $\underline{Z}(t) = \underline{Z}(t-\Delta t) + \Delta t \dot{\underline{Z}}(t-\Delta t)$. Then, Eq. (2.3) can be written as

$$\dot{\underline{Z}}(t) = \underline{g}[\underline{Z}(t-\Delta t) + \Delta t \dot{\underline{Z}}(t-\Delta t)] + \underline{B} \underline{U}(t) + \underline{W}_1 \ddot{\underline{X}}_0(t) \quad (2.24)$$

with zero initial conditions, i.e., $\dot{\underline{Z}}(0) = \underline{Z}(0) = 0$.

The Hamiltonian $H^*(t)$ is obtained from Eqs. (2.23) and (2.24) as

$$H^*(t) = \dot{\underline{Z}}'(t) \underline{Q}^* \dot{\underline{Z}}(t) + \underline{U}'(t) \underline{R} \underline{U}(t) + \underline{\lambda}' \{ \dot{\underline{Z}}(t) - \underline{g}[\underline{Z}(t - \Delta t) + \Delta t \dot{\underline{Z}}(t - \Delta t)] - \underline{B} \underline{U}(t) - \underline{W}_1 \ddot{\underline{X}}_o(t) \} \quad (2.25)$$

The necessary conditions for minimizing the objective function, $J^*(t)$, subjected to the constraint of Eq. (2.24) are as follows

$$\frac{\partial H^*(t)}{\partial \dot{\underline{Z}}} = 0 \quad ; \quad \frac{\partial H^*(t)}{\partial \underline{U}} = 0 \quad ; \quad \frac{\partial H^*(t)}{\partial \underline{\lambda}} = 0 \quad (2.26)$$

The optimal closed-loop control vector $\underline{U}(t)$ is obtained by substituting Eq. (2.25) into Eq. (2.26); with the result

$$\underline{U}(t) = -\underline{R}^{-1} \underline{B}' \underline{Q}^* \dot{\underline{Z}}(t) \quad (2.27)$$

Substituting Eq. (2.27) into Eq. (2.3), one obtains the nonlinear equation of motion with the instantaneous optimal control vector given by Eq. (2.27)

$$\dot{\underline{Z}}(t) = (\underline{I} + \underline{B} \underline{R}^{-1} \underline{B}' \underline{Q}^*)^{-1} \underline{g}[\underline{Z}(t)] + (\underline{I} + \underline{B} \underline{R}^{-1} \underline{B}' \underline{Q}^*)^{-1} \underline{W}_1 \ddot{\underline{X}}_o(t) \quad (2.28)$$

The response state vector $\underline{Z}(t)$ can be simulated numerically from Eq. (2.28) using the Fourth-Order Runge-Kutta method described previously.

2.5 Simulation of Controlled Response for Hysteretic Structural System

One objective of this report is to propose control algorithms suitable for applications to aseismic hybrid control systems. In order to evaluate the effectiveness of the proposed optimal algorithm and to compare the performance of various hybrid control systems, it is necessary to simulate the controlled response of the structure. To facilitate the simulation of the controlled structural response, the hysteretic component of the total deformation will be separated. With the instantaneous optimal control algorithm developed in the previous section, a method of simulation for the controlled response of the hysteretic structural system is presented in this section.

Various hysteretic models for the restoring force of an inelastic system have been developed in recent years [e.g., 25]. In this study, the differential equation model available in the literature [e.g., 1,2,15,19,25] will be used. The stiffness restoring force for a structural member or a story unit, $F_s(x)$, is expressed as

$$F_s(x) = \alpha k x + (1-\alpha) k D_y v \quad (2.29)$$

in which x = interstory deformation, k = elastic stiffness, α = ratio of post-yielding to pre-yielding stiffness, D_y = yield deformation = constant, and v is a non-dimensional variable introduced to describe the hysteretic component of the deformation, with $|v| \leq 1$, where

$$D_y \dot{v} = A \dot{x} - \beta |\dot{x}| |v|^{n-1} v - \gamma \dot{x} |v|^n \quad (2.30)$$

In Eq. (2.30), parameters A , β and γ govern the scale and general shape of the hysteresis loop, whereas the smoothness of the force-deformation curve is determined by the parameter n .

The hysteretic model given by Eq. (2.29) and (2.30) provides an explicit mathematical expression with many parameters flexible enough to reflect various hysteretic behaviors of inelastic systems. Likewise, Eq. (2.30) appears to be capable of describing the hysteretic behaviors of different base isolation systems, such as rubber bearings and sliding systems, which are the main concern of this study.

It follows from Eq. (2.29) that the stiffness of the i th story unit of the structure, denoted by $F_{si}(x)$, can be separated into an elastic component $\alpha_i k_i x_i$ and a hysteretic component $(1-\alpha_i) k_i D_{yi} v_i$, i.e., $F_{si}(x) = \alpha_i k_i x_i + (1-\alpha_i) k_i D_{yi} v_i$. The non-dimensional hysteretic variable v_i follows from Eq. (2.30) as

$$\dot{v}_i = D_{yi}^{-1} \left[A_i \dot{x}_i - \beta_i |\dot{x}_i| |v_i|^{n_i-1} v_i - \gamma_i \dot{x}_i |v_i|^{n_i} \right] = f_i(\dot{x}_i, v_i) \quad (2.31)$$

Consequently, the matrix equation of motion for a hysteretic structural system with a linear viscous damping model can be expressed as

$$\underline{M}\ddot{\underline{X}}(t) + \underline{C}\dot{\underline{X}}(t) + \underline{F}_s[\underline{X}(t)] = -\underline{M}\xi\ddot{X}_o(t) + \underline{H}U(t) \quad (2.32)$$

in which

$$\underline{F}_s[\underline{X}(t)] = \underline{K}_e \underline{X}(t) + \underline{K}_I \underline{V}(t) \quad (2.33)$$

where $\underline{V}(t) = [v_1(t), v_2(t), \dots, v_n(t)]'$ = an n vector denoting the hysteretic variable, v_i , of each story unit given by Eq. (2.31). In Eq. (2.33), \underline{K}_e is an $(n \times n)$ band-limited elastic stiffness matrix with all elements equal to zero, i.e., $K_e(i, j) = 0$, except $K_e(i, i) = \alpha_i k_i$ for $i = 1, 2, \dots, n$ and $K_e(i, i+1) = -\alpha_{i+1} k_{i+1}$ for $i = 1, 2, \dots, n-1$. Similarly, \underline{K}_I is an $(n \times n)$ band-limited hysteretic stiffness matrix with all elements equal to zero, i.e., $K_I(i, j) = 0$, except $K_I(i, i) = (1 - \alpha_i) k_i D_{y_i}$ for $i = 1, 2, \dots, n$ and $K_I(i, i+1) = -(1 - \alpha_{i+1}) k_{i+1} D_{y_{i+1}}$ for $i = 1, 2, \dots, n-1$. Matrices \underline{M} , \underline{K}_e and \underline{K}_I should be modified appropriately when an active mass damper is installed.

By introducing a $3n$ state vector $\tilde{\underline{Z}}(t)$,

$$\tilde{\underline{Z}}(t) = \begin{bmatrix} \underline{X} \\ \underline{V} \\ \dot{\underline{X}} \end{bmatrix} \quad (2.34)$$

the second order nonlinear matrix equation of motion, Eqs. (2.32) and (2.33), can be converted into a first order matrix equation as follows

$$\dot{\tilde{\underline{Z}}}(t) = \underline{g}[\tilde{\underline{Z}}(t)] + \underline{B}U(t) + \underline{W}_1 \ddot{X}_o(t) \quad (2.35)$$

in which \underline{B} and \underline{W}_1 are $3n$ vectors

$$\underline{B} = \begin{bmatrix} \underline{0} \\ \underline{0} \\ \underline{M}^{-1} \underline{H} \end{bmatrix} ; \quad \underline{W}_1 = \begin{bmatrix} \underline{0} \\ \underline{0} \\ -\xi \end{bmatrix} \quad (2.36)$$

and $\underline{g}[\tilde{\underline{Z}}(t)]$ is a $3n$ vector consisting of nonlinear functions of components of the vector $\tilde{\underline{Z}}(t)$,

$$\mathbf{g}[\tilde{\mathbf{Z}}(t)] = \begin{bmatrix} \dot{\mathbf{X}} \\ \text{-----} \\ \mathbf{f}(\dot{\mathbf{X}}, \mathbf{V}) \\ \text{-----} \\ -\mathbf{M}^{-1} (\mathbf{C}\dot{\mathbf{X}} + \mathbf{K}_e \mathbf{X} + \mathbf{K}_l \mathbf{V}) \end{bmatrix} \quad (2.37)$$

where $\mathbf{f}(\dot{\mathbf{x}}, \mathbf{v}) = [f_1(\dot{x}_1, v_1), f_2(\dot{x}_2, v_2), \dots, f_n(\dot{x}_n, v_n)]'$ = an n vector with the ith element, $f_i(\dot{x}_i, v_i)$, given by Eq. (2.31).

The optimal control vector $\mathbf{U}(t)$ is given by Eq. (2.14), which can be expressed as

$$\mathbf{U}(t) = -\frac{\Delta t}{3} \mathbf{R}^{-1} \mathbf{B}' \mathbf{Q} \begin{bmatrix} \mathbf{X} \\ \text{-----} \\ \dot{\mathbf{X}} \end{bmatrix} = \mathbf{G}_2 \mathbf{X}(t) + \mathbf{G}_1 \dot{\mathbf{X}}(t) \quad (2.38)$$

Substitution of Eq. (2.38) into Eq. (2.35) leads to the 3n matrix equation of motion for a hysteretic system under optimal control as follows

$$\dot{\tilde{\mathbf{Z}}}(t) = \mathbf{g}[\tilde{\mathbf{Z}}(t)] + \tilde{\mathbf{G}}\tilde{\mathbf{Z}}(t) + \mathbf{W}_1 \ddot{\mathbf{X}}_o(t) \quad (2.39)$$

in which

$$\tilde{\mathbf{G}} = \begin{bmatrix} \mathbf{0} & \mathbf{0} & \mathbf{0} \\ \mathbf{0} & \mathbf{0} & \mathbf{0} \\ \mathbf{M}^{-1} \mathbf{H} \mathbf{G}_2 & \mathbf{0} & \mathbf{M}^{-1} \mathbf{H} \mathbf{G}_1 \end{bmatrix} \quad (2.40)$$

With optimal control given by Eq. (2.14) or Eq. (2.38), the response for the hysteretic structural system can be simulated by solving Eq. (2.39) numerically using the Fourth-Order Runge-Kutta method.

SECTION 3

NUMERICAL EXAMPLE

To illustrate the application of the instantaneous optimal algorithm developed in this report to nonlinear and inelastic structural systems, several examples are presented in this section. Emphasis is placed on aseismic hybrid control systems. These aseismic hybrid control systems consist of active control devices, such as actuators or active mass dampers and base isolation systems, such as elastomeric bearings or sliding systems. The hysteretic behavior of elastomeric bearings is quite different from that of the sliding systems as will be described later.

An eight-story building that exhibits bilinear elasto-plastic behavior as shown in Fig. 3.1(a) is considered. The stiffness of each story unit is designed such that yielding occurs simultaneously for each story unit. The properties of the structure are as follows: (i) the mass of each floor is identical with $m_i = m = 345.6$ metric tons; (ii) the preyielding stiffnesses of the eight-story units are k_{i1} ($i=1,2,\dots,8$) = 3.4×10^5 , 3.26×10^5 , 2.85×10^5 , 2.69×10^5 , 2.43×10^5 , 2.07×10^5 , 1.69×10^5 and 1.37×10^5 kN/m, respectively, and the postyielding stiffnesses are $k_{i2} = 0.1 k_{i1}$ for $i=1,2,\dots,8$; and (iii) the viscous damping coefficients for each story unit are $c_i = 490, 467, 410, 386, 348, 298, 243$ and 196 kN.sec/m, respectively. The damping coefficients given above result in a classically damped structure with a damping ratio of 0.38% for the first vibrational mode. The natural frequencies of the unyielded structure are 5.24, 14.0, 22.55, 30.22, 36.89, 43.06, 49.54 and 55.96 rad./sec. The yielding level for each story unit varies with respect to the stiffness; with the results, $D_{yi} = 2.4, 2.3, 2.2, 2.1, 2.0, 1.9, 1.7,$ and 1.5 cm. The bilinear elasto-plastic behavior can be described by the hysteretic model, Eqs. (2.29) and (2.31), with $A_i=1.0$, $\beta_i=0.5$, $n_i=95$ and $\gamma_i=0.5$ for $i=1,2,\dots,8$. A simulated earthquake with a maximum ground acceleration of 0.3g as shown in Fig. 3.2 is used as the input excitation.

With the eight-story building structure described above and the earthquake ground acceleration shown in Fig. 3.2, time histories of all response quantities have been computed. Within 30 seconds of the earthquake episode, the maximum interstory

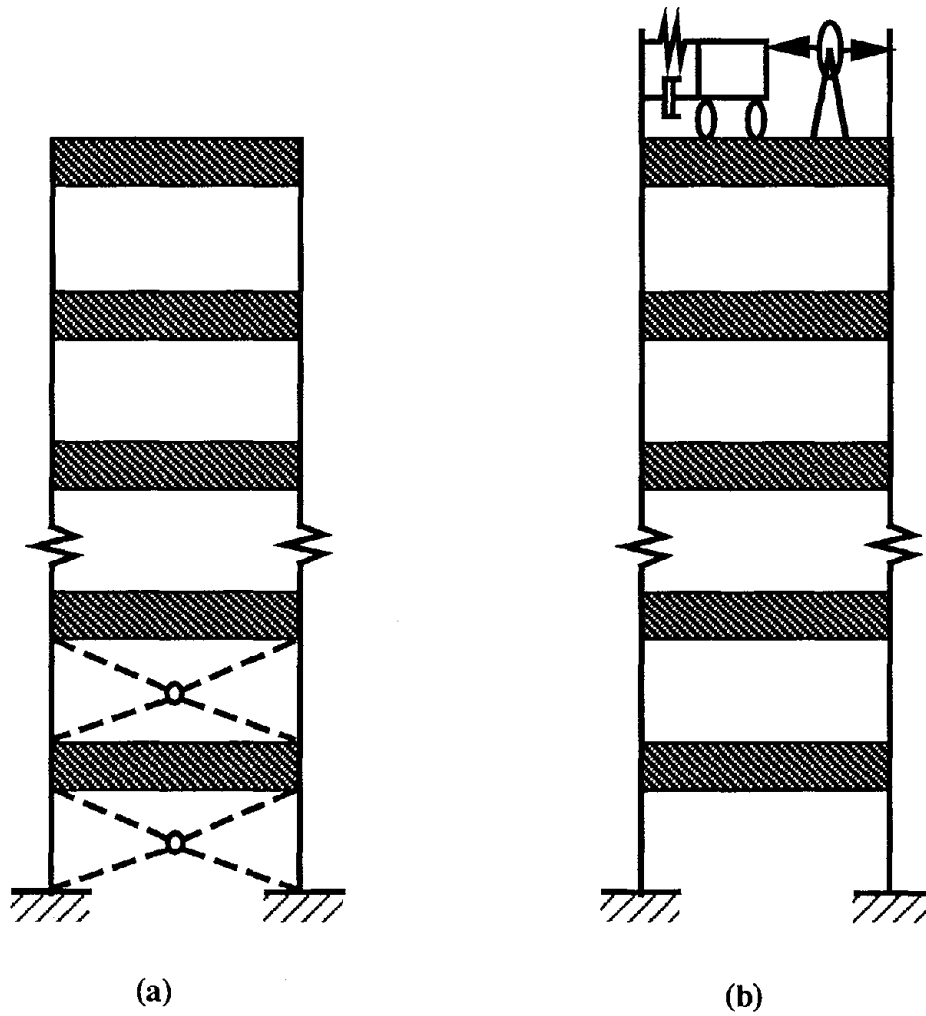


FIGURE 3.1 Structural Model of a Multi-Story Building with Active Control Systems:
(a) Active Tendon Control System; (b) Active Mass Damper

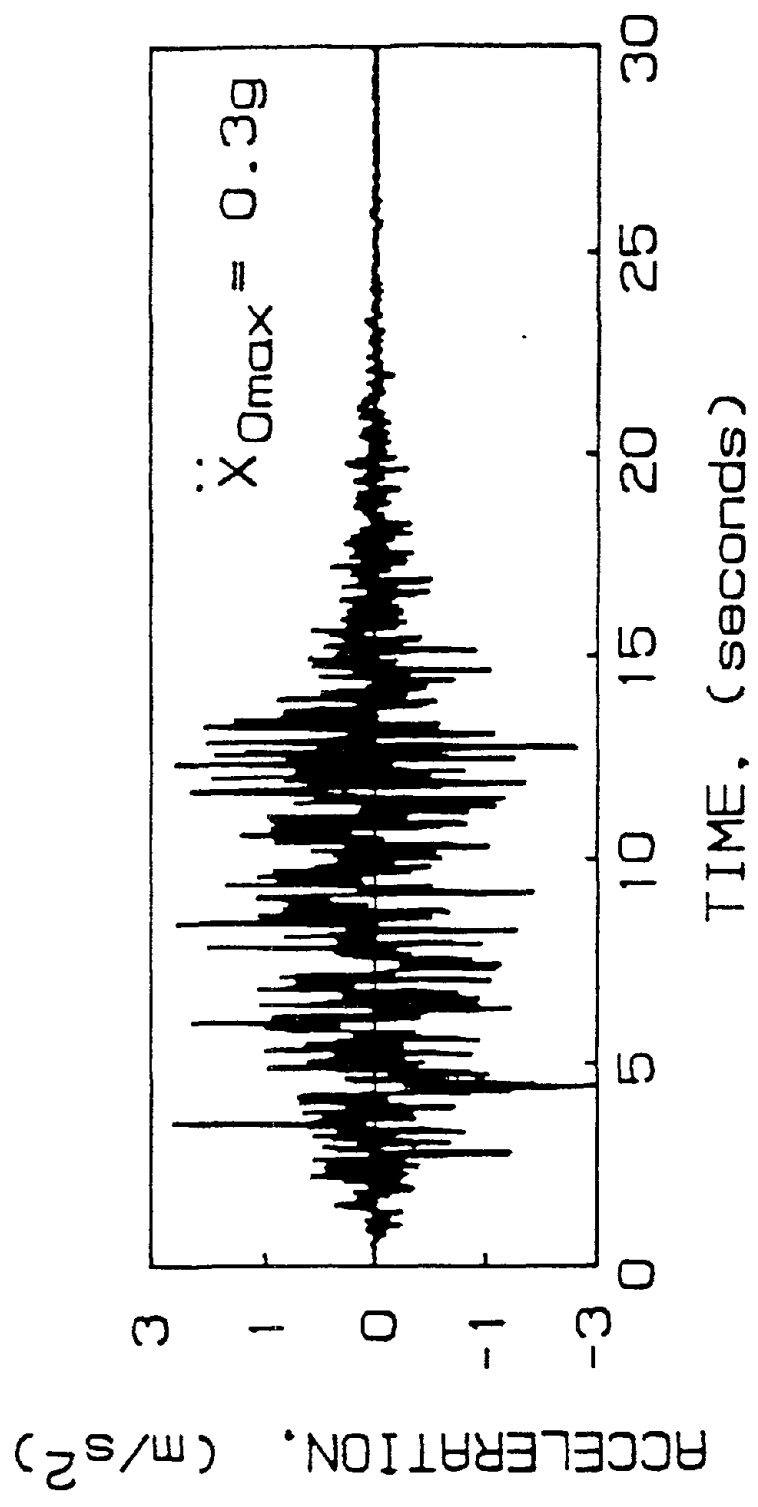


FIGURE 3.2 A Simulated Earthquake Ground Acceleration

deformation, x_{mi} , and the maximum absolute acceleration of each floor, a_i , are shown in Table 3.1. The time history of the first floor deformation, $x_1(t)$, is presented in Fig. 3.3(a). Further, the hysteresis loops of the shear force-deformation relation for the first, fourth, and eighth story units are displayed in Fig. 3.4(a) in which "i" signifies the ith story unit. As observed from Fig. 3.4(a) and Table 3.1, the deformation of the unprotected building is excessive and that yielding takes place in each story unit. These results also correspond to that obtained by Yang, et al [30-31].

Example 1: Building Equipped with Active Mass Damper on Top Floor

Consider that the building is equipped with an active mass damper on the top floor as shown in Fig. 3.1(b). The mass, stiffness and damping coefficient of the active mass damper are as follows: $m_d=36.3$ metric tons; $k_d=957.5$ kN/m; $c_d=27.97$ kN.sec./m. Hence, the mass ratio of the damper with respect to the first generalized mass is 10.5%, the damping ratio of the damper is 7.5% and the frequency of the damper is 98% of the fundamental frequency of the unyielded building.

With the active mass damper, the building response depends on the active control force that is determined by the weighting matrices \underline{Q} and \underline{R} . The weighting matrix \underline{R} consists of only one element, denoted by R_0 , since only one controller is installed on the top floor. The weighting matrix \underline{Q} is (18x18) and it is partitioned as follows

$$\underline{Q} = \alpha \left[\begin{array}{c|c} \underline{Q} & \underline{Q} \\ \hline \underline{Q}_{21} & \underline{Q}_{22} \end{array} \right] \quad (3.1)$$

in which \underline{Q}_{21} and \underline{Q}_{22} are (2x9) matrices and \underline{Q} is a (16x9) matrix with all elements equal to zero.

It is mentioned that the \underline{Q} matrix is symmetric. Since the active control forces from the actuator are acting on the mass damper and the top floor, only elements in two rows of the \underline{Q} matrix are relevant to the control vector $\underline{U}(t)$, Eq. (2.21). In the present case, only elements in the first two rows of \underline{Q}_{21} and \underline{Q}_{22} matrices are related to the control vector $\underline{U}(t)$. As a result, all elements of the \underline{Q} matrix which have no effect on

TABLE 3.1 : Maximum Response Quantities of Building Equipped with Active Mass Damper :

\bar{x}_d =maximum relative displacement of the mass damper; x_{mi} =maximum deformation of i th story unit; a_i =maximum absolute acceleration of i th floor; U_m =maximum active control force

Floor No.	Yield Displ. D_{yi} (cm)	without control		with AMD $\alpha/R=4.05 \times 10^8$ $\bar{x}_d=115$ cm $U_m=558.3$ kN		with AMD $\alpha/R=4.05 \times 10^9$ $\bar{x}_d=199$ cm $U_m=1417$ kN	
		x_{mi} (cm)	a_i (cm/s ²)	x_{mi} (cm)	a_i (cm/s ²)	x_{mi} (cm)	a_i (cm/s ²)
1	2.4	3.05	486	1.38	404	1.13	282
2	2.3	2.80	456	1.35	583	1.16	297
3	2.2	3.14	571	1.43	585	1.25	251
4	2.1	2.95	529	1.48	381	1.22	280
5	2.0	2.70	558	1.66	433	1.16	326
6	1.9	2.91	720	1.84	497	1.15	293
7	1.7	2.90	580	1.68	554	1.17	304
8	1.5	2.08	617	1.83	658	1.00	420

AMD = Active Mass Damper

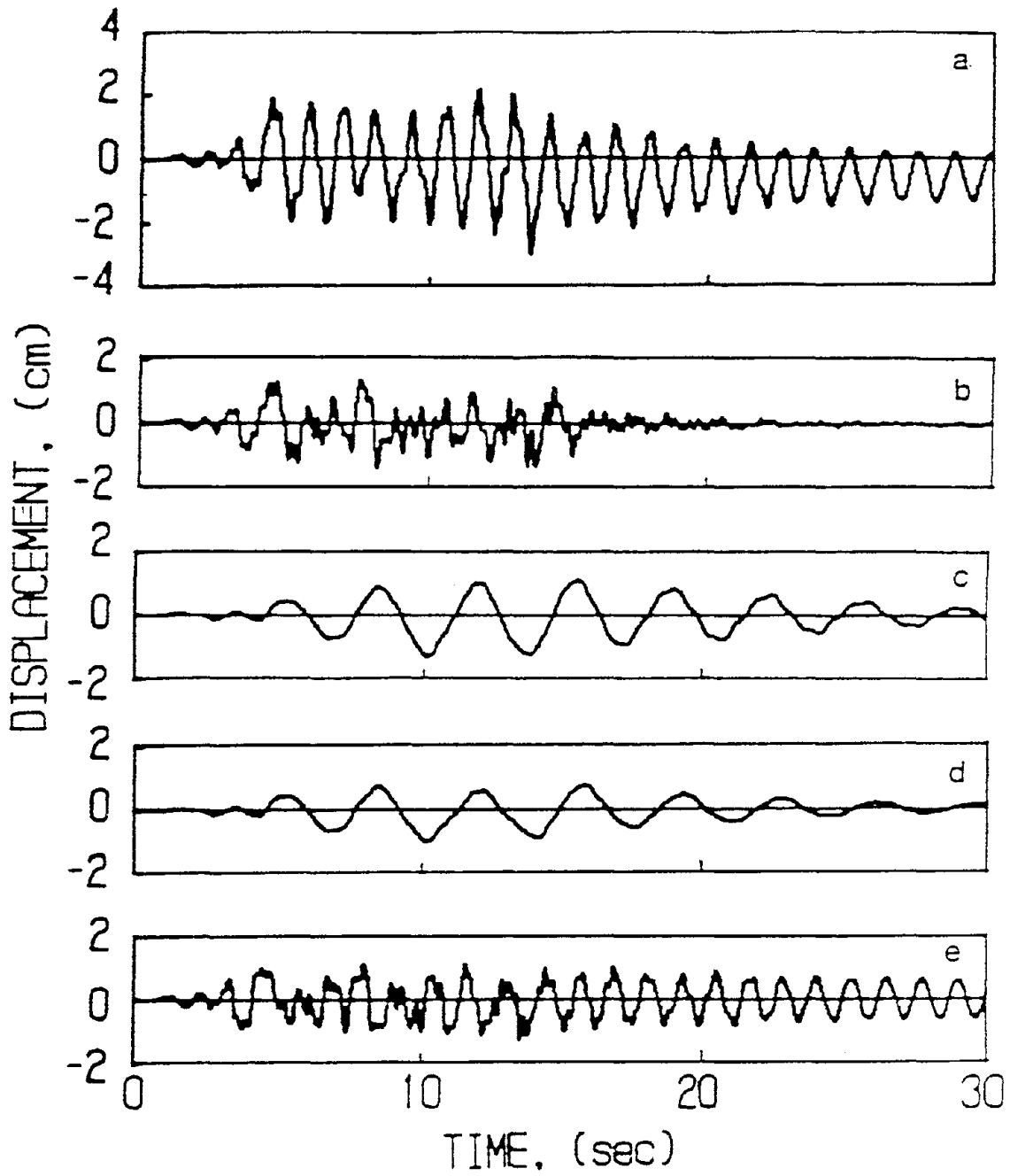


FIGURE 3.3 Deformation of First Story Unit Using Passive Control Systems: (a) Without Control; (b) With Active Mass Damper; (c) With Base Isolation System alone; (d) With Base Isolation System and Passive Mass Damper ($m_d = 50\%m_j$); (e) With Base Sliding System

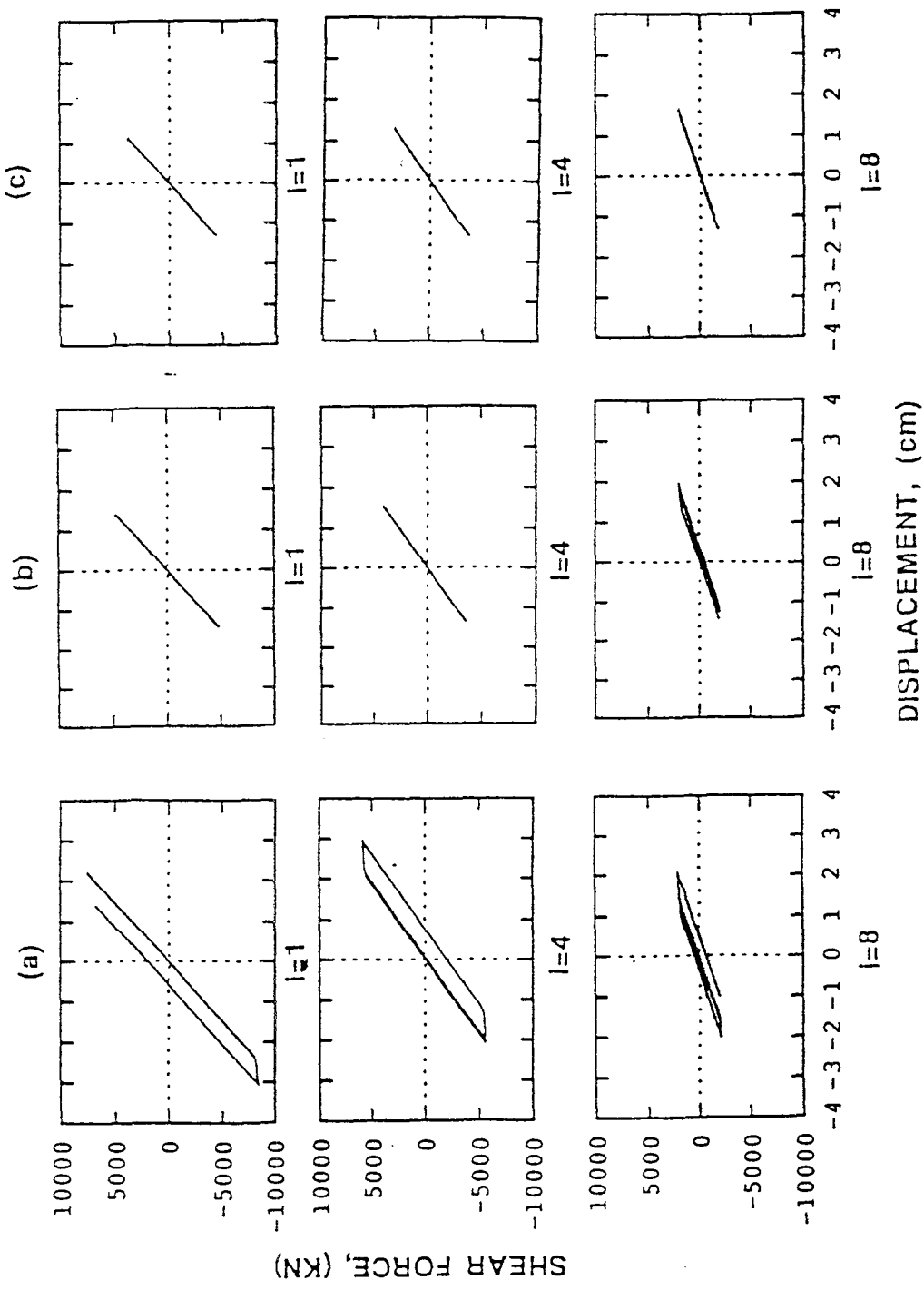


FIGURE 3.4 Hysteresis Loops for Shear Force in i th Story-Unit: (a) Without Control; (b) With Active Mass Damper; (c) With Base Sliding System

the control vector $\underline{U}(t)$ are set to be zero for convenience.

For illustrative purposes, $R_0=10^{-3}$ and Q_{21} and Q_{22} are given as follows

$$\begin{aligned} Q_{21} &= \begin{bmatrix} -1, & -1, & -1, & -1, & -1, & -1, & -1.59, & -2.68, & 0.0125 \\ -1, & -1, & -1, & -1, & -1, & -1, & -1.59, & -2.68, & 0.0107 \end{bmatrix} \\ Q_{22} &= \begin{bmatrix} 20, & 20, & 20, & 20, & 20, & 20, & 20, & 20, & 20, & 0.107 \\ 1.73, & 1.73, & 1.73, & 1.73, & 1.73, & 1.73, & 1.73, & 1.73, & 1.73, & 0.107 \end{bmatrix} \times 10^{-1} \end{aligned} \quad (3.2)$$

Time histories of all the response quantities were computed for an α/R_0 ratio of 4.05×10^8 . The deformation of the first story unit, $x_1(t)$, is plotted in Fig. 3.3(b) and the hysteresis loops for the first, fourth and eighth story unit are displayed in Fig. 3.4(b). Within 30 seconds of the earthquake episode, the following quantities are summarized in Table 3.1: (i) the maximum interstory deformation, x_{mi} , (ii) the maximum acceleration, a_i , of each floor, (iii) the maximum relative displacement of the mass damper with respect to the top floor, \bar{x}_d , and (iv) the maximum active control force U_m . A value of $\Delta t=0.15 \times 10^{-3}$ sec was used in the numerical computation. The time history of the required active control force is shown in Fig. 3.5.

For comparison, the response quantities for an α/R_0 of 4.05×10^9 are also shown in Table 3.1. It is observed from Table 3.1 that the active mass damper is capable of reducing the building response and that the response quantities reduce as the active control force increases. All the response quantities are within the elastic range for the case of $\alpha/R_0=4.05 \times 10^9$. A further comparison of the results in Table 3.1 with that in Ref. 30 indicates that the present formulation may be more efficient.

Example 2: Building Equipped With Rubber-Bearing Base Isolation System

To reduce the structural response, a lead-core rubber-bearing isolation system is implemented as shown in Fig. 3.6(a). The restoring force of the lead-core rubber-bearing system is modeled as

$$F_{sb} = \alpha_b k_b x_b + (1 - \alpha_b) k_b D_{yb} v_b \quad (3.3)$$

in which v_b is given by Eq. (2.31) with $i=b$. The mass of the base isolation system is $m_b=450$ metric tons and the viscous damping coefficient is assumed to be linear with

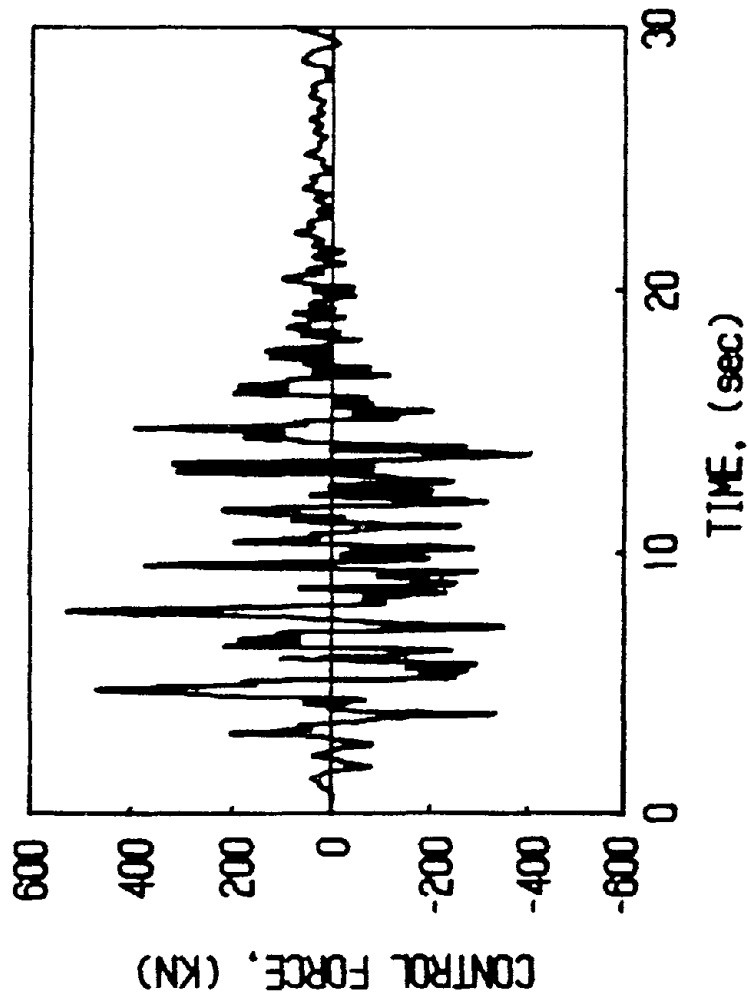


FIGURE 3.5 Required Active Control Force (Active Mass Damper Alone)

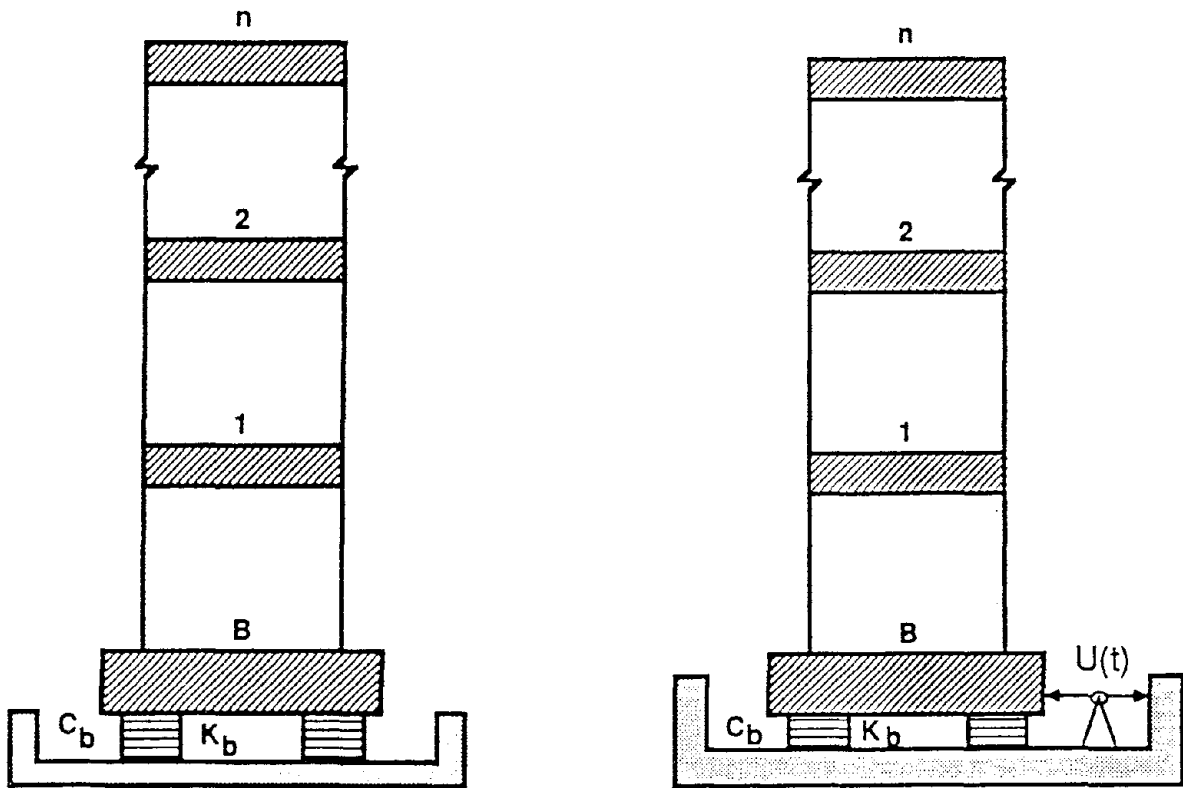


FIGURE 3.6 Structure Model of a Multi-Story Building: (a) With Base Isolation System; (b) With Base Isolation System and Actuator

$c_b=26.17$ kN.sec/m. The restoring force of the base isolation system given by Eq. (3.3) is not bilinear elasto-plastic and the parameter values are given as follows: $k_b=18050.0$ kN/m, $\alpha_b=0.6$ and $D_{yb}=4$ cm. The parameters governing the scale and general shape of the hysteresis loop of the isolation system, Eq. (2.31), were assumed to be $A_b=1.0$, $\beta_b=0.5$, $n_b=3$ and $\gamma_b=0.5$. The hysteretic characteristics of such a base isolation system, i.e., the hysteretic component v_b versus the displacement x_b , is shown in Fig. 3.8(a). With the base isolation system, the 9 natural frequencies of the preyielding structure are 2.21, 9.31, 17.29, 25.18, 32.19, 38.29, 44.12, 50.37, and 56.74 rad/sec. The damping ratio for the first vibrational mode is 0.15%. It is observed that the fundamental frequency is reduced significantly by the implementation of the base isolation system. The response vector $\underline{X}(t)$ is given by $\underline{X}=[x_b, x_1, \dots, x_8]'$.

Time histories of all the response quantities were computed. The time history, $x_1(t)$, of the deformation of the first story unit is depicted in Fig. 3.3(c) and that of the base isolation system, $x_b(t)$, is presented in Fig. 3.9(a). Further, the hysteresis loop for the shear force of the base isolation system is shown in Fig. 3.10(a). The maximum response quantities of the structure in 30 seconds of the earthquake episode are shown in Table 3.2, in which the row designated by "B" indicates the response of the base isolation system. As observed from Table 3.2 and Fig. 3.3(c), the interstory deformation and the floor acceleration are drastically reduced. The advantage of using a base isolation system to protect the building is clearly demonstrated. However, the deformation of the base isolation system shown in row B of Table 3.2 may be excessive.

Example 3: Building Equipped With Passive Hybrid Control System

To protect the safety and integrity of the base isolation system, a passive mass damper was proposed [Refs. 34-36] to be connected to the base isolation system as shown in Fig. 3.7(a). This is referred to as the passive hybrid control system [Refs. 35-36]. The properties of the mass damper are as follows. The mass of the mass damper, m_d , is expressed in terms of the ϕ percentage of the floor mass m_i , i.e. $m_d=\phi m_i$, and it will be varied to examine the effect of the mass ratio ϕ . The natural frequency of the mass damper is the same as the first natural frequency of the base isolated building, i.e.

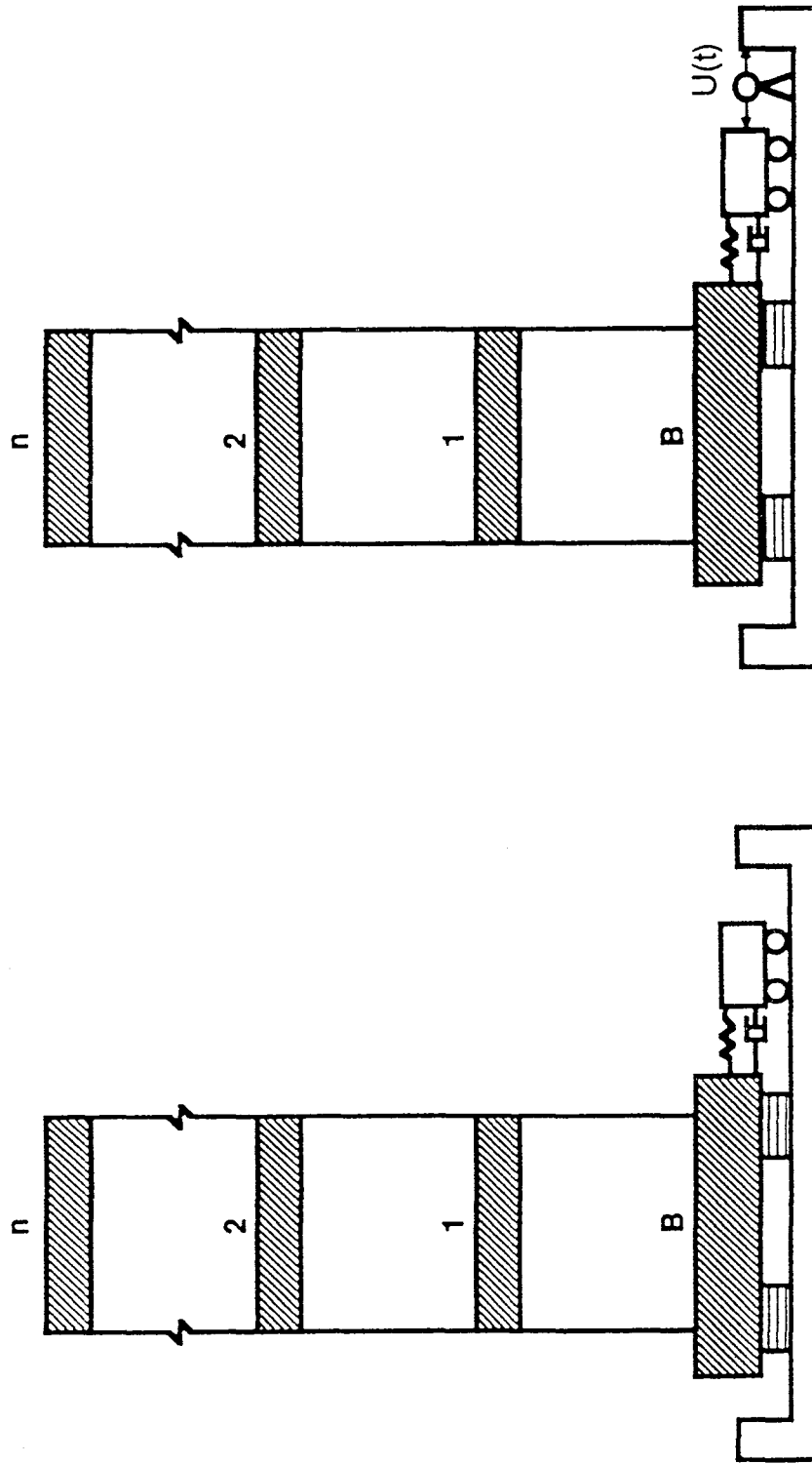
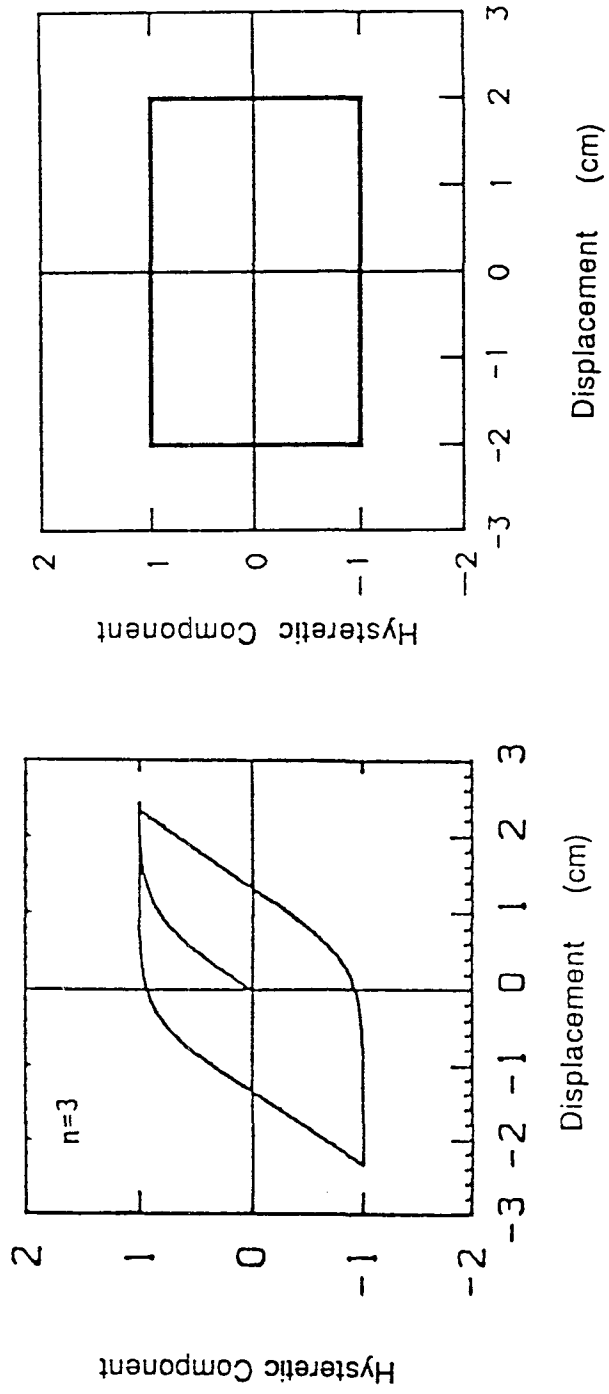


FIGURE 3.7 Structure Model of a Multi-Story Building: (a) With Base Isolation System and Passive Mass Damper; (b) With Base Isolation System and Active Mass Damper



(a) (b)

FIGURE 3.8 Hysteretic Characteristics of Base Isolation System :
 (a) Lead-core Rubber Bearing System; (b) Frictional-type Sliding System

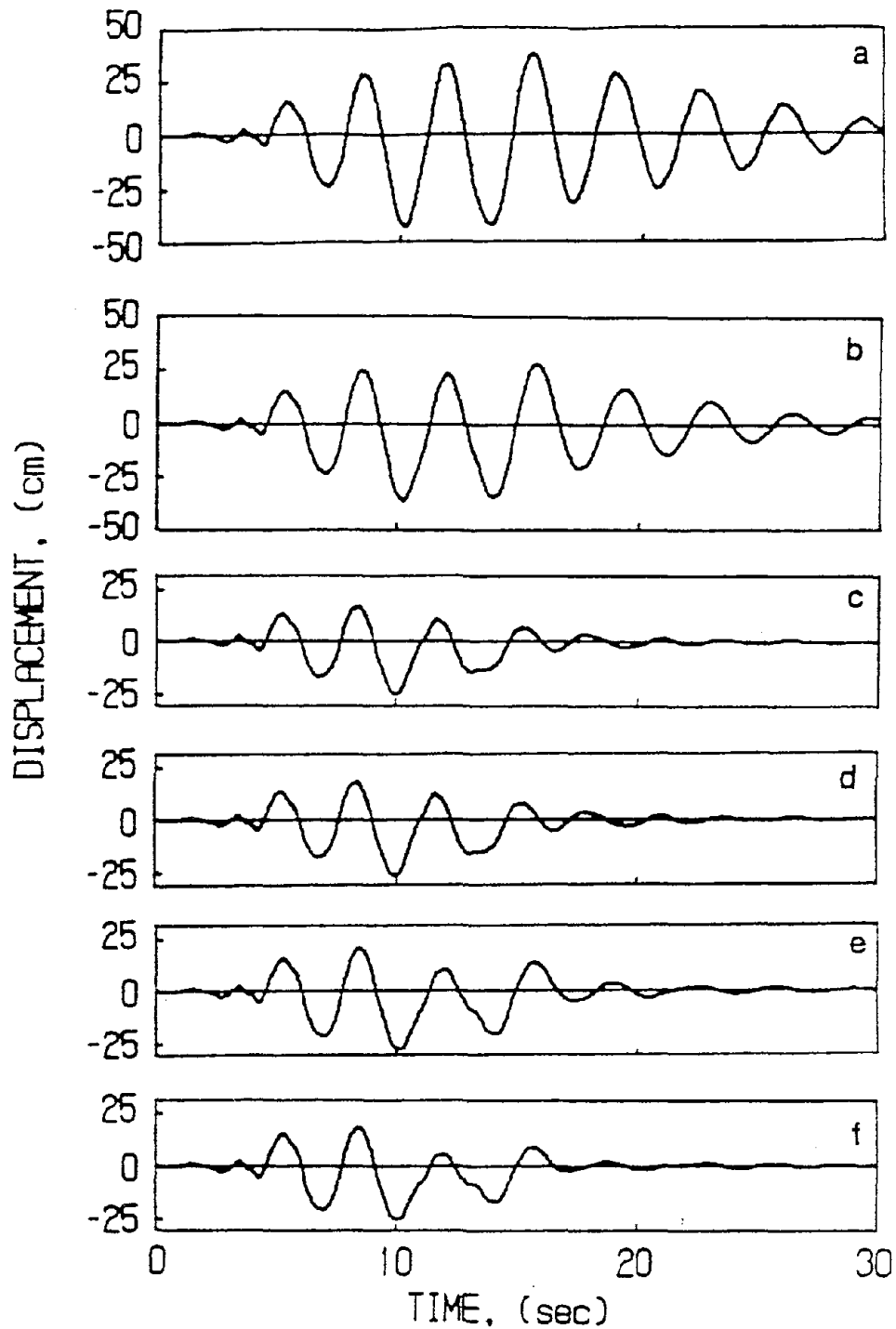


FIGURE 3.9 Deformation of Rubber Bearing Base Isolation System:
 (a) Without Control; (b) With Passive Mass Damper ($m_d = 50\%m_i$); (c) With Actuator; (d) With Actuator (Limited No. of Sensors); (e) With Active Mass Damper (f) With Active Mass Damper (Limited No. of Sensors)

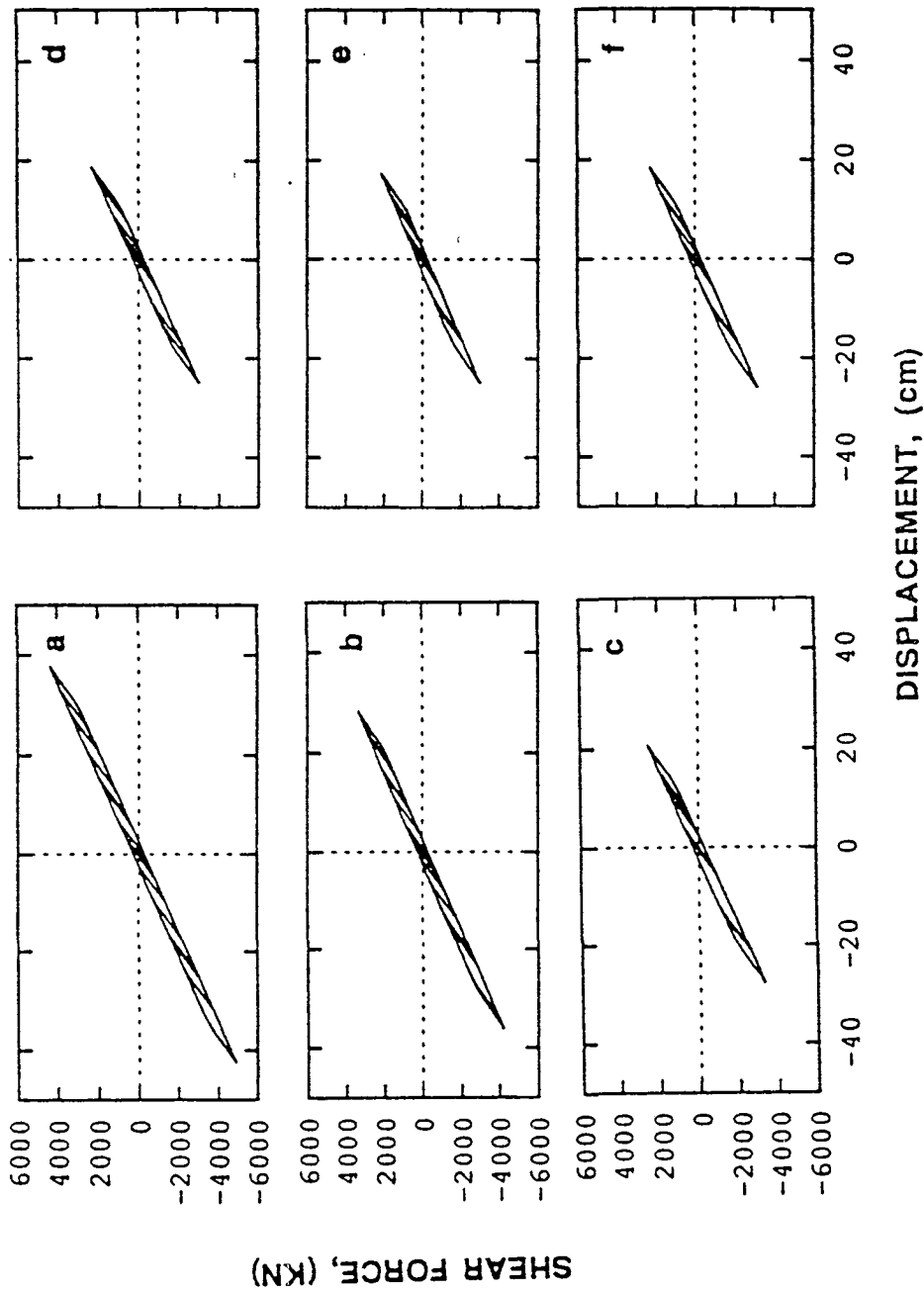


FIGURE 3.10 Hysteresis Loops for Shear Force in Rubber Bearing Base Isolation System: (a) Without Control; (b) With Passive Mass Damper; (c) With Active Mass Damper; (d) With Active Mass Damper (Limited No. of Sensors); (e) With Actuator; (f) With Actuator (Limited No. of Sensors)

TABLE 3.2 : Maximum Response Quantities of Building Equipped with Base Isolation System and Passive Mass Damper : \bar{x}_d =maximum relative displacement of the mass damper; x_{mi} =maximum deformation of i th floor; a_i =maximum absolute acceleration of i th floor

FLOOR NO	Yield Displ. D_{yi} (cm)	with BIS Alone		$m_d=0.5 m_i$ $\bar{x}_d=93\text{cm}$		$m_d=1.0 m_i$ $\bar{x}_d=80\text{cm}$		$m_d=2.0 m_i$ $\bar{x}_d=60\text{cm}$		$m_d=3.0 m_i$ $\bar{x}_d=47\text{cm}$	
		x_{mi} (cm)	a_i (cm/s ²)	x_{mi} (cm)	a_i (cm/s ²)	x_{mi} (cm)	a_i (cm/s ²)	x_{mi} (cm)	a_i (cm/s ²)	x_{mi} (cm)	a_i (cm/s ²)
B	4.0	42.70	158	36.29	127	32.07	119	29.27	104	25.28	93
1	2.4	1.31	155	1.01	128	0.87	113	0.72	102	0.57	88
2	2.3	1.25	152	0.98	132	0.84	112	0.68	96	0.54	82
3	2.2	1.28	157	1.01	128	0.88	108	0.69	96	0.56	81
4	2.1	1.17	164	0.94	127	0.84	104	0.65	95	0.53	79
5	2.0	1.07	177	0.86	140	0.79	122	0.61	104	0.49	86
6	1.9	0.97	185	0.78	150	0.72	140	0.55	115	0.46	94
7	1.7	0.82	198	0.66	162	0.61	147	0.47	112	0.42	94
8	1.5	0.52	206	0.41	161	0.38	151	0.32	128	0.29	114

2.21 rad/sec. The damping ratio of the mass damper is 10%. With such a passive hybrid control system, the maximum deformation of each story unit, x_{mi} , and the maximum acceleration of each floor, a_i , within 30 seconds of the earthquake episode are presented in Table 3.2 for different mass ratio, ϕ , of the mass damper. Also shown in row B of Table 3.2 is the maximum deformation of the base isolation system. The maximum deformations for the base isolation system and the first story unit are plotted in Fig. 3.11 as function of the mass ratio $\phi = m_d/m_i$. The maximum relative displacement of the mass damper, denoted by \bar{x}_d , is also shown in Table 3.2. Time histories of the deformation of both the first story unit and the base isolation system are shown in Figs. 3.3(d) and 3.9(b), respectively, for $\phi = 0.5$. It is observed from Table 3.2 and Figs. 3.3 and 3.9 that the passive mass damper is capable of reducing not only the deformation of the base isolation system but also the response of the building; the bigger the passive mass damper, the better the performance of the passive hybrid control system.

Example 4: Building Equipped With Rubber-Bearing Isolation System and Active Devices

Instead of using a passive mass damper, an active mass damper has been proposed in Refs. 34-36 for protecting the base isolation system. It is referred to as the active hybrid control system in Refs 34-36. For the active mass damper, a mass ratio of 50% is considered, i.e., $m_d = 0.5m_i$. With the active mass damper, the structural response depends on the weighting matrices \underline{R} and \underline{Q} . For this example, the weighting matrix \underline{R} consists of only one element, denoted by R_0 , whereas the dimension of the \underline{Q} matrix is (20x20). R_0 is chosen to be 10^{-3} for simplicity and the \underline{Q} matrix is partitioned as shown in Eq. (3.1), in which \underline{Q}_{21} and \underline{Q}_{22} are (10x10) matrices.

Note that the weighting matrix \underline{Q} is symmetric. Because there is only one actuator installed on the basement floor, see Fig. 3.6(b), only elements in one row of the \underline{Q} matrix are relevant to the control vector $\underline{U}(t)$, Eq. (2.21). For the present hybrid control system, only elements in the first row of the \underline{Q}_{21} and \underline{Q}_{22} matrices are related to the

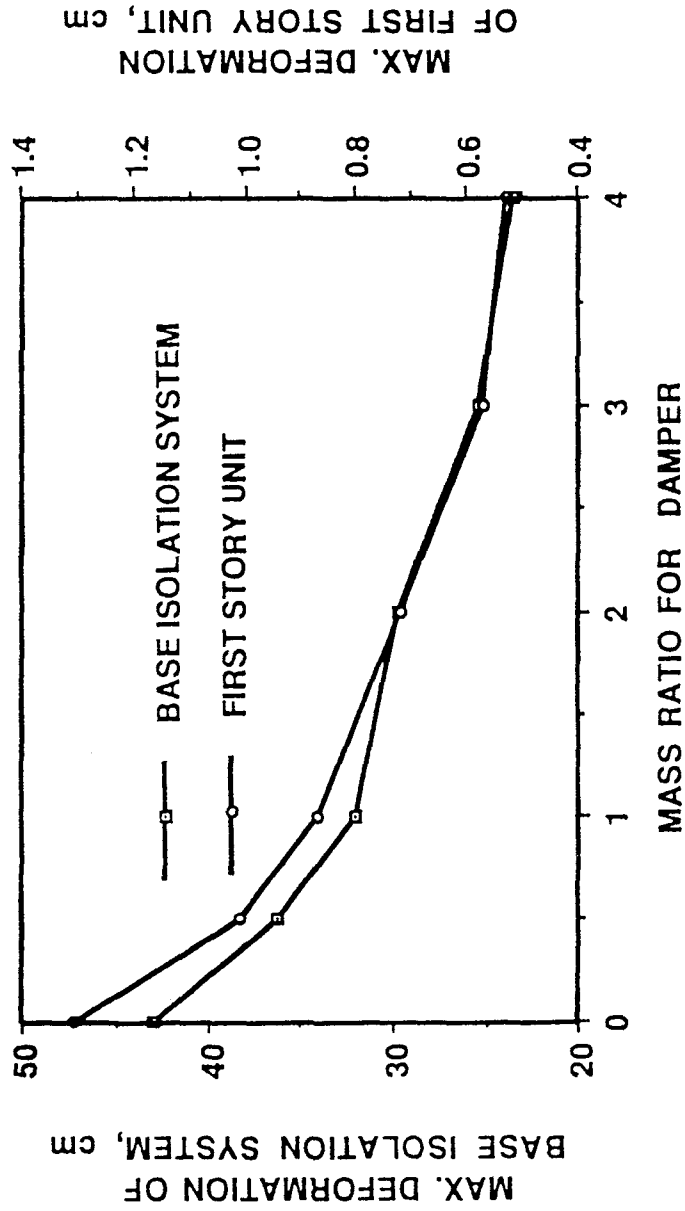


FIGURE 3.11 Maximum Deformation of First Story Unit and Base Isolation System as Function of Mass Ratio of Passive Mass Damper

control vector $\underline{U}(t)$. As a result, all elements of the \underline{Q} matrix which have no effect on the control vector $\underline{U}(t)$ are set to be zero for convenience.

First, we consider the case in which displacement and velocity sensors are installed on all the degrees of freedom of the structure. For illustrative purposes, the following values are assigned for $Q_{21}(1,j)$ and $Q_{22}(1,j)$ for $j=1,2,\dots,10$.

$$\begin{aligned} Q_{21}(1,j) &= [102 \quad -2362 \quad -11 \quad -840 \quad -1397 \quad -1649 \quad -1645 \quad -1433 \quad -1057 \quad -561] \\ Q_{22}(1,j) &= [67 \quad 731 \quad 646 \quad 621 \quad 584 \quad 529 \quad 457 \quad 366 \quad 257 \quad 133] \end{aligned} \quad (3.4)$$

and $Q_{21}(i,j)=Q_{22}(i,j)=0$ for $i=2,3,\dots,10$ and $j=1,2,\dots,10$.

Time histories of all the response quantities have been computed. In particular, the time histories of the deformation of the base isolation system and the first story unit are shown in Fig. 3.9(e) and 3.12(b), respectively, for $\alpha/R_0=50000$ and $\Delta t = 0.375 \times 10^{-2}$. The hysteresis loop for the shear force of the base isolation system is plotted in Fig. 3.10(c) and the required active control force is displayed in Fig. 3.13.

Within 30 seconds of the earthquake episode, the maximum interstory deformations, x_{mi} ($i=B,1,2,\dots,8$), the maximum acceleration of each floor, a_i , the maximum active control force U_m and force rate \dot{U}_m , as well as the maximum relative displacement of the mass damper, \bar{x}_d , are summarized in the columns designated as "BIS&AMD¹" of Table 3.3.

The building equipped with a base isolation system tends to behave like a rigid body since the interstory deformation is small compared to that of the base isolation system. As a result, sensors may not be needed for the building. Consider the second case in which displacement and velocity sensors are installed on the active mass damper and the base isolation system only, i.e. no sensor is installed on the building. In this case, all the elements of Q_{21} and Q_{22} matrices are zero except $Q_{21}(1,1)$, $Q_{21}(1,2)$, $Q_{22}(1,1)$, and $Q_{22}(1,2)$. For simplicity, the following values are assigned: $Q_{21}(1,1)=102$, $Q_{21}(1,2)=-2363$, $Q_{22}(1,1)=67$, and $Q_{22}(1,2)=731$. The maximum response quantities for $\alpha/R_0=60000$ and $\Delta t=0.375 \times 10^{-2}$ have been computed and summarized in the columns designated as "BIS&AMD²" of Table 3.3. Time histories

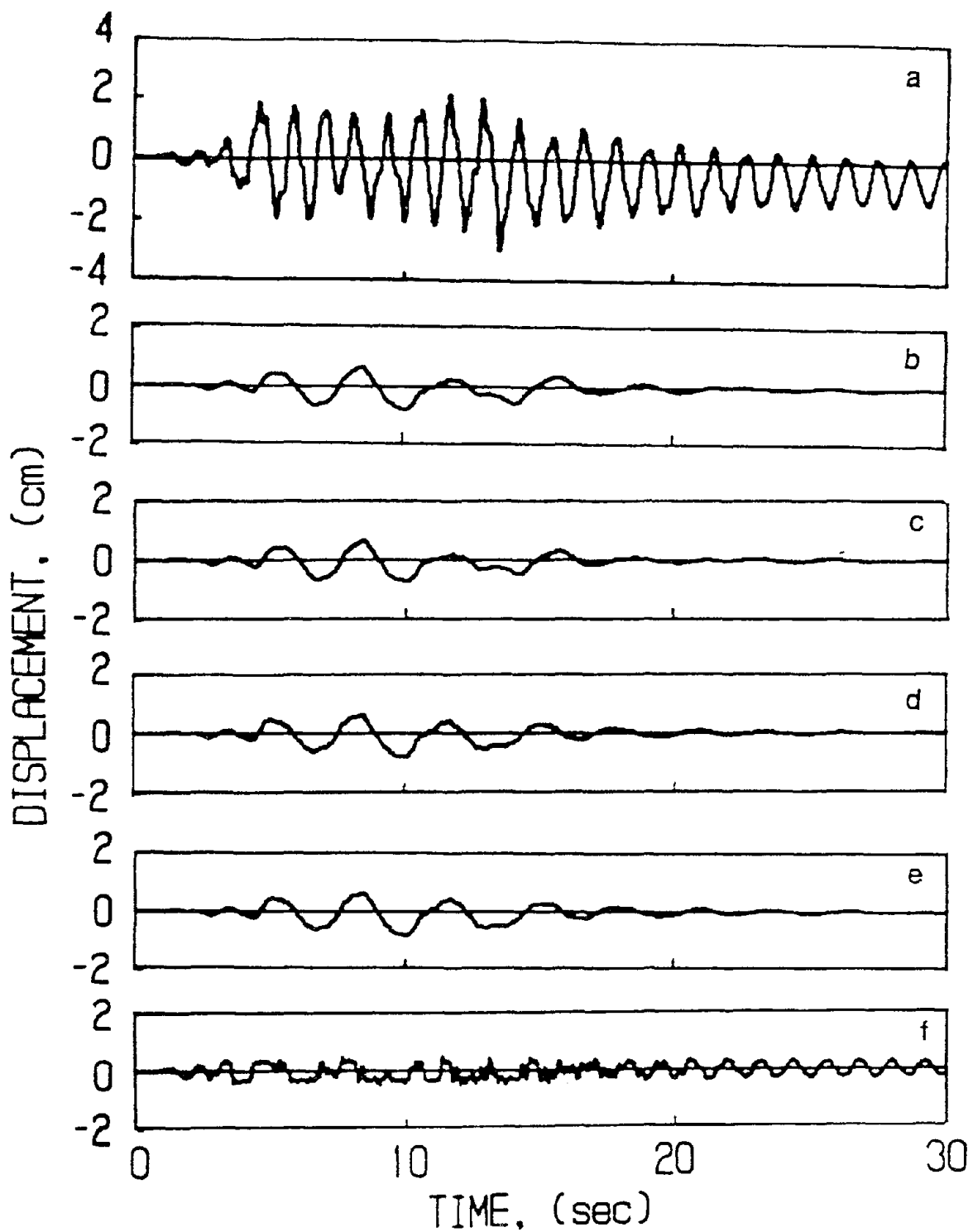


FIGURE 3.12 Deformation of First Story Unit: (a) Without Control; (b) With Base Isolation System and Active Mass Damper; (c) With Base Isolation System and Active Mass Damper (Limited No. of Sensors); (d) With Base Isolation System and Actuator; (e) With Base Isolation System and Actuator (Limited No. of Sensors); (f) With Base Sliding System and Actuator

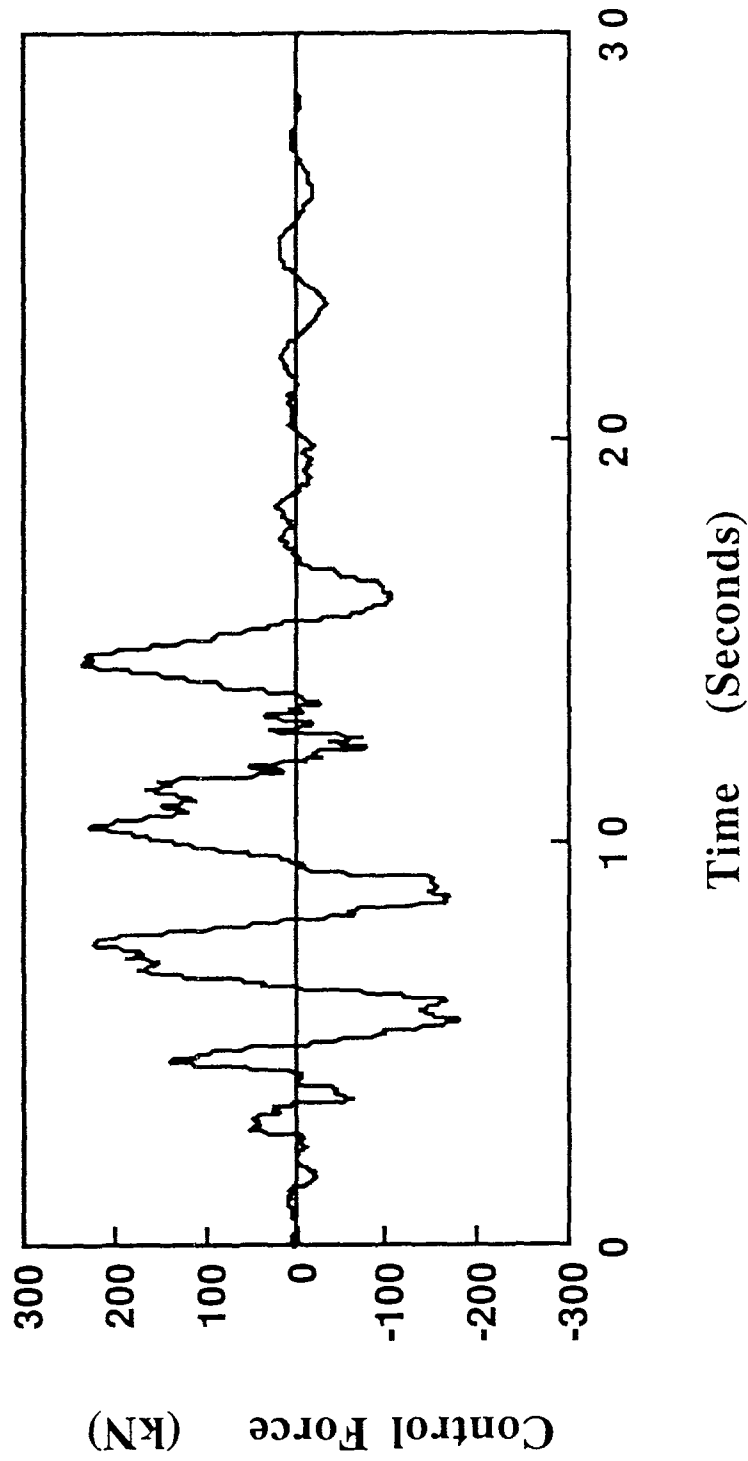


FIGURE 3.13 Required Active Control Force for Building With Base Isolation System and Active Mass Damper

TABLE 3.3 : Maximum Response Quantities of Building Equipped with Base Isolation System and Active Mass Damper : \bar{x}_d =maximum relative displacement of the mass damper; x_{mi} =maximum deformation of *i*th story unit; a_i =maximum absolute acceleration of *i*th floor; U_m =maximum active control force; \dot{U}_m =maximum active control force rate

FLOOR	Yield Displ. D_{yi} (cm)	BIS & AMD ¹ $\bar{x}_d=135$ cm $U_m=225.5$ kN $\dot{U}_m=984.8$ kN/s		BIS & AMD ² $\bar{x}_d=136$ cm $U_m=234.4$ kN $\dot{U}_m=1218.9$ kN/s		BIS & AF ³ $U_m=855.4$ kN $\dot{U}_m=4883.1$ kN/s		BIS & AF ⁴ $U_m=808.6$ kN $\dot{U}_m=4490.6$ kN/s	
		x_{mi} (cm)	a_i (cm/s ²)	x_{mi} (cm)	a_i (cm/s ²)	x_{mi} (cm)	a_i (cm/s ²)	x_{mi} (cm)	a_i (cm/s ²)
B	4.0	24.80	118	24.21	118	24.85	118	26.11	117
1	2.4	0.71	112	0.69	112	0.82	119	0.86	118
2	2.3	0.70	108	0.69	109	0.79	123	0.82	123
3	2.2	0.73	105	0.72	105	0.80	121	0.83	122
4	2.1	0.69	94	0.68	94	0.71	112	0.74	116
5	2.0	0.63	102	0.63	101	0.63	124	0.66	125
6	1.9	0.59	111	0.59	111	0.56	112	0.58	117
7	1.7	0.53	121	0.53	119	0.47	126	0.48	131
8	1.5	0.36	141	0.36	142	0.33	131	0.33	129

BIS = Base Isolation System; AMD¹ = Active Mass Damper with full sensors; AMD² = Active Mass Damper with limited No. of sensors; AF³ = Active Control Force with full sensors; AF⁴ = Active Control Force with limited No. of sensors

for the deformation of the base isolation system and the first story unit are shown in Fig. 3.9(f) and 3.12(c), respectively. The hysteresis loop for the shear force of the base isolation system is plotted in Fig. 3.10(d). A comparison of the results in this case with those of the first case in which sensors are installed on all floors of the building indicates that installations of displacement and velocity sensors on the building are not necessary. This conclusion is very important because it is expensive to install sensors. It is further observed from Table 3.3 that a significant reduction of the building response, in particular the response of the base isolation system, can be achieved using an active mass damper with a small active control force and force rate.

Instead of using an active mass damper described above, the base isolation system can be connected directly to an actuator. Such an active hybrid control system will be considered. Consider the first case in which displacement and velocity sensors are installed on every degree of freedom. The (18x18) \underline{Q} matrix is partitioned as shown in Eq. (3.1) in which \underline{Q}_{21} , and \underline{Q}_{22} are (9x9) matrices. For the isolation system connected to an actuator, the control force $\underline{U}(t)$ depends on the difference between the first two rows of the \underline{Q}_{21} and \underline{Q}_{22} matrices, i.e., $\underline{Q}_{21}(1,j)-\underline{Q}_{21}(2,j)$ and $\underline{Q}_{22}(1,j)-\underline{Q}_{22}(2,j)$. For simplicity, elements of $\underline{Q}_{21}(2,j)$ and $\underline{Q}_{22}(2,j)$ rows will be assigned to be zero. The following values are assigned to the elements of $\underline{Q}_{21}(1,j)$ and $\underline{Q}_{22}(1,j)$ rows for illustrative purposes:

$$\begin{aligned} \underline{Q}_{21}(1,j) &= [0.25 \quad 5.5 \quad 4.5 \quad 3.4 \quad 2.4 \quad 1.4 \quad 1.3 \quad 1.3 \quad 1.3] \\ \underline{Q}_{22}(1,j) &= [3.5 \quad 0.5 \quad 0.5 \quad 0.5 \quad 0.5 \quad 0.4 \quad 0.4 \quad 0.3 \quad 0.3] \end{aligned} \quad (3.5)$$

and $\underline{Q}_{21}(i,j)=\underline{Q}_{22}(i,j)=0$ for $i=2,\dots,9$. The weighting matrix \underline{R} consists of only one element denoted by R_0 . R_0 is chosen to be 10^{-3} . Time histories of all the structural response quantities have been computed. In particular, the time histories of the deformation of the base isolation system and the first story unit are shown in Fig. 3.9(c) and 3.12(d), respectively, for $\alpha/R_0=1.55 \times 10^8$ and $\Delta t=0.357 \times 10^{-2}$. The hysteresis loop for the shear force of the base isolation system is plotted in Fig. 3.10(e) and the required active control force is displayed in Fig. 3.14.

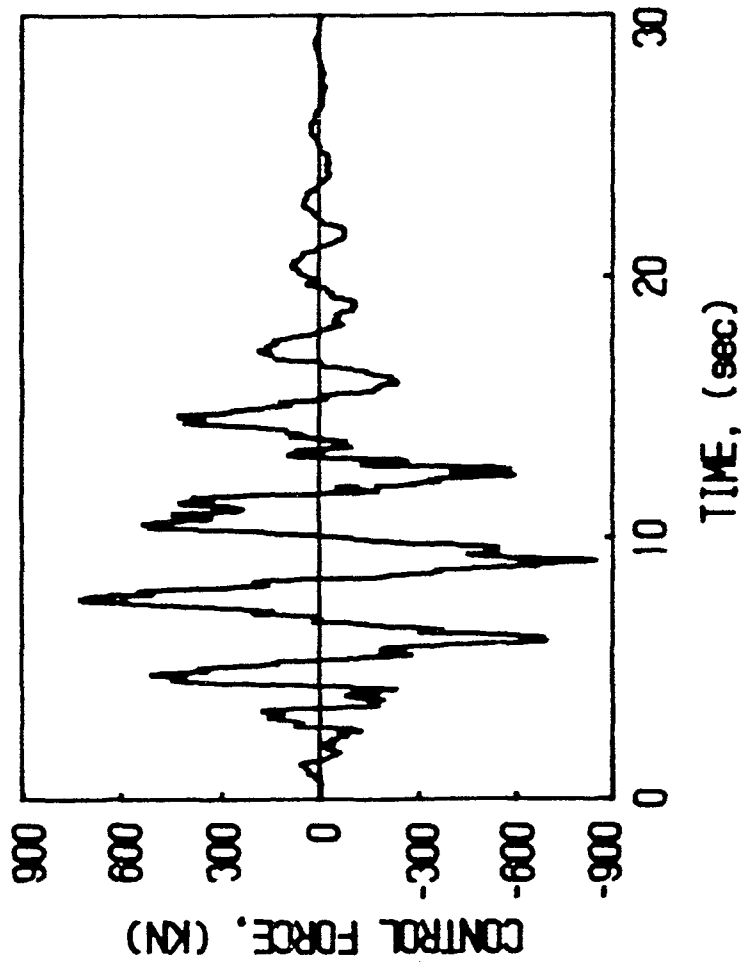


FIGURE 3.14 Required Active Control Force for Building With Base Isolation System and Actuator

Within 30 seconds of the earthquake episode, the maximum interstory deformations, x_{mi} , the maximum acceleration, a_i , of each floor, the maximum active control force, U_m , and force rate, \dot{U}_m , are summarized in the columns designated as "BIS&AF³" of Table 3.3.

Again, for convenience of instrumentation, we consider the second case in which displacement and velocity sensors are installed on the base isolation system only, i.e., no sensor is installed on the building. In this case, all the elements of Q_{21} and Q_{22} matrices are zero except $Q_{21}(1,1)$ and $Q_{23}(1,1)$. For simplicity, the following values are assigned: $Q_{21}(1,1)=0.9$ and $Q_{23}(1,1)=3.4$. The maximum response quantities for $\alpha/R_0=1.5 \times 10^8$ have been computed and summarized in the columns designated as "BIS&AF⁴" of Table 3.3. Time histories of the deformation of the base isolation system and the first story unit are shown in Fig. 3.9(d) and 3.12(e), respectively. The hysteresis loop for the shear force of the base isolation is plotted in Fig. 3.10(f). A comparison of these results with those of Case 1 using 18 sensors indicates that installing only the displacement and velocity sensors on the base isolation system is as good as installing displacement and velocity sensors on all degrees of freedom of the structural system.

It is observed from the results presented in Table 3.3 that the performance of the actuator is about the same as that of an active mass damper. However, the required active control force, U_m , and the force rate, \dot{U}_m , are much bigger using an actuator alone. This has been expected because the idea of using a mass damper is to absorb energies from the base isolation system, thus reducing the capacity of the actuator. The passive hybrid control system considered in the previous example demonstrates very well such a conclusion.

Example 5: Building Equipped With Sliding-Type Base Isolator and Actuator

Instead of using a rubber-bearing base isolation system, a frictional-type sliding base isolation system, as shown schematically in Fig. 3.15(a), is considered herein. This type of isolators allows greater resistance to damage by permitting the building to slide on its foundation during severe earthquakes. This isolation system decouples the building

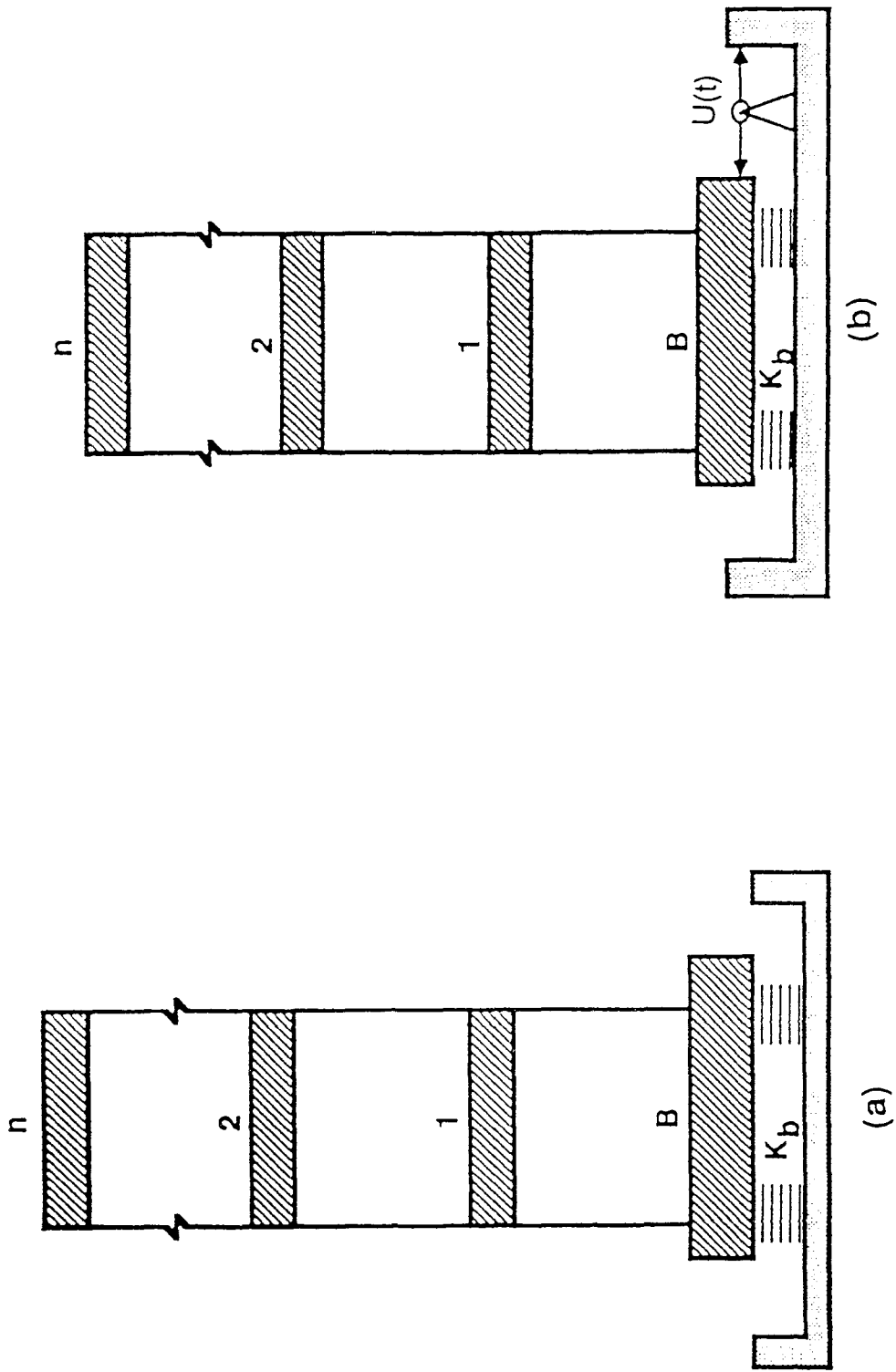


FIGURE 3.15 Structure Model of a Multi-Story Building: (a) With Base Sliding System; (b) With Base Sliding System and Actuator

from its foundation with nearly frictionless teflon on stainless steel sliding plates that have very low frictional resistance [e.g., 5-8, 17-18].

When the sliding system slides, the frictional force developed in the sliding system, F_{sb} , is given by

$$F_{sb} = \mu \bar{m} g \operatorname{sgn}(\dot{x}_b) \quad (3.6)$$

in which $\bar{m}g = w$ is the weight of the building system above the sliding bearings and μ is the coefficient of friction. When the sliding system sticks to the structure, the frictional force F_{sb} is smaller than the one given by Eq. (3.6). In the dynamic analysis of the sliding system for computing the time history of the structural response, a judgement is needed at every time instant t to determine whether the system is sticking or sliding. This is because the nonlinear frictional force varies from time to time. As a result, such an approach is quite tedious in the numerical computation of the structural response and it does not provide a systematic approach for the control problem.

To overcome the problem described above, the highly nonlinear frictional force is represented by the following analytical function

$$F_{sb} = \mu \bar{m} g v_b \quad (3.7)$$

in which v_b is a nondimensional hysteretic quantity described by Eq. (2.30) for $i=b$. It is mentioned that during the sliding phase (yielding), v_b takes a value of either 1 or -1. During the sticking phase (elastic behavior), the absolute value of v_b is less than unity, i.e., $|v_b| \leq 1$. The conditions of sticking and sliding are accounted for by Eq. (2.30) automatically. The parameters governing the scale and general shape of the hysteresis loop of the sliding system are $A_b=1.0$, $\beta_b=0.5$, $n_b=2$, $v_b=0.5$ and $D_{yb}=0.012\text{cm}$. A hysteresis loop for this set of parameters, i.e., v_b vs. x_b , representing the hysteretic behavior of the sliding system is schematically shown in Fig. 3.8(b). The mass of the sliding system is $m_b=450$ metric tons and the coefficient of friction is $\mu=10\%$. The response vector is given by $\underline{X}=[x_b, x_1, \dots, x_8]'$. The integration time step Δt is 0.03×10^{-2} sec.

Time histories of all the response quantities have been computed for the building equipped with the sliding base isolation alone. The time history, $x_1(t)$, of the first story deformation is depicted in Fig. 3.3(e) and that of the sliding system, $x_b(t)$, is presented in Fig. 3.16(a), where $x_b(t)$ denotes the relative displacement of the teflon and the stainless steel plate. Further, the hysteresis loops for the frictional force of the sliding system and the shear force of the first, fourth, and eighth story units are shown in Figs. 3.17(a) and 3.4(c), respectively. The maximum response quantities of the structure within 30 seconds of the earthquake episode are shown in the columns designated as "With SIS" of Table 3.4. As observed from Table 3.4 and Figs. 3.3(e) and 3.4(c), the interstory deformations and floor accelerations are significantly reduced. The advantage of using a sliding type base isolation system to protect the building is clearly demonstrated. However, the deformation of the eighth story unit is still in the inelastic range.

To further reduce the structural response and to bring the deformation of the 8th story unit into the elastic range, an actuator is connected to the sliding system as shown in Fig. 3.15(b). The actuator will apply the active control force directly on the sliding system. The basic idea of the active force, in this case, is to counteract the frictional force in order to maintain the system in the sliding condition as much as possible, so that the transmission of the earthquake ground motion to the building can be kept to a minimum.

With the active control force, the structural response depends on the weighting matrices \underline{R} and \underline{Q} . Again, the weighting matrix \underline{R} consists of only one element, denoted by R_0 , whereas the dimension of the \underline{Q} matrix is (18x18). R_0 is chosen to be 10^{-3} for simplicity and the \underline{Q} matrix is partitioned as shown in Eq. (3.1).

It is noticed that the deformation of the building is in-phase with the frictional force and the velocity of the building is out of phase of the frictional force. As a result, $\underline{Q}_{22} = \underline{Q}$ and only the elements in the \underline{Q}_{21} matrix which correspond to the deformation of the building are needed. These elements are assigned in the following for illustrative purposes:

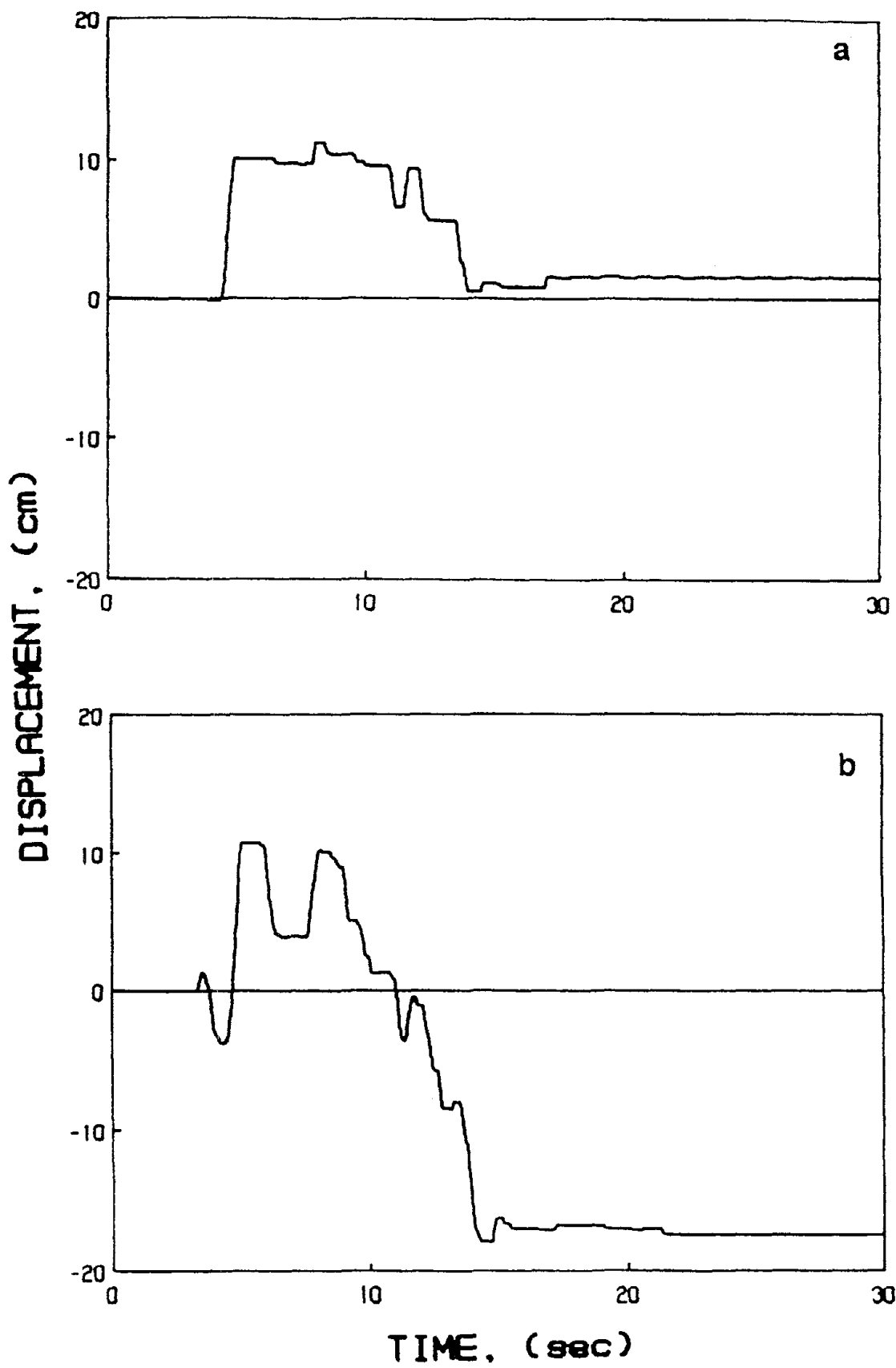


FIGURE 3.16 Relative Displacement of Base Sliding System: (a) Without Control; (b) With Actuator

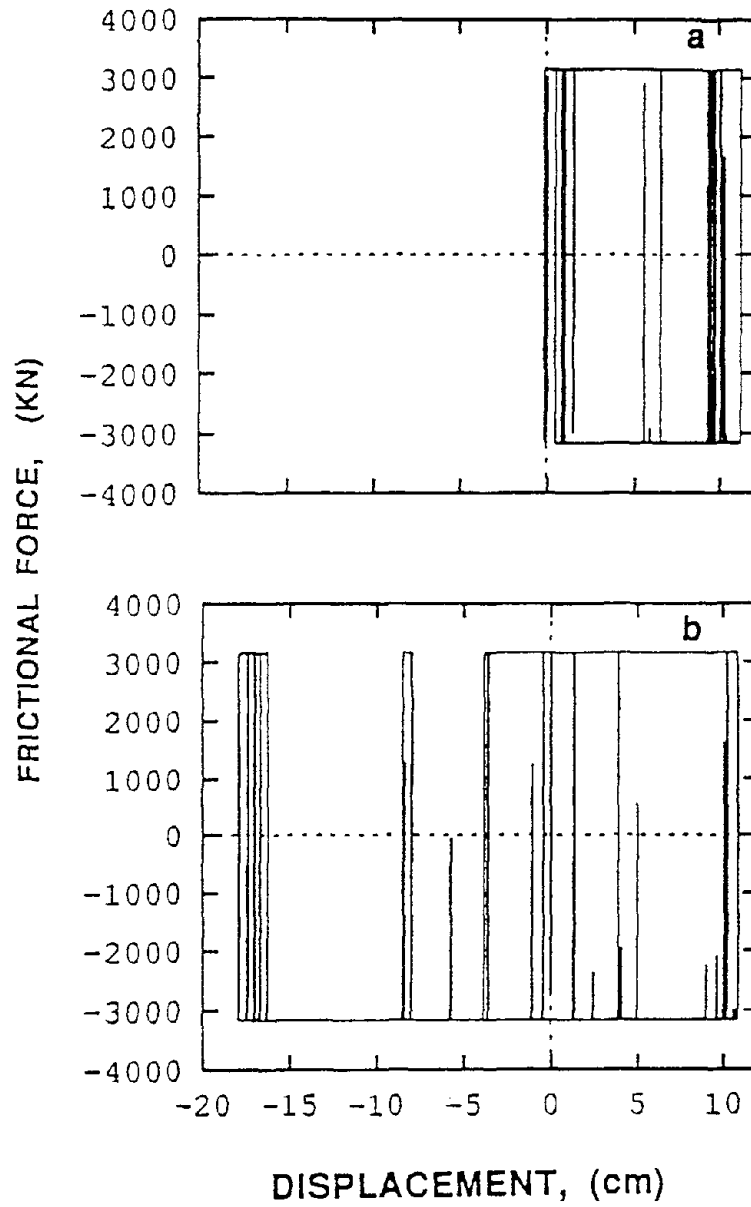


FIGURE 3.17 Hysteresis Loop for Frictional Force in Base Sliding System : (a) Without Control; (b) With Actuator

TABLE 3.4 : Maximum Response Quantities of Building Equipped with Sliding-type Isolation System and Actuator : x_d =maximum relative displacement of the mass damper; x_{mi} =maximum deformation of i th story unit; a_i =maximum absolute acceleration of i th floor; U_m =maximum active control force

Floor No.	Yield Displ. (cm)	without control		with SIS		SIS & AF	
		x_{mi} (cm)	a_i (cm/s ²)	x_{mi} (cm)	a_i (cm/s ²)	x_{mi} (cm)	a_i (cm/s ²)
B	-	-	-	11.54	658	18.13	688
1	2.4	3.05	486	1.30	370	0.56	325
2	2.3	2.80	456	1.23	547	0.76	342
3	2.2	3.14	571	1.38	531	0.91	379
4	2.1	2.95	529	1.40	404	0.83	300
5	2.0	2.70	558	1.50	424	0.89	379
6	1.9	2.91	720	1.72	462	1.00	412
7	1.7	2.90	580	1.82	541	1.09	341
8	1.5	2.08	617	1.64	601	0.99	391

SIS = Sliding-type Isolation System; AF = Active Control Force

$$Q_{21}(1,j) = [0, -30000, -3000, -300, -30, -3, -0.3, -0.03, -0.003] \quad (3.8)$$

All other elements of the Q_{21} matrix are set to be zero.

Time histories of all the structural response quantities have been computed. In particular, the time histories of the deformation of the sliding system and the first story unit are shown in Fig. 3.16(b) and 3.12(f), respectively, for $\alpha/R_0=2.25 \times 10^8$. The hysteresis loop for the sliding system is plotted in Fig. 3.17(b). The required active control force is displayed in Fig. 3.18. Within 30 seconds of the earthquake episode, the maximum interstory deformations, $x_{mi}(i=b,1,2,\dots,8)$, the maximum floor acceleration, a_i , and the maximum active control force, U_m , are summarized in the columns designated as "SIS&AF" of Table 3.4.

It is observed from Table 3.4 and Figs. 3.16(b) and 3.12(f) that the actuator connected to the sliding system is capable of reducing the response of the building significantly.

Example 6: Hybrid Control System Consisting of a Base Isolation System and an Actuator With Velocity and Acceleration Feedbacks

The instantaneous optimal control algorithm using velocity and acceleration feedbacks has been developed, Eq. (2.27). The application of such an algorithm and its performance will be demonstrated using an eight-story bilinear elasto-plastic building implemented by a hybrid control system. The hybrid control system consists of a rubber-bearing isolation system connected to an actuator, see Fig. 3.6(b), identical to that presented in Example 4. In the present case, however, instead of using the displacement and velocity feedbacks, i.e., $\underline{Z}(t)$, the velocity and acceleration feedbacks, $\dot{\underline{Z}}(t)$, will be used, Eq. (2.27).

The structural response $\underline{X}(t)=[x_b, x_1, \dots, x_8]'$ depends on the weighting matrices \underline{Q}^* and \underline{R}^* . Since there is only one actuator, the \underline{R}^* matrix consists of only one element, denoted by R_0^* . The dimension of the \underline{Q}^* matrix is 18×18 and it is partitioned as follows

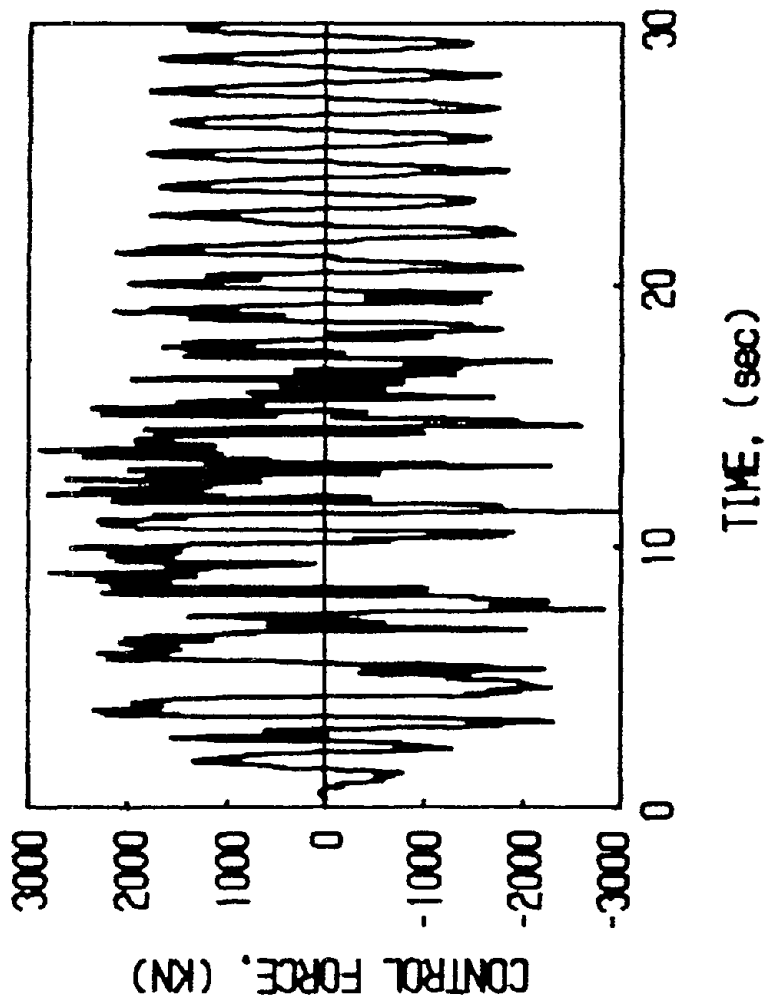


FIGURE 3.18 Required Active Control Force for Building With Base Sliding System and Actuator

$$\mathbf{Q}^* = \alpha \begin{bmatrix} \mathbf{0} & \mathbf{0} \\ \mathbf{Q}_{21}^* & \mathbf{Q}_{22}^* \end{bmatrix} \quad (3.9)$$

in which \mathbf{Q}_{21}^* and \mathbf{Q}_{22}^* are (9x9) matrices.

Again, the \mathbf{Q}^* matrix is symmetric. Since there is only one actuator installed on the basement floor, see Fig. 3.6(b), the control vector $\underline{\mathbf{U}}(t)$ depends only on the difference between the first two rows of the \mathbf{Q}_{21}^* and \mathbf{Q}_{22}^* matrices, Eq. (2.27). For convenience, only elements in the first row of the \mathbf{Q}_{21}^* and \mathbf{Q}_{22}^* are assigned with values and all other elements are set to be zero.

With a base isolation system, the building usually behaves like a rigid body, since its deformation is relatively small compared to that of the base isolation system. As a result, the performance of the control system will not be affected adversely if sensors are not installed on the building as demonstrated in Example 4. Since the installation of sensors is quite expensive, only a velocity sensor and an acceleration sensor will be installed on the base isolation system and the foundation. Consequently, all the elements in \mathbf{Q}_{21}^* and \mathbf{Q}_{22}^* matrices are zero except $Q_{21}^*(1,1)$ and $Q_{22}^*(1,1)$. For illustrative purpose, the following values are assigned to these two elements: $Q_{21}^*(1,1)=35$ and $Q_{22}^*(1,1)=0.5$.

Within 30 seconds of the earthquake episode, the following quantities are presented in the last two columns designated as "BIS&AF²" of Table 3.5 for $\alpha=18,750$ and $R_0^*=1$: (i) the maximum interstory deformations, x_{mi} , (ii) the maximum floor accelerations a_i and (iii) the maximum active control force U_m . Also presented in the columns designated as "BIS&AF¹" of Table 3.5 for comparison are the corresponding results using $\underline{\mathbf{Z}}(t)$ feedback taken from Table 3.3. The structural response quantities without active control are also shown in Table 3.5, which are taken from Tables 3.1 and 3.2.

It is observed from Table 3.5 that the performance of the instantaneous optimal control algorithm using velocity and acceleration feedbacks is as good as that using the

TABLE 3.5 : Maximum Response Quantities of Building Equipped with Base Isolation System and Actuator Using \dot{Z} feedback : x_{mi} =maximum deformation of i th story unit; a_i =maximum absolute acceleration of i th floor; U_m =maximum active control force

FLOOR	Yield Displ (cm)	without control		with BIS		BIS & AF ¹ $U_m=808.6$ kN		BIS & AF ² $U_m=807$ kN	
		x_{mi} (cm)	a_i (cm/s ²)	x_{mi} (cm)	a_i (cm/s ²)	x_{mi} (cm)	a_i (cm/s ²)	x_{mi} (cm)	a_i (cm/s ²)
B	-	-	-	42.70	158	26.11	117	25.77	109
1	2.4	3.05	486	1.31	155	0.86	118	0.82	111
2	2.3	2.80	456	1.25	152	0.82	123	0.78	114
3	2.2	3.14	571	1.28	157	0.83	122	0.79	116
4	2.1	2.95	529	1.17	164	0.74	116	0.70	113
5	2.0	2.70	558	1.07	177	0.66	125	0.62	116
6	1.9	2.91	720	0.97	185	0.58	117	0.55	113
7	1.7	2.90	580	0.82	198	0.48	131	0.46	124
8	1.5	2.08	617	0.52	206	0.33	129	0.30	120

BIS = Base Isolation System; AF¹ = Active Control Force with \dot{Z} feedback; AF² = Active Control Force with \dot{Z} feedback

displacement and velocity feedbacks. Further, the active control system using the instantaneous optimal algorithms presented herein is capable of significantly reducing both the responses of the building and the base isolation system.

Example 7: Hybrid Control System Consisting of A Base Isolation System and An Active Mass Damper With Velocity and Acceleration Feedbacks

The control algorithm using velocity and acceleration feedbacks, Eq. (2.27), will be used for a hybrid control system consisting of a base isolation system and an active mass damper presented in Example 4. In this case the structural response vector is $\underline{X}(t)=[x_d, x_b, x_1, \dots, x_8]'$. The weighting matrix \underline{R}^* consists of only one element, denoted by R_0^* , and the (20x20) weighting matrix \underline{Q}^* is partitioned as shown in Eq. (3.9), where \underline{Q}_{21}^* and \underline{Q}_{22}^* are (10x10) matrices. For illustrative purposes, velocity and acceleration sensors are installed on every degree of freedom of the structural system, i.e., a total of 20 velocity and acceleration sensors are installed. The elements of $\underline{Q}_{21}^*(1,j)$ and $\underline{Q}_{22}^*(1,j)$ are assigned in the following for illustrative purpose

$$\begin{aligned} Q_{21}^*(1,j) &= [102, -1353, 11, 840, 1397, 1649, 1645, 1433, 1057, 561] \\ Q_{22}^*(1,j) &= [67, 731, 646, 621, 584, 529, 457, 366, 257, 133] \end{aligned} \quad (3.10)$$

where $Q_{21}^*(i,j)=Q_{22}^*(i,j)=0$ for $i=2,3,\dots,10$,

With $R_0^*=1$ and $\alpha=300$, Eq. (3.9), the following maximum response quantities in 30 seconds of the earthquake episode are presented in the columns designated as "I(B)" of Table 3.6: (i) the maximum interstory deformation x_{im} , (ii) the maximum floor acceleration a_i , and (iii) the maximum active control force U_m . Also presented in the columns designated as "I(A)" of Table 3.6 for comparison are the corresponding results using the displacement and velocity feedbacks, $\underline{Z}(t)$, taken from Table 3.3.

We now consider the case in which sensors are not installed on the building, i.e., sensors are installed only on the base isolation system and on the mass damper. In this case all the elements of the $\underline{Q}_{21}^*(1,j)$ and $\underline{Q}_{22}^*(1,j)$ matrices are zero, except $Q_{21}^*(1,1)$, $Q_{21}^*(1,2)$, $Q_{22}^*(1,1)$ and $Q_{22}^*(1,2)$. For illustrative purpose, the following values are

TABLE 3.6: Maximum Response Quantities of Building Equipped with Base Isolation System and Active Mass Damper Using \underline{Z} feedback : x_{mi} =maximum deformation of i th story unit; a_i =maximum absolute acceleration of i th floor; U_m =maximum active control force; I = full Sensors; II = Limited No. of Sensors; (A) = with \underline{Z} feedback; (B) = with $\underline{\dot{Z}}$ feedback

FLOOR NO	Yield Displ D_{yi}	I				II			
		(A)		(B)		(A)		(B)	
		$U_m=225.5\text{kN}$		$U_m=212.3\text{kN}$		$U_m=2344\text{kN}$		$U_m=2184\text{kN}$	
i	x_{mi} (cm)	a_i (cm/s ²)	x_{mi} (cm)	a_i (cm/s ²)	x_{mi} (cm)	a_i (cm/s ²)	x_{mi} (cm)	a_i (cm/s ²)	
B	-	24.80	118	14.6	108	24.21	118	15.7	103
1	2.4	0.71	112	0.51	104	0.69	112	0.48	97
2	2.3	0.70	108	0.52	92	0.69	109	0.49	87
3	2.2	0.73	105	0.57	80	0.72	105	0.54	79
4	2.1	0.69	94	0.56	80	0.68	94	0.54	72
5	2.0	0.63	102	0.55	77	0.63	101	0.52	77
6	1.9	0.59	111	0.52	97	0.59	111	0.50	92
7	1.7	0.53	121	0.48	107	0.53	119	0.44	103
8	1.5	0.36	141	0.35	141	0.36	142	0.33	132

assigned: $Q^*_{21}(1,1)=102$, $Q^*_{21}(1,2)=-1353$, $Q^*_{22}(1,1)=67$ and $Q^*_{22}(1,2)=731$.

Within 30 seconds of the earthquake episode, the maximum response quantities are presented in the last two columns of Table 3.6 designated as "II(B)". For comparison, the corresponding results using the response state vector $\underline{Z}(t)$ as feedback are shown in the columns designated as "II(A)" of Table 3.6. These results were taken from Table 3.3.

Although the control algorithm using the $\dot{\underline{Z}}$ feedback is capable of reducing the structural response quantities, the required active control force is about one order of magnitude bigger than that using the \underline{Z} feedback as observed from Table 3.6. With the same order of magnitude of the control force, i.e., $U_m=225.5$ kN, and the $\dot{\underline{Z}}$ feedback algorithm, the response quantities are much larger than those obtained using the control algorithm with the \underline{Z} feedback, Case (A) of Table 3.6.

Consequently, it is concluded that the control algorithm using the $\dot{\underline{Z}}$ feedback is not suitable for the base-isolated building connected to an active mass damper. The applicability and limitation of the control algorithm using the velocity and acceleration feedbacks for different types of aseismic protective systems will be presented in a different report.

SECTION 4 CONCLUSION

A refined version of the instantaneous optimal control algorithm for nonlinear or inelastic structural systems is presented. The optimal algorithm is simple and reliable for on-line operations without tracking any system characteristics. Applications of the optimal algorithm to various types of hybrid control systems have been demonstrated. These include (i) an active mass damper installed on the top floor of the building, (ii) active control of base-isolated buildings using lead-core elastomeric bearings, and (iii) active control of base-isolated buildings using sliding type isolation systems. The building itself considered is bilinear elasto-plastic.

A method of simulating the seismic response of inelastic (hysteretic) systems using the proposed optimal algorithm is presented. This method has been used to evaluate and compare numerically the performance of various control systems. The advantages of aseismic hybrid control systems are clearly demonstrated. It is shown that the optimal algorithm proposed is effective for practical applications.

Because of possible difficulties involved in measuring the displacement response of the building during an earthquake, it is desirable not to use the displacement response as feedbacks. A variation of the instantaneous optimal algorithm utilizing the acceleration response rather than the displacement response as feedback is also presented. Numerical examples demonstrate that the performance of the control algorithm using the velocity and acceleration feedbacks is at least as good as that of the optimal algorithm using the displacement and velocity feedbacks for the hybrid control systems considered.

Another contribution of this report is the analysis methodology presented for evaluating the performance of aseismic hybrid control systems using frictional-type sliding isolation systems. The highly nonlinear frictional force is described by an analytical function of the equivalent hysteretic component, thus facilitating the analysis of controlled response of the entire structural system.

SECTION 5

REFERENCES

1. Baber, T.T., and Wen, Y.K. (1981), "Random Vibration of Hysteretic Degrading Systems", Journal of Engineering Mechanics Division, ASCE, Vol. 107, No. EM6, pp. 1069-1987.
2. Bouc, R. (1967), "Forced Vibration of Mechanical Systems With Hysteresis, abstract", Proceedings of 4th Conference on Nonlinear Oscillation, Prague, Czechoslovakia.
3. Chong, K.P., Liu, S.C., and Li, J.C., Editors, Intelligent Structures (1990). Elsevier Applied Science, London and New York.
4. Chung, L.L., Lin, R.C., Soong, T.T., and Reinhorn, A.M. (1988), "Experimental Study of Active Control of MDOF Structures Under Seismic Excitations". Technical Report NCEER-88-0025.
5. Constantinou, M.C., and Papageorgiou, A.S. (1990), "Stochastic Response of Practical Sliding Isolation System", Probabilistic Engineering Mechanics, Vol. 5, No. 1, pp. 27-34.
6. Contantinou, M.C., Mokha, A., and Reinhorn, A. (1990), "Teflon Bearings in Base Isolation. II: Modeling", Journal of Structural Engineering, ASCE, Vol. 116, No. 2, February, pp. 455-474.
7. Constantinou, M.C., and Tadjbakhsh, I.G. (1984), "Response of a Sliding Structures to Filtered Random Excitation", Journal of Structural Mechanics, Vol. 12, pp. 401-418.
8. Fan, F.G., Ahmadi, G., and Tadjbakhsh, I.G. (1988), "Base Isolation of a Multi-Story Building Under a Harmonic Ground Motion - A Comparison of Performances of Various Systems", National Center for Earthquake Engineering Research, Technical Report NCEER-88-0010, SUNY, Buffalo.
9. Housner, G.W. and Masri, S. (1990), Editors, Proceedings of U.S. National Workshop on Structural Control Research, October USC publication, CE-9013.
10. Kelly, J.M., Leitmann, G., and Soldators, A.G. (1987), "Robust Control of Base-Isolated Structures Under Earthquake Excitation", Journal of Optimization Theory and Applications, Vol. 53, No. 2, pp. 159-180.
11. Kelly, J.M. (1986), "Aseismic Base Isolation: Review and Bibliography", Journal of Soil Dynamics and Earthquake Engineering, Vol. 5, No. 3, pp. 202-216.

12. Kobori, T., Koshika, N., Yamada, K., and Ikeda, Y. (1991), "Seismic-Response-Controlled Structure with Active Mass Driver System. Part 1: Design". Earthquake Engineering and Structural Dynamics, Vol. 20, pp. 133-149.
13. Kobori, T., Koshika, N., Yamada, K., and Ikeda, Y. (1991), "Seismic-Response-Controlled Structure with Active Mass Driver System. Part 2: Verification". Earthquake Engineering and Structural Dynamics, Vol. 20, pp. 151-166.
14. Kobori, T. (1990), "Technology Development and Forecast of Dynamical Intelligent Building (D.I.B.)", Intelligent Structure by K.P. Chong, S.C. Liu and J.C. Li, Published by Elsevier Applied Science, pp. 42-59.
15. Li, Z., Katukura, H., and Izumi, M. (1991), "Synthesis and Extension of One-Dimensional Nonlinear Hysteretic Models", J. Engineering Mechanics, ASCE, Vol 117, No. 1, pp. 100-109.
16. Masri, S.F., Bekey, G.A., and Caughey, T.K. (1981a), "On-Line Control of Nonlinear Flexible Structures", Journal of Applied Mechanics, ASME, Vol. 49, No. 4, pp. 871-884.
17. Mokha, A., Constantinou, M., and Reinhorn, A. (1990), "Teflon Bearings in Base Isolation. I: Testing", Journal of Structural Engineering, ASCE, Vol. 116, No. 2, February, pp. 438-454.
18. Mokha, A., Constantinou, M., and Reinhorn, A. (1988), "Teflon Bearings in Aseismic Base Isolation: Experimental Studies and Mathematical Modeling", Technical Report NCEER-88-0038, SUNY, Buffalo, NY.
19. Park, Y.J., Wen, Y.K., and Ang, A.H-S. (1986), "Two Dimensional Random Vibration of Hysteretic Structures", Journal of Earthquake Engineering and Structural Dynamics, Vol. 14, pp. 543-557.
20. Reinhorn, A.M., Soong, T.T., Lin, R.C., Wang, Y.P., Fukao, Y., Abe, H., and Hakai, M. (1989), "1:4 Scale Model Studies of Active Tendon Systems and Active Mass Dampers for Aseismic Protection". Technical Report NCEER-89-0026.
21. Reinhorn, A.M., Manolis, G.D., and Wen, C.Y. (1987), "Active Control of Inelastic Structures", Journal of Engineering Mechanics, ASCE, Vol. 113, No. 3, pp. 315-332.
22. Reinhorn, A.M., Soong, T.T., and Yen, C.Y. (1987), "Base Isolated Structures with Active Control", Seismic Engineering, Recent Advances in Design, Analysis, Testing and Qualification Methods, edited by T.H. Liu and A. Marr, ASME, PVP-Vol. 127, pp. 413-419.
23. Soong, T.T. (1990), Active Structural Control: Theory and Practice, Longman Scientific and Technical, New York, SUNY, August.

24. Su, L., Ahmadi, G., and Tadjbakhsh, I.G. (1987), "A Comparative Study of Performance of Various Base Isolation Systems Part I: Shear Beam Structures", Report No. MIE-153, Clarkson University, October.
25. Wen, Y.K. (1989), "Methods of Random Vibration for Inelastic Structures", Journal of Applied Mechanics Reviews, Vol. 42, No. 2, February, pp. 39-52.
26. Yang, J.N., Akbarpour, A., and Ghaemmaghami, P. (1985) "Optimal Control Algorithms for Earthquake Excited Building Structures", Structural Control, Proceedings of 2nd International Symposium on Structural Control, editor H.H.E. Leipholz, Martinus Nijhoff, Amsterdam, pp. 748-761.
27. Yang, J.N., Akbarpour, A., and Ghaemmaghami, P. (1987) "New Optimal Control Algorithms for Structural Control", Journal of Engineering Mechanics, ASCE, Vol. 113, No. 9, June, pp. 1369-1386.
28. Yang, J.N., Akbarpour, A., and Ghaemmaghami, P. (1987) "Instantaneous Optimal Control Laws For Building Structures Under Earthquake Excitations", National Center for Earthquake Engineering Research, Technical Report NCEER-TR-87-0007, SUNY, Buffalo.
29. Yang, J.N., and Soong, T.T. (1988) "Recent Advancement in Active Control of Civil Engineering Structures", Journal of Probabilistic Engineering Mechanics, Vol. 3, No. 4, December, pp. 179-188.
30. Yang, J.N., Long, F.X., and Wong, D. (1988) "Optimal Control of Nonlinear Structures", Journal of Applied Mechanics, ASME, Vol. 55, December, pp. 931-938.
31. Yang, J.N., Long, F.X., and Wong, D. (1988) "Optimal Control of Nonlinear Flexible Structures", National Center for Earthquake Engineering Research, Technical Report NCEER-TR-88-0002.
32. Yang, J.N., and Akbarpour, A. (1990), "Effect of System Uncertainty on Control of Seismic-Excited Buildings", J. of Engineering Mechanics, ASCE, Vol. 116, No. 2, February, pp. 462-478.
33. Yang, J.N., Akbarpour, A., and Askar, G. (1990), "Effect of Time Delay on Control of Seismic-Excited Buildings", J. of Structural Engineering, ASCE, Vol. 116, No. 10, October, pp. 2801-2814.
34. Yang, J.N., and Wong, D. (1989) "On Aseismic Hybrid Control System," Proceedings of 5th International Conference on Structural Safety and Reliability, ICOSSAR '89, edited by A. H-S. Ang, M. Shinozuka and G.T. Schueller, ASCE, August, pp. 471-478.

35. Yang, J.N, Danielians, A. and Liu, S.C. (1990) "Aseismic Hybrid Control Systems For Building Structures Under Strong Earthquakes", Intelligent Structures, edited by K.P. Chong, S.C. Liu and J.C. Li, Elsevier Applied Science, pp. 179-195, Proceedings of International Workshop on Intelligent Structures, July 23-26, Taipei, Taiwan. Also Journal of Intelligent Material Systems and Structures, Vol. 1, No. 4, October, pp. 432-446.
36. Yang, J.N., Danielians, A., and Liu, S.C. (1991), "Aseismic Hybrid Control Systems for Building Structures", Journal of Engineering Mechanics, ASCE, Vol. 117, No. 4, April, pp. 836-853.
37. Yang, J.N., Li, Z., and Liu, S.C. (1990) "Instantaneous Optimal Control With Acceleration and Velocity Feedback", Proceedings of the 2nd International Conference on Stochastic Structural Dynamics, May 7-9, Boca Raton, FL.
38. Yang, J.N., Li, Z., and Liu, S.C. (1991) "Instantaneous Optimal Control With Acceleration and Velocity Feedback", paper to appear in Journal of Probabilistic Engineering Mechanics, Sept. 1991.
39. Yang, J.N., Li, Z., Danielians, A., and Liu, S.C., "Instantaneous Optimal Control of Nonlinear Hybrid Systems," paper presented at the Eighth VPI&SU Symposium on Dynamics and Control of Large Structures, May 6-8, 1991, Blacksburg, VA.
40. Yang, J.N., Li, Z. and Liu, S.C., "Hybrid Control of Seismic-Excited Inelastic System Using Velocity and Acceleration Feedbacks", paper presented at the IUTAM Symposium on Nonlinear Stochastic Mechanics, July 1-5, 1991, in Trino, Italy.
41. Yang, J.N., Li, Z., Danielians, A. and Liu, S.C., "Optimal Hybrid Control of Seismic-Excited Nonlinear and Inelastic Structures", paper presented at the U.S.-Japan-Italy Workshop/Seminar on Intelligent Systems, June 27-29, 1991, Perugia, Italy, to appear in the Conference Proceedings.

APPENDIX A
FOURTH-ORDER RUNGE-KUTTA METHOD

The Runge-Kutta method has been used extensively to solve the first order nonlinear differential equation numerically. In this method, the solution at time $t + \Delta\tau$ is approximated by a truncated Taylor's series around the solution at the previous time t . Let

$$\dot{y}(t) = f[y(t), t] \quad (\text{A-1})$$

be a first order nonlinear differential equation. Given the solution $y(t_n)$ at time t_n , the solution $y(t_n + \Delta\tau)$ at $t_n + \Delta\tau$ is obtained using the Runge-Kutta method as

$$y(t_n + \Delta\tau) = y(t_n) + \frac{1}{6} \Delta\tau (A_0 + 2A_1 + 2A_2 + A_3) \quad (\text{A-2})$$

where

$$\begin{aligned} A_0 &= f[y(t_n), t_n] \\ A_1 &= f[y(t_n) + 0.5A_0, t_n + 0.5\Delta\tau] \\ A_2 &= f[y(t_n) + 0.5A_1, t_n + 0.5\Delta\tau] \\ A_3 &= f[y(t_n) + A_2, t_n + \Delta\tau] \end{aligned} \quad (\text{A-3})$$

The matrix equation of motion given by Eq. (2.3) can be written as

$$\dot{\underline{Z}}(t) = f[\underline{Z}(t), t] \quad (\text{A-4})$$

in which

$$f[\underline{Z}(t), t] = \underline{g}[\underline{Z}(t)] + \underline{B}\underline{U}(t) + \underline{W}_1 \ddot{\underline{X}}_0(t) \quad (\text{A-5})$$

Equation (A-4) is analogy to Eq. (A-1). Hence, using Eqs. (A-2) and (A-3) with $t_n + \Delta\tau = t$ and $\Delta\tau = 2\Delta t$, the solution for $\underline{Z}(t)$ can be expressed as

$$Z(t) = Z(t - 2\Delta t) + \frac{1}{6}(A_0 + 2A_1 + 2A_2 + A_3) \quad (\text{A-6})$$

in which \underline{A}_0 , \underline{A}_1 , \underline{A}_2 and \underline{A}_3 are defined as Eq. (2.7).

APPENDIX B
INSTANTANEOUS OPTIMAL CONTROL ALGORITHMS

Substituting Eq. (2.12) and Eq. (2.13), one obtains the following three matrix equations

$$2\mathbf{Q}\mathbf{Z}(t) + \boldsymbol{\lambda}(t) = \mathbf{0} \quad (\text{B-1})$$

$$2\mathbf{R}\mathbf{U}(t) - \frac{\Delta t}{3} \mathbf{B}'\boldsymbol{\lambda}(t) = \mathbf{0} \quad (\text{B-2})$$

$$\mathbf{Z}(t) = \mathbf{D}(t-2\Delta t, t-\Delta t) + \frac{\Delta t}{3} [\mathbf{B}\mathbf{U}(t) + \mathbf{W}_1\ddot{\mathbf{X}}_0(t)] \quad (\text{B-3})$$

(i) Instantaneous Optimal Open-Loop Control (Feedforward)

Let the control vector $\mathbf{U}(t)$ be regulated by the earthquake excitation alone, i.e.

$$\boldsymbol{\lambda}(t) = \mathbf{q}(t) \quad (\text{B-4})$$

Then equations (B-1), (B-2) and (B-3) become

$$2\mathbf{Q}\mathbf{Z}(t) + \mathbf{q}(t) = \mathbf{0} \quad (\text{B-5})$$

$$2\mathbf{R}\mathbf{U}(t) - \frac{\Delta t}{3} \mathbf{B}'\mathbf{q}(t) = \mathbf{0} \quad (\text{B-6})$$

$$\mathbf{Z}(t) = \mathbf{D}(t-2\Delta t, t-\Delta t) + \frac{\Delta t}{3} [\mathbf{B}\mathbf{U}(t) + \mathbf{W}_1\ddot{\mathbf{X}}_0(t)] \quad (\text{B-7})$$

The unknown vectors $\mathbf{U}(t)$, $\mathbf{q}(t)$, and $\mathbf{Z}(t)$ can be solved from Eqs. (B-5)-(B-7) as follows. The vector $\mathbf{Z}(t)$ is eliminated by substituting Eq. (B-7) into Eq. (B-5) resulting in

$$2Q = D(t-2\Delta t, t-\Delta t) + \frac{\Delta t}{3} [BU(t) + W_1 \ddot{X}_0(t)] + q(t) = 0 \quad (\text{B-8})$$

Premultiplying Eq. (B-8) by $\Delta t/3 B'$ and adding to Eq. (B-6), one obtains the control vector $\underline{U}(t)$ in the following

$$\underline{U}(t) = \underline{L}G(t) \quad (\text{B-9})$$

in which

$$\underline{L} = \left[\left(\frac{\Delta t}{3} \right)^2 B'QB + R \right]^{-1} \quad (\text{B-10})$$

$$\underline{G}(t) = \frac{\Delta t}{3} B'QD(t-2\Delta t, t-\Delta t) - \left(\frac{\Delta t}{3} \right)^2 B'QW_1 \ddot{X}_0(t) \quad (\text{B-11})$$

It is observed from Eqs. (B-9)-(B-11) that the control vector $\underline{U}(t)$ at time t is regulated by the earthquake excitation $\ddot{X}_0(t)$ at time t and $D(t-2\Delta t, t-\Delta t)$, that consists of quantities at $t-\Delta t$ and $t-2\Delta t$. The response state vector $\underline{Z}(t)$ is obtained by substituting Eq. (B-9) into Eq. (B-7).

$$\underline{Z}(t) = D(t-2\Delta t, t-\Delta t) + \frac{\Delta t}{3} [BLG(t) + W_1 \ddot{X}_0(t)] \quad (\text{B-12})$$

(ii) Instantaneous Optimal Closed-Loop Control (Feedback)

Let the control vector $\underline{U}(t)$ be regulated by the feedback response state vector $\underline{Z}(t)$ alone, i.e.

$$\underline{\lambda}(t) = \underline{\Lambda} \underline{Z}(t) \quad (\text{B-13})$$

Then, substitution of Eq. (B-13) into Eq. (B-1) yields

$$(2Q + \underline{\Lambda}) \underline{Z}(t) = 0 \quad (\text{B-14})$$

The unknown matrix $\underline{\Lambda}$ is obtained, for $\underline{Z}(t) \neq 0$, as

$$\underline{\Lambda} = 2Q \quad (\text{B-15})$$

The control vector $\underline{U}(t)$ is obtained by substituting Eq. (B-15) into Eq. (B-13) and then into Eq. (B-2) as follows

$$\underline{U}(t) = - \frac{\Delta t}{3} \underline{R}^{-1} \underline{B}' Q \underline{Z}(t) \quad (\text{B-16})$$

Substituting Eq. (B-16) into Eq. (B-3) and simplifying the resulting expression, one obtains the response vector $\underline{Z}(t)$ under instantaneous optimal closed-loop control

$$\underline{Z}(t) = \left[\underline{I} + \left(\frac{\Delta t}{3} \right)^2 \underline{B} \underline{R}^{-1} \underline{B}' Q \right]^{-1} \{ \underline{D}[(t-\Delta t), (t-2\Delta t)] + \frac{\Delta t}{3} \underline{W}_1 \ddot{\underline{X}}_0(t) \} \quad (\text{B-17})$$

(iii) Instantaneous Optimal Closed-Open-Loop Control (Feedforward-Feedback)

Let the control vector $\underline{U}(t)$ or $\underline{\lambda}(t)$ be regulated by both the feedback response state vector $\underline{Z}(t)$ and the measured earthquake ground acceleration $\ddot{\underline{X}}_0(t)$, i.e.

$$\underline{\lambda}(t) = \underline{\Lambda}_1 \underline{Z}(t) + \underline{q}(t) \quad (\text{B-18})$$

The control vector $\underline{U}(t)$ can be eliminated by substituting Eq. (B-2) into (B-3)

$$\underline{Z}(t) = \underline{D}(t-2\Delta t, t-\Delta t) + \frac{\Delta t}{3} \left[\frac{\Delta t}{6} \underline{B} \underline{R}^{-1} \underline{B}' \underline{\lambda}(t) + \underline{W}_1 \ddot{\underline{X}}_0(t) \right] \quad (\text{B-19})$$

Equation (B-1) can be rewritten as

$$Q [\underline{Z}(t) + \underline{Z}(t)] + \underline{\lambda}(t) = 0 \quad (\text{B-20})$$

Substituting Eq. (B-19) for the second term of $\underline{Z}(t)$ in Eq. (B-20) and simplifying the resulting expression, one obtains

$$\left\{ Q + \left[\frac{(\Delta t)^2}{18} QBR^{-1}B' + I \right] \underline{\Delta}_1 \right\} \underline{Z}(t) + Q \{ D(t-2\Delta t, t-\Delta t) + \frac{\Delta t}{3} W_1 \ddot{X}_0(t) \} + \left\{ \frac{(\Delta t)^2}{18} QBR^{-1}B' + I \right\} \underline{q}(t) = 0 \quad (\text{B-21})$$

For $\underline{Z}(t) \neq 0$ and $\underline{q}(t) \neq 0$, the solution of unknown matrix, $\underline{\Delta}_1$, and vector, $\underline{q}(t)$, are obtained as follows

$$\underline{\Delta}_1 = - \left[\frac{(\Delta t)^2}{18} QBR^{-1}B' + I \right]^{-1} Q \quad (\text{B-22})$$

$$\underline{q}(t) = \underline{\Delta}_1 \left[D(t-2\Delta t, t-\Delta t) + \frac{\Delta t}{3} W_1 \ddot{X}_0(t) \right] \quad (\text{B-23})$$

Thus, the control vector $\underline{U}(t)$ and the response state vector $\underline{Z}(t)$ with instantaneous optimal closed-open-loop control are determined in the following:

$$\underline{U}(t) = \frac{\Delta t}{6} R^{-1}B' \left[\underline{\Delta}_1 \underline{Z}(t) + \underline{q}(t) \right] \quad (\text{B-24})$$

$$\underline{Z}(t) = \left[I - \frac{(\Delta t)^2}{18} BR^{-1}B'\underline{\Delta}_1 \right]^{-1} \left\{ D(t-2\Delta t, t-\Delta t) + \frac{(\Delta t)^2}{18} BR^{-1}B'\underline{q}(t) + \frac{\Delta t}{3} W_1 \ddot{X}_0(t) \right\} \quad (\text{B-25})$$

in which $\underline{\Delta}_1$ and $\underline{q}(t)$ are given in Eqs. (B-22) and (B-23).

HYBRID CONTROL OF SEISMIC-EXCITED STRUCTURAL SYSTEMS

PART II



SECTION 1 INTRODUCTION

It has been shown recently that a combined use of active and passive control systems, referred to as the hybrid control system, is more effective, beneficial and practical, in some cases, for reducing the building response under strong earthquakes [e.g., 3,9,23,24,28,29]. However, the use of hybrid control systems involves active control of nonlinear or inelastic structural systems, since passive control systems, such as base isolation systems, usually behave nonlinearly or inelastically under dynamic loads. Instantaneous optimal control algorithms for linear, nonlinear or inelastic structures were proposed in Refs. 19-22. Recently, a refined version of such optimal control algorithms was presented in Refs. 28-29, with emphasis placed on applications to aseismic hybrid control systems. An aseismic hybrid control system consists of active control devices, such as an active mass damper, and passive base isolation systems. In Refs. 28-29, the optimal control vector $\underline{U}(t)$ was obtained from the measured $2n$ state vector $\underline{Z}(t)$.

For inelastic structural systems, such as base-isolated buildings using either lead-core rubber bearing isolators or sliding-type isolations [e.g., 4-8,10,12-14], the total deformation consists of an elastic component and a hysteretic component. Various mathematical models to describe the behavior of the hysteretic component have been proposed in the literature [e.g., 1,2,4-8,11-15,17-18]. To-date, the hysteretic component of the structural response has not been incorporated in the formulation of the optimal control problem, although the hysteretic model has been used in the simulation of the controlled response of buildings equipped with aseismic hybrid control systems [28-29].

Based on the concept of instantaneous optimal control [19-22,28-29], the optimal control problem is formulated incorporating the specific hysteretic model in this report. This is accomplished by including the hysteretic component explicitly in the equations of motion, which are used as the constraints for the determination of the optimal control vector. For an n -degree-of-freedom system, the dimension of the state vector $\underline{Z}(t)$ used in Refs. 28-29 is $2n$. Including the hysteretic component explicitly in the present

formulation, the dimension of the new state vector $\tilde{\mathbf{Z}}(t)$ becomes $3n$. The optimal control vector $\mathbf{U}(t)$ is obtained by minimizing a time dependent quadratic performance index [16,19-21] exactly in the same manner as that described in Refs. 19-22 and 28-29. In this report, we also prove that the optimal control vector satisfies not only the necessary conditions but also the sufficient condition of optimality. Since the control vector $\mathbf{U}(t)$ is obtained as a linear function of the $3n$ state vector $\tilde{\mathbf{Z}}(t)$, it depends not only on the measured deformation and velocity but also on the hysteretic component of the structural response. The hysteretic component of the structural response can be estimated from an observer using the measured structural response and the specific hysteretic model used. A simple method of constructing the observer for the estimation of the hysteretic component is also presented.

Specific applications of the present control algorithm to two important types of aseismic hybrid control systems are demonstrated. These include (i) a frictional-type sliding isolation system connected to an actuator, and (ii) a lead-core rubber bearing isolation system connected to either an actuator or an active mass damper. These two types of aseismic hybrid systems are highly nonlinear and hysteretic in nature. Theoretically, the performance of the present optimal algorithm should be better than that proposed in Refs. 28-29, because more information is used in the determination of the control vector. Several examples have been worked out and the performance of the present optimal algorithm has been investigated, evaluated and compared numerically with that of the previous algorithm [Ref. 28-29]. It is shown numerically that the performance of the present optimal algorithm is indeed better than that of the previous one for the two types of aseismic hybrid control systems investigated herein.

SECTION 2
OPTIMAL CONTROL OF INELASTIC STRUCTURAL SYSTEMS

2.1 Nonlinear Hysteretic Model for Inelastic Systems

Various hysteretic models for the restoring force of an inelastic system have been developed in recent years [e.g. 1,2,4-8,11-15,17-18]. In this study, the differential equation model available in the literature [e.g., 1,2,11,15,18] will be used for both structures and passive protective systems. The stiffness restoring force for a structural member or a story unit, $F_s(x,t)$, is expressed as

$$F_s(x,t) = \alpha k x + (1 - \alpha) k D_y v \quad (2.1)$$

in which x =deformation, k =elastic stiffness, α = ratio of post-yielding to pre-yielding stiffness, D_y =yield deformation=constant, and v is a nondimensional variable introduced to describe the hysteretic component of the deformation, with $|v| \leq 1$, where

$$D_y \dot{v} = A \dot{x} - \beta |\dot{x}| |v|^{n-1} v - \gamma \dot{x} |v|^n \quad (2.2)$$

In Eq. (2.2), parameters A , β and γ govern the scale and general shape of the hysteresis loop, whereas the smoothness of the force-deformation curve is determined by the parameter n . It is noticed that D_y is the measure of the yielding level if the hysteresis loop is not bilinear. In this case, however, D_y can be chosen as a large number such that $|v| \leq 1$ as will be described later.

The hysteretic model given by Eqs. (2.1) and (2.2) is phenomenological in nature; however, it does provide an explicit mathematical expression with many parameters flexible enough to reflect various hysteretic behaviors of inelastic systems. Likewise, Eq. (2.2) appears to be capable of describing the hysteretic behaviors of different base isolation systems, such as rubber bearings and sliding systems, which are the main concern of this study.

2.2 Equations of Motion

For simplicity, consider a base-isolated one-dimensional inelastic building

implemented by a hybrid control system as shown in Fig. 2.1(a). The structure system is idealized by an n-degree-of-freedom system and subjected to a one-dimensional earthquake ground acceleration $\ddot{X}_0(t)$. Let $x_i(t)$ be the relative displacement between the i th floor and the $(i-1)$ th floor, i.e., the deformation of the i th story unit. The stiffness restoring force, $F_{s_i}(t)$, of the i th story unit is given by

$$F_{s_i}(t) = \alpha_i k_i x_i + (1 - \alpha_i) k_i D_{y_i} v_i \quad (2.3)$$

in which the subscript i represents the quantity associated with the i th story unit and

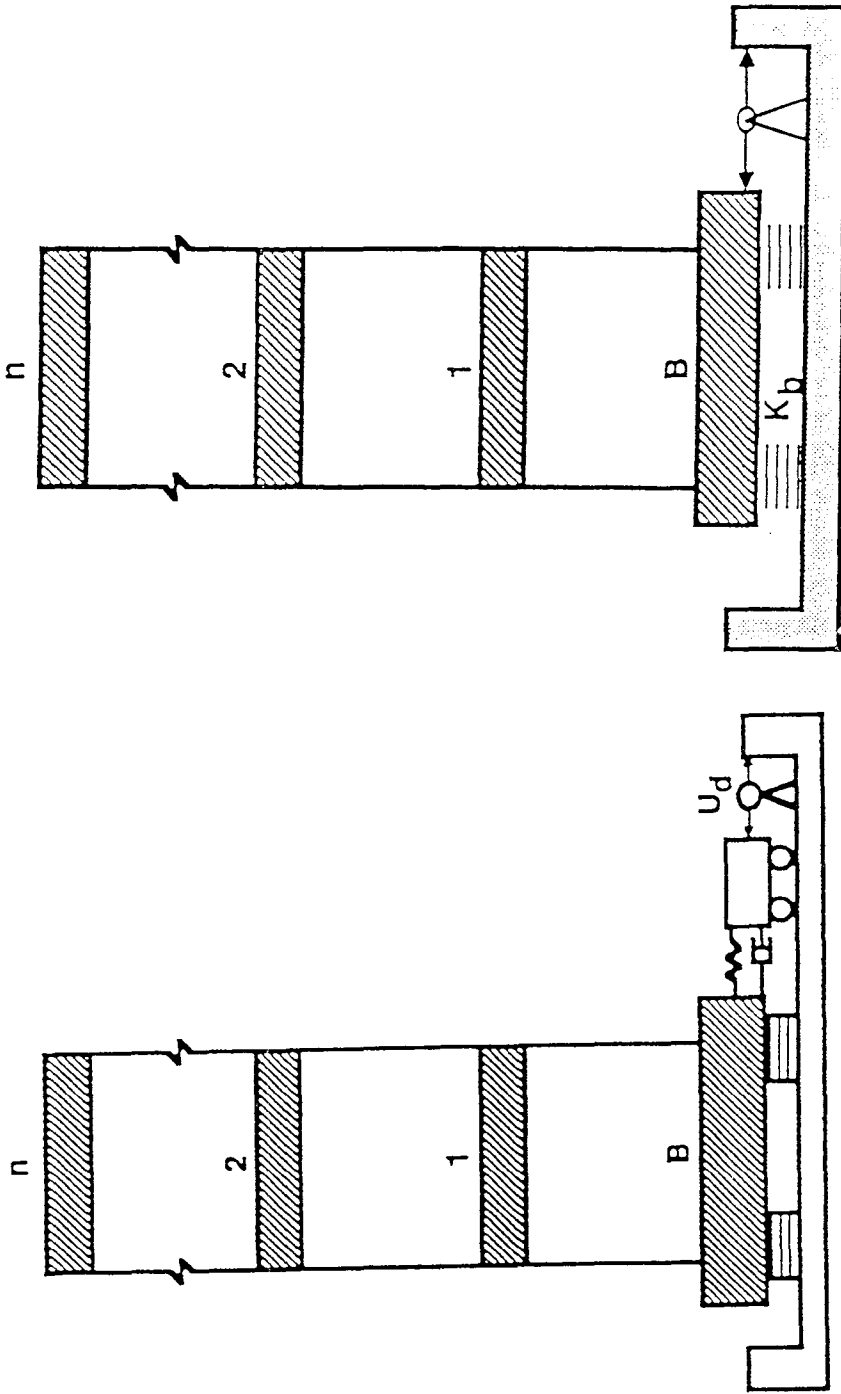
$$D_{y_i} \dot{v}_i = A_i \dot{x}_i - \beta_i |\dot{x}_i| |v_i|^{n_i-1} v_i - \gamma_i \dot{x}_i |v_i|^{n_i} \quad (2.4)$$

The matrix equation of motion of the entire building system can be expressed as follows

$$\underline{M} \ddot{\underline{X}}(t) + \underline{C} \dot{\underline{X}}(t) + \underline{K}_e \underline{X}(t) + \underline{K}_I \underline{V}(t) = \underline{H} \underline{U}(t) + \underline{F} \ddot{X}_0(t) \quad (2.5)$$

in which a linear viscous damping model has been assumed, $\underline{X}(t)=[x_1, x_2, \dots, x_n]'$ = an n vector denoting the deformation of each story unit, and $\underline{V}(t)=[v_1, v_2, \dots, v_n]'$ = an n vector denoting the hysteretic variable of each story unit. For the notations above, an under bar denotes a vector or a matrix and a prime indicates the transpose of a vector or a matrix.

In Eq. (2.5), \underline{M} is an $(n \times n)$ mass matrix with the i - j th element $M(i,j)=m_i$ for $i=1,2,\dots,n$ and $j=1,2,\dots,i$ and $M(i,j)=0$ for $j>i$, where m_i is the mass of the i th floor, \underline{C} is an $(n \times n)$ band-limited damping matrix with all elements equal to zero except $C(i,i)=c_i$ for $i=1,2,\dots,n$ and $C(i,i+1)=-c_{i+1}$ for $i=1,2,\dots,n-1$, where c_i is the damping coefficient of the i th story unit. \underline{K}_e and \underline{K}_I are $(n \times n)$ band-limited elastic stiffness matrix and hysteretic stiffness matrix, respectively. All elements of \underline{K}_e and \underline{K}_I are zero except $K_e(i,i)=\alpha_i k_i$, $K_I(i,i)=(1-\alpha_i)k_i D_{y_i}$ for $i=1,2,\dots,n$ and $K_e(i,i+1)=-\alpha_{i+1} k_{i+1}$, $K_I(i,i+1)=- (1-\alpha_{i+1})k_{i+1} D_{y_{i+1}}$ for $i=1,2,\dots,n-1$. \underline{H} is an $(n \times r)$ matrix denoting the location of r controllers and \underline{F} is an n vector denoting the influence of the earthquake ground acceleration. The matrices \underline{M} , \underline{C} , \underline{K}_e and \underline{K}_I described above hold when the base-isolated



(a) (b)

FIGURE 2.1 : Structural Model of a Multi-Story Building Equipped with Aseismic Hybrid Control Systems : (a) Rubber Bearing Isolation System and Active Mass Damper; (b) Base Sliding Isolation System and Actuator

building is connected to an actuator as shown in Fig. 2.1(b). These matrices should be modified appropriately when the base-isolated building is connected to an active mass damper.

From Eq. (2.4), the vector \underline{V} appearing in Eq. (2.5) is given by

$$\dot{\underline{V}} = f(\dot{\underline{X}}, \underline{V}) \quad (2.6)$$

in which the i th element of $\dot{\underline{V}}$ or $f(\dot{\underline{X}}, \underline{V})$, denoted by \dot{v}_i or $f_i(\dot{x}_i, v_i)$, is given by

$$\dot{v}_i = f_i(\dot{x}_i, v_i) = D_{yi}^{-1} \left[A_i \dot{x}_i - \beta_i |\dot{x}_i| |v_i|^{n_i-1} v_i - \gamma_i \dot{x}_i |v_i|^{n_i} \right] \quad (2.7)$$

By introducing a $3n$ state vector $\tilde{\underline{Z}}(t)$,

$$\tilde{\underline{Z}}(t) = \begin{bmatrix} \underline{X} \\ \underline{V} \\ \dot{\underline{X}} \end{bmatrix} \quad (2.8)$$

the second-order nonlinear matrix equation of motion, Eq. (2.5), can be converted into a first order matrix equation as follows:

$$\dot{\tilde{\underline{Z}}}(t) = \underline{g}[\tilde{\underline{Z}}(t)] + \underline{B}\underline{U}(t) + \underline{W}_1 \ddot{\underline{X}}_0(t) \quad (2.9)$$

in which \underline{B} and \underline{W}_1 are $3n$ vectors

$$\underline{B} = \begin{bmatrix} \underline{0} \\ \underline{0} \\ \underline{M}^{-1} \underline{H} \end{bmatrix} \quad ; \quad \underline{W}_1 = \begin{bmatrix} \underline{0} \\ \underline{0} \\ \underline{M}^{-1} \underline{E} \end{bmatrix} \quad (2.10)$$

and $\underline{g}[\tilde{\underline{Z}}(t)]$ is a $3n$ vector consisting of nonlinear functions of components of the vector $\tilde{\underline{Z}}(t)$,

$$\underline{g}[\tilde{\underline{Z}}(t)] = \begin{bmatrix} \dot{\underline{X}} \\ \text{-----} \\ f(\dot{\underline{X}}, \underline{V}) \\ \text{-----} \\ -\underline{M}^{-1}(\underline{C} \dot{\underline{X}} + \underline{K}_e \underline{X} + \underline{K}_l \underline{V}) \end{bmatrix} \quad (2.11)$$

The first-order nonlinear matrix equation, Eq. (2.9), can be solved step-by-step

numerically using the Fourth-Order Runge-Kutta method as follows [Ref.29]:

$$\tilde{\mathbf{Z}}(t) = \tilde{\mathbf{Z}}(t - 2\Delta t) + \frac{1}{6} [\mathbf{A}_0 + 2\mathbf{A}_1 + 2\mathbf{A}_2 + \mathbf{A}_3] \quad (2.12)$$

in which Δt is the integration time step, and \mathbf{A}_0 , \mathbf{A}_1 , \mathbf{A}_2 , and \mathbf{A}_3 are $3n$ vectors

$$\begin{aligned} \mathbf{A}_0 &= 2\Delta t \{ \mathbf{g}[\tilde{\mathbf{Z}}(t - 2\Delta t)] + \mathbf{B} \mathbf{U}(t - 2\Delta t) + \mathbf{W}_1 \ddot{\mathbf{X}}_0(t - 2\Delta t) \} \\ \mathbf{A}_1 &= 2\Delta t \{ \mathbf{g}[\tilde{\mathbf{Z}}(t - 2\Delta t) + 0.5\mathbf{A}_0] + \mathbf{B} \mathbf{U}(t - \Delta t) + \mathbf{W}_1 \ddot{\mathbf{X}}_0(t - \Delta t) \} \\ \mathbf{A}_2 &= 2\Delta t \{ \mathbf{g}[\tilde{\mathbf{Z}}(t - 2\Delta t) + 0.5\mathbf{A}_1] + \mathbf{B} \mathbf{U}(t - \Delta t) + \mathbf{W}_1 \ddot{\mathbf{X}}_0(t - \Delta t) \} \\ \mathbf{A}_3 &= 2\Delta t \{ \mathbf{g}[\tilde{\mathbf{Z}}(t - 2\Delta t) + \mathbf{A}_2] + \mathbf{B} \mathbf{U}(t) + \mathbf{W}_1 \ddot{\mathbf{X}}_0(t) \} \end{aligned} \quad (2.13)$$

As observed from Eq. (2.13), \mathbf{A}_0 , \mathbf{A}_1 , \mathbf{A}_2 , \mathbf{A}_3 are functions of $t-2\Delta t$, $t-\Delta t$ and t . For simplicity of presentation, the arguments, $t-2\Delta t$, $t-\Delta t$ and t , have been omitted.

To simplify the mathematical operation, it is desirable to group all vectors in Eq. (2.12), which are functions of $\tau < t$, into one term, denoted by $\mathbf{D}(t-2\Delta t, t-\Delta t)$, as follows:

$$\begin{aligned} \mathbf{D}(t - 2\Delta t, t - \Delta t) &= \tilde{\mathbf{Z}}(t - 2\Delta t) + \frac{1}{3} \Delta t \{ \mathbf{g}[\tilde{\mathbf{Z}}(t - 2\Delta t)] + \mathbf{B} \mathbf{U}(t - 2\Delta t) \\ &\quad + \mathbf{W}_1 \ddot{\mathbf{X}}_0(t - 2\Delta t) + 2 \mathbf{g}[\tilde{\mathbf{Z}}(t - 2\Delta t) + 0.5\mathbf{A}_0] + 4 \mathbf{B} \mathbf{U}(t - \Delta t) \\ &\quad + 4 \mathbf{W}_1 \ddot{\mathbf{X}}_0(t - \Delta t) + 2 \mathbf{g}[\tilde{\mathbf{Z}}(t - 2\Delta t) + 0.5\mathbf{A}_1] + \mathbf{g}[\tilde{\mathbf{Z}}(t - 2\Delta t) + \mathbf{A}_2] \} \end{aligned} \quad (2.14)$$

Then, Eq. (2.12) can be expressed as

$$\tilde{\mathbf{Z}}(t) = \mathbf{D}(t - 2\Delta t, t - \Delta t) + \frac{\Delta t}{3} [\mathbf{B} \mathbf{U}(t) + \mathbf{W}_1 \ddot{\mathbf{X}}_0(t)] \quad (2.15)$$

It is mentioned that for the regular Fourth-Order Runge-Kutta method, the integration time step is $\Delta\tau$ that is twice of Δt used in Eqs. (2.12)-(2.15), i.e., $\Delta\tau = 2\Delta t$ or $\Delta t = \Delta\tau/2$. In other words, the integration step size Δt used in the current numerical scheme is one-half of that used in the regular Fourth-Order Runge-Kutta method.

As observed from Eqs. (2.6), (2.7) and (2.11), the \mathbf{g} vector is a function of \mathbf{X} , \mathbf{V} and $\ddot{\mathbf{X}}$ which are elements of the vector $\tilde{\mathbf{Z}}$. Thus, the \mathbf{g} vector can be expressed as a

function of the response state vector $\tilde{\mathbf{Z}}$, i.e., $\mathbf{g} = \mathbf{g}(\tilde{\mathbf{Z}})$. To evaluate $\mathbf{g}(\tilde{\mathbf{Z}})$, the argument vector $\tilde{\mathbf{Z}} = [\mathbf{X}', \mathbf{V}', \dot{\mathbf{X}}']'$ is computed first and then its components, \mathbf{X} , \mathbf{V} and $\dot{\mathbf{X}}$, are substituted into the right hand side of Eq. (2.11). For the $\mathbf{g}[\tilde{\mathbf{Z}}(t-2\Delta t) + 0.5 \mathbf{A}_1]$ vector appearing in Eq. (2.14), the argument vector (3n-dimensional), denoted by $\underline{\mathbf{S}}$,

$$\underline{\mathbf{S}} = \tilde{\mathbf{Z}}(t - 2\Delta t) + 0.5\mathbf{A}_1 \quad (2.16)$$

is computed first from Eq. (2.16). Then, $\underline{\mathbf{S}}$ is partitioned in the same form as the vector $\tilde{\mathbf{Z}}$, i.e., $\underline{\mathbf{S}} = [\underline{\mathbf{S}}_1', \underline{\mathbf{S}}_2', \underline{\mathbf{S}}_3']'$, where $\underline{\mathbf{S}}_1$, $\underline{\mathbf{S}}_2$ and $\underline{\mathbf{S}}_3$ are n-dimensional vectors. Finally, the $\mathbf{g}[\tilde{\mathbf{Z}}(t-2\Delta t) + 0.5 \mathbf{A}_1]$ vector is obtained from Eq. (2.11) by replacing \mathbf{X} , \mathbf{V} and $\dot{\mathbf{X}}$, respectively, by $\underline{\mathbf{S}}_1$, $\underline{\mathbf{S}}_2$ and $\underline{\mathbf{S}}_3$. Likewise, the other two vectors $\mathbf{g}[\tilde{\mathbf{Z}}(t-2\Delta t) + 0.5 \mathbf{A}_0]$ and $\mathbf{g}[\tilde{\mathbf{Z}}(t-2\Delta t) + \mathbf{A}_2]$ appearing in Eq. (2.14) are similarly defined.

2.3 Instantaneous Optimal Control

The instantaneous optimal control algorithm proposed by Yang, et al for linear structures [19-20] was extended later to nonlinear structures [21,28-29]. It is used herein for applications to control of inelastic systems.

The time dependent quadratic objective function $J(t)$ is given as follows

$$J(t) = \dot{\tilde{\mathbf{Z}}}'(t) \mathbf{Q} \dot{\tilde{\mathbf{Z}}}(t) + \mathbf{U}'(t) \mathbf{R} \mathbf{U}(t) \quad (2.17)$$

in which \mathbf{Q} and \mathbf{R} are (3n x 3n) and (rxr) weighting matrices, respectively, representing the relative importance of the response vector $\tilde{\mathbf{Z}}(t)$ and the control vector $\mathbf{U}(t)$. The optimal control vector obtained by minimizing the time-dependent objective function, $J(t)$, is referred to as the instantaneous optimal control algorithm [e.g., 16,19-22].

To minimize the objective function, Eq. (2.17), subjected to the constraint given by Eq. (2.15), the Hamiltonian H is constructed by introducing a 3n-dimensional Lagrangian multiplier vector $\underline{\lambda}(t)$

$$H = \tilde{\mathbf{Z}}'(t) \mathbf{Q} \tilde{\mathbf{Z}}(t) + \mathbf{U}'(t) \mathbf{R} \mathbf{U}(t) + \lambda'(t) \{ \tilde{\mathbf{Z}}(t) - \mathbf{D}(t - 2\Delta t, t - \Delta t) - \frac{\Delta t}{3} [\mathbf{B} \mathbf{U}(t) + \mathbf{W}_1 \ddot{\mathbf{X}}_0(t)] \} \quad (2.18)$$

The necessary conditions for minimizing $J(t)$, subjected to the constraint of Eq. (2.15), are

$$\frac{\partial H}{\partial \tilde{\mathbf{Z}}} = 0, \quad \frac{\partial H}{\partial \mathbf{U}} = 0, \quad \frac{\partial H}{\partial \lambda} = 0 \quad (2.19)$$

Substituting Eq. (2.18) into Eq. (2.19), one obtains the optimal control vector $\mathbf{U}(t)$ in the following manner: (i) when the control vector $\mathbf{U}(t)$ is assumed to be regulated by the response state vector $\tilde{\mathbf{Z}}(t)$, the instantaneous optimal closed-loop (feedback) control algorithm is obtained

$$\mathbf{U}(t) = - \frac{\Delta t}{3} \mathbf{R}^{-1} \mathbf{B}' \mathbf{Q} \tilde{\mathbf{Z}}(t) \quad (2.20)$$

(ii) when the control vector $\mathbf{U}(t)$ is regulated by the measurement of the earthquake ground acceleration $\ddot{\mathbf{X}}_0(t)$ without a feedback response state vector $\tilde{\mathbf{Z}}(t)$, the instantaneous optimal open-loop (feedforward) control algorithm is obtained, and (iii) the instantaneous optimal closed-open-loop (feedback and feedforward) control algorithm is obtained by assuming that the control vector $\mathbf{U}(t)$ is regulated by the measurements of both the response state vector $\tilde{\mathbf{Z}}(t)$ and the earthquake ground acceleration $\ddot{\mathbf{X}}_0(t)$ [see Ref. 29]. Although the control operations for the three optimal algorithms are different, the resulting state vector $\tilde{\mathbf{Z}}(t)$ and control vector $\mathbf{U}(t)$ remain the same under ideal control environments.

With the control vector given by Eq. (2.20), the response state vector $\tilde{\mathbf{Z}}(t)$ is obtained by substituting Eq. (2.20) into Eq. (2.15) as follows

$$\tilde{\mathbf{Z}}(t) = \left[\mathbf{I} + \left(\frac{\Delta t}{3} \right)^2 \mathbf{B} \mathbf{R}^{-1} \mathbf{B}' \mathbf{Q} \right]^{-1} \left[\mathbf{D}(t - 2\Delta t, t - \Delta t) + \frac{\Delta t}{3} \mathbf{W}_1 \ddot{\mathbf{X}}_0(t) \right] \quad (2.21)$$

in which \mathbf{I} is a $(3n \times 3n)$ identity matrix.

2.4 Sufficient Condition For Optimal Control

In the original derivations for the instantaneous optimal control algorithms, such as Refs. 19-21,28 and 29, the optimal control vector $\underline{U}(t)$ was obtained from the necessary conditions, such as Eq. (2.19), i.e., $\partial H/\partial \tilde{\underline{Z}}=0$, $\partial H/\partial \underline{U}=0$ and $\partial H/\partial \underline{\lambda}=0$. In fact, the derived optimal control vector $\underline{U}(t)$ also satisfies the sufficient condition of optimality as will be proved in the following.

The sufficient condition for the optimal solution is given by [Ref. 31]

$$\left[\partial \tilde{\underline{Z}}', \partial \underline{U}' \right] \begin{bmatrix} \frac{\partial^2 H}{\partial \tilde{\underline{Z}}^2} & \frac{\partial^2 H}{\partial \tilde{\underline{Z}} \partial \underline{U}} \\ \frac{\partial^2 H}{\partial \underline{U} \partial \tilde{\underline{Z}}} & \frac{\partial^2 H}{\partial \underline{U}^2} \end{bmatrix} \begin{bmatrix} \partial \tilde{\underline{Z}} \\ \partial \underline{U} \end{bmatrix} > 0 \quad (2.22)$$

Taking derivatives of H in Eq. (2.18), one obtains

$$\begin{aligned} \frac{\partial H}{\partial \tilde{\underline{Z}}} &= 2Q\tilde{\underline{Z}} - \underline{\lambda} ; & \frac{\partial H}{\partial \underline{U}} &= 2R\underline{U} - \frac{\Delta t}{3} \underline{B}'\underline{\lambda} \\ \frac{\partial^2 H}{\partial \tilde{\underline{Z}}^2} &= 2Q ; & \frac{\partial^2 H}{\partial \underline{U}^2} &= 2R ; & \frac{\partial^2 H}{\partial \tilde{\underline{Z}} \partial \underline{U}} &= \frac{\partial^2 H}{\partial \underline{U} \partial \tilde{\underline{Z}}} = 0 \end{aligned} \quad (2.23)$$

Substitution of Eq. (2.23) into the left hand side of Eq. (2.22) leads to the following expression

$$2 \left[\partial \tilde{\underline{Z}}', \partial \underline{U}' \right] \begin{bmatrix} Q & 0 \\ 0 & R \end{bmatrix} \begin{bmatrix} \partial \tilde{\underline{Z}} \\ \partial \underline{U} \end{bmatrix} = 2 (\partial \tilde{\underline{Z}}' Q \partial \tilde{\underline{Z}} + \partial \underline{U}' R \partial \underline{U}) > 0 \quad (2.24)$$

Since Q is a positive semi-definite matrix and R is a positive definite matrix, Eq. (2.24) is greater than zero. Thus, the sufficient condition for the optimal solution, Eq. (2.22), is satisfied.

2.5 Estimation of Hysteretic Component Vector \underline{V}

The optimal control vector $\underline{U}(t)$ given by Eq. (2.20) is regulated by the $3n$ response state vector $\tilde{\underline{Z}}(t)=[\underline{X}'(t), \underline{V}'(t), \dot{\underline{X}}'(t)]'$. The displacement and velocity response vectors, $\underline{X}(t)$ and $\dot{\underline{X}}(t)$, are available from measurements using sensors. However, the hysteretic

component vector $\underline{V}(t)=[v_1(t),v_2(t),\dots,v_n(t)]'$ is not measurable and hence it should be estimated. An approach to estimate $v_i(t)$ for $i=1,2,\dots,n$ is by use of a reduced order nonlinear state observer. In the present case, the observer can be constructed easily, since $v_i(t)$ is only a function of the interstory velocity $\dot{x}_i(t)$ as shown in Eq. (2.7). As a result, the estimate of the hysteretic component $v_i(t)$, denoted by $\hat{v}_i(t)$, follows from Eq. (2.7) as

$$\dot{\hat{v}}_i(t) = f_i(\dot{x}_i, \hat{v}_i) = D_{yi}^{-1} \left[A_i \dot{x}_i - \beta_i |\dot{x}_i| |\hat{v}_i|^{n_i-1} \hat{v}_i - \gamma_i \dot{x}_i |\hat{v}_i|^{n_i} \right] \quad (2.25)$$

in which the argument t for $\dot{x}_i(t)$ and $\hat{v}_i(t)$ has been omitted for simplicity and $\dot{x}_i(t)$ is obtained from measurements.

Given the measured $\dot{x}_i(t)$, Eq. (2.25) can be integrated on-line to obtain the estimate $\hat{v}_i(t)$ for $v_i(t)$ without any difficulty. It is mentioned that when the response level is within the elastic limit, the hysteretic component v_i is very closed to the interstory deformation x_i , Eq. (2.1). As in the case of any observer, the accuracy of the estimates $\hat{v}_i(t)$ for $i=1,2,\dots,n$, depends on the accuracy of the hysteretic model representing the behavior of the system as well as the corresponding parameters, such as A_i , β_i , γ_i and n_i . This subject, however, is beyond the scope of this report.

SECTION 3

NUMERICAL EXAMPLE

To illustrate the application of the optimal control algorithm developed in this report for inelastic structural systems, several examples are presented in this section. Emphasis is placed on aseismic hybrid control systems. The same eight-story building that exhibits bilinear elasto-plastic behavior used in Refs. 28 and 29 is considered. The stiffness of each story unit is designed such that yielding occurs simultaneously for each story unit. The properties of the structure are as follows: (i) the mass of each floor is identical with $m_i = m = 345.6$ metric tons; (ii) the preyielding stiffnesses of the eight-story units are k_{i1} ($i=1,2,\dots,8$) = 3.4×10^5 , 3.26×10^5 , 2.85×10^5 , 2.69×10^5 , 2.43×10^5 , 2.07×10^5 , 1.69×10^5 and 1.37×10^5 kN/m, respectively, and the postyielding stiffnesses are $k_{i2} = 0.1 k_{i1}$ for $i=1,2,\dots,8$; and (iii) the viscous damping coefficients for each story unit are $c_i = 490, 467, 410, 386, 348, 298, 243$ and 196 kN.sec/m, respectively. The damping coefficients given above result in a classically damped structure with a damping ratio of 0.38% for the first vibrational mode. The natural frequencies of the unyielded structure are 5.24, 14.0, 22.55, 30.22, 36.89, 43.06, 49.54 and 55.96 rad./sec. The yielding level for each story unit varies with respect to the stiffness; with the results, $D_{yi} = 2.4, 2.3, 2.2, 2.1, 2.0, 1.9, 1.7,$ and 1.5 cm. The bilinear elasto-plastic behavior can be described by the hysteretic model, Eqs. (2.3) and (2.4), with $A_i=1.0$, $\beta_i=0.5$, $n_i=95$ and $\gamma_i=0.5$ for $i=1,2,\dots,8$. A simulated earthquake with a maximum ground acceleration of 0.3g as shown in Fig. 3.1 is used as the input excitation.

With the eight-story bilinear elasto-plastic building structure described above and the earthquake ground acceleration shown in Fig. 3.1, time histories of all the response quantities have been computed. Within 30 seconds of the earthquake episode, the maximum interstory deformation, x_{mi} , and the maximum absolute acceleration of each floor, a_i , are shown in Table 3.1. Other response quantities have been presented in Ref. 29. As observed from Table 3.1, the deformation of the unprotected building is excessive and that yielding takes place in each story unit.

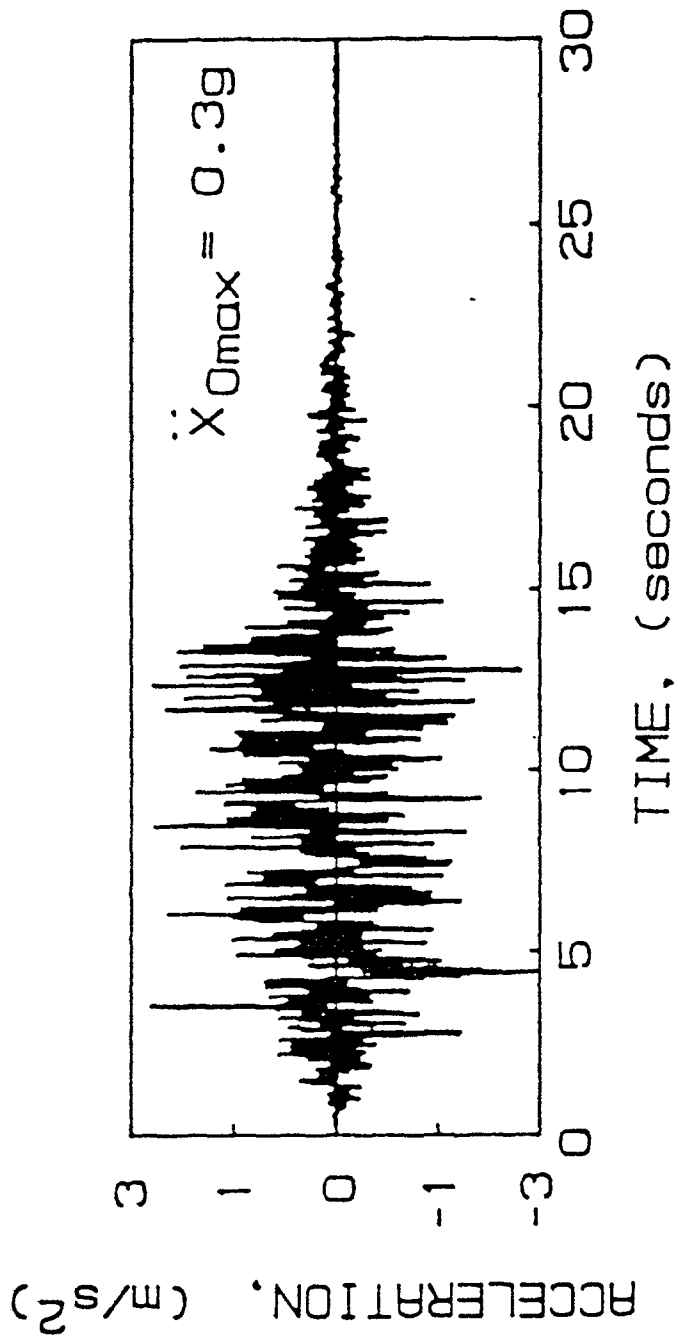


FIGURE 3.1: A Simulated Earthquake Ground Acceleration

TABLE 3.1: Maximum Response Quantities of Building Equipped with Base Isolation System and Active Mass Damper (BIS & AMD) :
 \bar{x}_d =maximum relative displacement of the mass damper; x_{mi} =maximum deformation of i th story unit; a_i =maximum absolute acceleration of i th floor; U_m =maximum active control force

FLOOR NO	without control		with BIS		Full Sensors BIS & AMD				Limited No. of Sensors BIS & AMD			
	x_{mi} (cm)	a_i (cm/s ²)	x_{mi} (cm)	a_i (cm/s ²)	(A) $U_m=225.5$ kN $\bar{x}_d=135$ cm	(B) $U_m=201.5$ kN $\bar{x}_d=110$ cm	(A) $U_m=234.4$ kN $\bar{x}_d=136$ cm	(B) $U_m=196$ kN $\bar{x}_d=110$ cm	(A) x_{mi} (cm)	(A) a_i (cm/s ²)	(B) x_{mi} (cm)	(B) a_i (cm/s ²)
B	-	-	42.70	158	24.80	118	23.2	117	24.21	118	23.3	118
1	2.4	3.05	1.31	155	0.71	112	0.67	112	0.69	112	0.66	111
2	2.3	2.80	1.25	152	0.70	108	0.66	109	0.69	109	0.65	108
3	2.2	3.14	1.28	157	0.73	105	0.69	107	0.72	105	0.68	106
4	2.1	2.95	1.17	164	0.69	94	0.64	98	0.68	94	0.64	97
5	2.0	2.70	1.07	177	0.63	102	0.60	99	0.63	101	0.59	98
6	1.9	2.91	0.97	185	0.59	111	0.54	106	0.59	111	0.54	106
7	1.7	2.90	0.82	198	0.53	121	0.49	116	0.53	119	0.49	117
8	1.5	2.08	0.52	206	0.36	141	0.33	131	0.36	142	0.33	130

(A) = without \bar{V} feedback; (B) = with \bar{V} feedback

Example 1: Building Equipped With Rubber-Bearing Base Isolation System
and Active Mass Damper

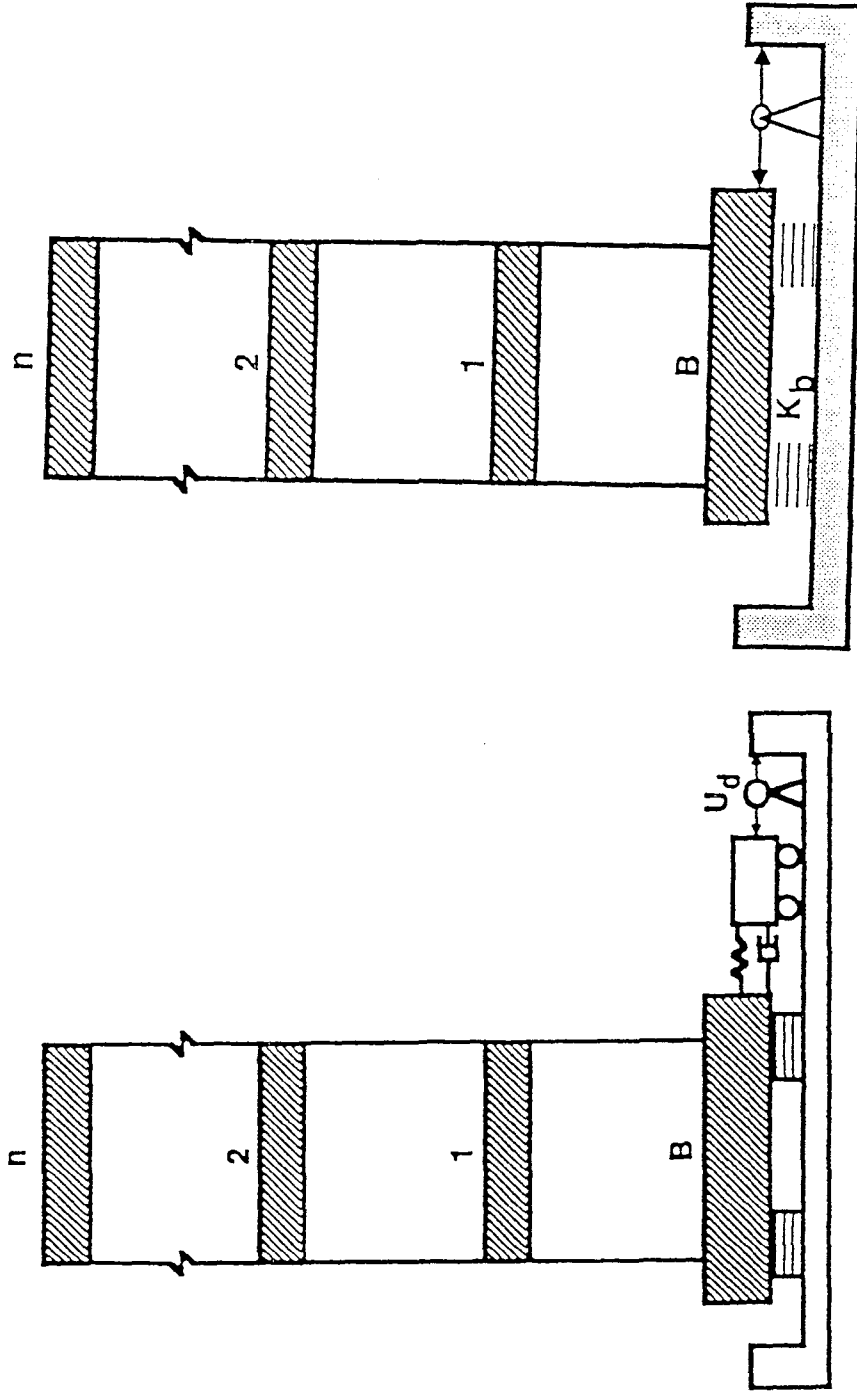
To reduce the structural response, a lead-core rubber-bearing isolation system connected to an active mass damper is implemented as shown in Fig. 3.2(a). The restoring force of the lead-core rubber-bearing system is modeled as

$$F_{sb} = \alpha_b k_b x_b + (1 - \alpha_b) k_b D_{yb} v_b \quad (3.1)$$

in which v_b is given by Eq. (2.4) with $i=b$. The mass of the base isolation system is $m_b=450$ metric tons and the viscous damping coefficient is assumed to be linear with $c_b=26.17$ kN.sec/m. The restoring force of the base isolation system given by Eq. (3.1) is not bilinear elasto-plastic and the parameter values are given as follows: $k_b=18050$ kN/m, $\alpha_b=0.6$ and $D_{yb}=4$ cm. The parameters governing the scale and general shape of the hysteresis loop of the isolation system, Eq. (2.4), were assumed to be $A_b=1.0$, $\beta_b=0.5$, $n_b=3$ and $\gamma_b=0.5$. The hysteretic characteristics of such a base isolation system, i.e., x_b versus v_b , are shown in Fig. 3.3(a). For the building with the base isolation system without an active mass damper, the 9 natural frequencies of the preyielding structure are 2.21, 9.31, 17.29, 25.18, 32.19, 38.29, 44.12, 50.37, and 56.74 rad/sec. The damping ratio for the first vibrational mode is 0.15%. It is observed that the fundamental frequency is reduced significantly by the implementation of the base isolation system. The response vector $\underline{X}(t)$ is given by $\underline{X}=[x_b, x_1, \dots, x_8]'$.

Without an active mass damper, time histories of all the response quantities were computed and presented in Ref. 29. The maximum response quantities of the structure in 30 seconds of the earthquake episode are shown in the column of Table 3.1 designated as "With BIS". As observed from Table 3.1, the interstory deformation and the floor acceleration are drastically reduced. However, the deformation of the base isolation system shown in row B of Table 3.1 may be excessive.

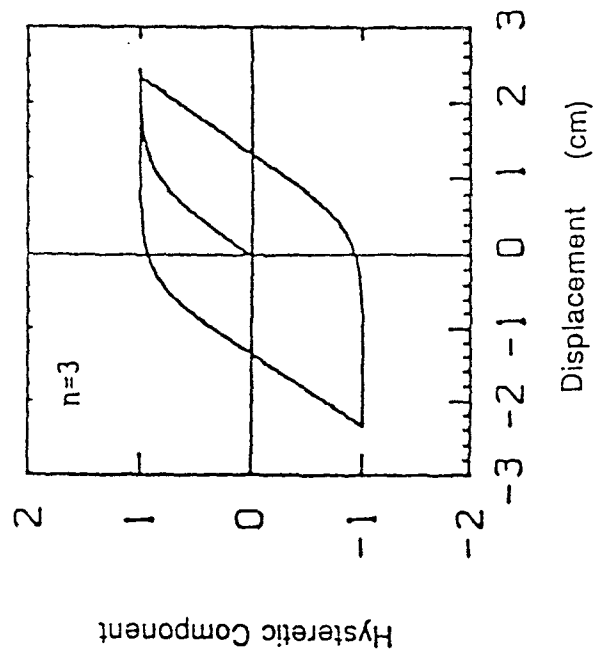
To protect the safety and integrity of the base isolation system, an active mass damper was proposed in Refs. 23-24 to be connected to the base isolation system as shown in Fig. 3.1(a). The properties of the mass damper are as follows. The mass of



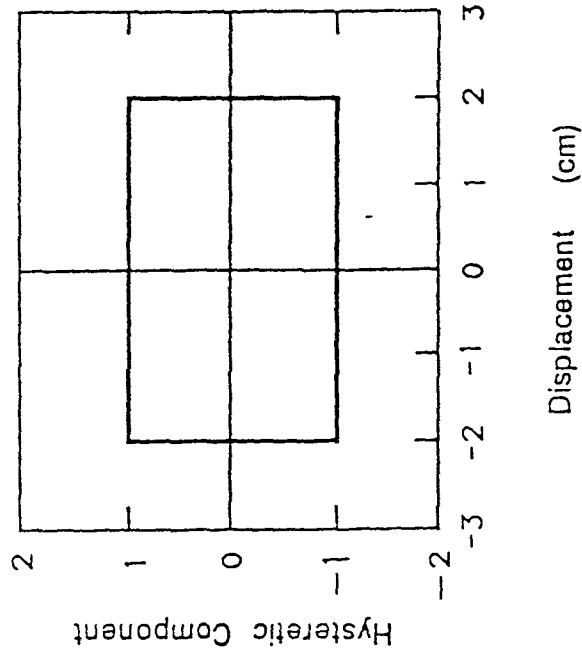
(a)

(b)

FIGURE 3.2: Structural Model of a Multi-Story Building Equipped with Aseismic Hybrid Control Systems : (a) Rubber Bearing Isolation System and Active Mass Damper; (b) Base Sliding Isolation System and Actuator



(a)



(b)

FIGURE 3.3: Hysteretic Characteristics of Base Isolation System :
 (a) Rubber Bearing Isolation System;
 (b) Sliding Isolation System

the mass damper, m_d , is equal to 50% of the floor mass, i.e., $m_d=0.5m_i$ and the natural frequency of the mass damper is the same as the first natural frequency of the base isolated building, i.e. 2.21 rad/sec. The damping ratio of the mass damper is 10%. With the active mass damper, the response vector is given by $\underline{X}(t)=[x_d, x_b, x_1, \dots, x_8]'$ and the structural response depends on the weighting matrices \underline{R} and \underline{Q} . For this example, the weighting matrix \underline{R} consists of only one element, denoted by R_0 , whereas the dimension of the \underline{Q} matrix is (30x30). R_0 is chosen to be 10^{-3} for simplicity. The \underline{Q} matrix is partitioned as follows

$$\underline{Q} = \alpha \begin{bmatrix} \underline{0} & \underline{0} & \underline{0} \\ \underline{Q}_{21} & \underline{Q}_{22} & \underline{Q}_{23} \end{bmatrix} \quad (3.2)$$

in which $\underline{0}$ is a (20x10) matrix with all elements equal to zero, and \underline{Q}_{21} , \underline{Q}_{22} and \underline{Q}_{23} are (10x10) matrices.

Note that \underline{Q} is a symmetric matrix. Because of the fact that there is only one actuator installed on the basement floor as shown in Fig. 3.2(a), only the elements in one row of the \underline{Q} matrix are relevant to the control vector $\underline{U}(t)$, see Eq. (2.20). In the present case, only the elements in the first row of \underline{Q}_{21} , \underline{Q}_{22} and \underline{Q}_{23} matrices are related to the control vector $\underline{U}(t)$. As a result, all elements of the \underline{Q} matrix which have no effect on the control vector $\underline{U}(t)$ are set to be zero for convenience.

It is mentioned that matrices \underline{Q}_{21} , \underline{Q}_{22} and \underline{Q}_{23} are associated with the feedbacks of $\underline{X}(t)$, $\underline{V}(t)$ and $\dot{\underline{X}}(t)$, respectively. For instance, setting all the elements of \underline{Q}_{21} equal to zero, the control vector $\underline{U}(t)$ given by Eq. (2.20) is no longer a function of $\underline{X}(t)$. Hence, the main difference between the current control algorithm and that presented in Refs. 28 and 29 lies in the matrix \underline{Q}_{22} . If all elements of \underline{Q}_{22} are zero, there is no feedback of $\underline{V}(t)$ and the results will be identical to those presented in Refs. 28 and 29.

Consider the case in which there is no feedback of $\underline{V}(t)$, i.e., all elements of \underline{Q}_{22} are zero. Since there is only one actuator, all the elements of \underline{Q}_{21} and \underline{Q}_{23} are set to be zero, except $Q_{21}(1,j)$ and $Q_{23}(1,j)$ for $j=1,2,\dots,10$. For illustrative purpose, the following values are assigned.

$$\begin{aligned} Q_{21}(1,j) &= [102 \quad -2362 \quad -11 \quad -840 \quad -1397 \quad -1649 \quad -1645 \quad -1433 \quad -1057 \quad -561] \\ Q_{23}(1,j) &= [67 \quad 731 \quad 646 \quad 621 \quad 584 \quad 529 \quad 457 \quad 366 \quad 257 \quad 133] \end{aligned} \quad (3.3)$$

and $Q_{21}(i,j)=Q_{23}(i,j)=0$ for $i=2,3,\dots,10$ and $j=1,2,\dots,10$.

Time histories of all the structural response quantities have been computed for $\alpha/R_0=50000$ and $\Delta t=0.375 \times 10^{-2}$. Within 30 seconds of the earthquake episode, the maximum interstory deformations, x_{mi} ($i=B,1,2,\dots,8$), the maximum acceleration of each floor, a_i , the maximum active control force, U_m , and the maximum relative displacement of the mass damper, \bar{x}_d , are summarized in column (A) of Table 3.1 designated as "Full sensors". Time histories of many response quantities were plotted and presented in Ref. 29.

We consider now the case in which the hysteretic component $\underline{V}(t)$ is also a feedback to the control vector $\underline{U}(t)$. In this case, elements of $Q_{21}(1,j)$, $Q_{22}(i,j)$ and $Q_{23}(1,j)$ are assigned in the following for illustrative purposes

$$\begin{aligned} Q_{21}(1,j) &= [102 \quad -3363 \quad -11 \quad 840 \quad 1397 \quad 1649 \quad 1645 \quad 1433 \quad 1057 \quad 561] \\ Q_{22}(1,j) &= [0, \quad -100, \quad 0, \quad 0, \quad 0, \quad 0, \quad 0, \quad 0, \quad 0, \quad 0] \\ Q_{23}(1,j) &= [67 \quad 931 \quad 646 \quad 621 \quad 584 \quad 529 \quad 457 \quad 366 \quad 257 \quad 133] \end{aligned} \quad (3.4)$$

and all other elements are zero. Eq. (3.4) indicates that only the hysteretic component of the base isolation system is used as a feedback.

Within 30 seconds of the earthquake episode, all the maximum response quantities are summarized in column (B) of Table 3.1 designated as "Full sensors" for comparison. It is observed from Table 3.1 that (i) the performance of the present optimal algorithm with an additional feedback of the hysteretic component is slightly better than that of the optimal algorithm without a feedback of the hysteretic component, and (ii) the aseismic hybrid control system using a lead-core rubber bearing isolation system and an active mass damper is very effective in protecting building structures against strong earthquakes.

The base-isolated building tends to behave like a rigid body and the interstory deformation is small compared with that of the base isolation system. As a result,

sensors may not be needed for the building. Consider the case in which displacement and velocity sensors are installed on the active mass damper and the base isolation system only, i.e., no sensor is installed on the building. For the first case in which the hysteretic component $\underline{V}(t)$ is not accounted for in the determination of $\underline{U}(t)$, one has $\underline{Q}_{22}=\underline{0}$. Further, all elements of \underline{Q}_{21} and \underline{Q}_{23} are zero, except $Q_{21}(1,1)$, $Q_{21}(1,2)$, $Q_{23}(1,1)$ and $Q_{23}(1,2)$. For simplicity, the following values are assigned; $Q_{21}(1,1)=102$, $Q_{21}(1,2)=-2363$, $Q_{23}(1,1)=67$ and $Q_{23}(1,2)=731$. The maximum response quantities for $\alpha/R_0=50000$ and $\Delta t=0.375 \times 10^{-2}$ sec. were computed and summarized in column (A) of Table 3.1 under the heading of limited number of sensors.

We next consider the case in which the hysteretic component $\underline{V}(t)$ is used for the determination of $\underline{U}(t)$. In this case, the following elements are assigned: $Q_{21}(1,1)=102$, $Q_{21}(1,2)=-3363$, $Q_{22}(1,1)=0$, $Q_{22}(1,2)=-100$, $Q_{23}(1,1)=67$, and $Q_{23}(1,2)=931$. All other elements of the \underline{Q} matrix are zero. The maximum response quantities for $\alpha/R_0=50,000$ and $\Delta t=0.375 \times 10^{-2}$ sec. are summarized in the last two columns of Table 3.1 designated as "limited number of sensors."

A comparison of the results for the case using a limited number of sensors with those of the case in which sensors are installed on all floors of the building indicates that installations of displacement and velocity sensors on the building are not necessary. This conclusion is very important because it is expensive to install sensors. It is further observed from the last four columns of Table 3.1 that the performance of the present control algorithm is slightly better than that of the previous algorithm without considering the hysteretic component $\underline{V}(t)$ as a feedback.

Example 2: Building Equipped with Rubber Bearing Isolation System and Actuator

Instead of using an active mass damper described above, the base isolation system can be connected directly to an actuator. With such a hybrid control system, the (27×27) \underline{Q} matrix is partitioned as shown in Eq. (3.1), where \underline{Q}_{21} , \underline{Q}_{22} and \underline{Q}_{23} are (9×9) matrices. From the conclusions above, it is not necessary to install sensors on the base-isolated building. Hence, we consider only the case in which displacement and velocity sensors are installed on the base isolation system only, i.e., no sensor is installed on the

building. When $\underline{V}(t)$ is not considered as a feedback for the determination of $\underline{U}(t)$, all elements of Q_{21} , Q_{22} and Q_{23} are zero, except $Q_{21}(1,1)$ and $Q_{23}(1,1)$. For simplicity, the following values are assigned: $Q_{21}(1,1)=0.9$ and $Q_{23}(1,1)=3.4$. The maximum response quantities for $\alpha/R_0=1.55 \times 10^8$ and $\Delta t=0.375 \times 10^{-2}$ sec. are summarized in the columns designated as "BIS&AF¹" of Table 3.2 [Ref. 29].

When $\underline{V}(t)$ is used in the determination of $\underline{U}(t)$, one additional non-zero element from the Q_{22} matrix is assigned. For illustrative purposes, the following values are assigned: $Q_{21}(1,1)=0.1$, $Q_{22}(1,1)=0.5$ and $Q_{23}(1,1)=3.5$, and all other elements of the Q matrix are zero. The maximum response quantities in 30 seconds of the earthquake episode are presented in the columns designated as "BIS&AF²" of Table 3.2 for comparison. It is observed from Table 3.2 that the performance of the present control algorithm is slightly better than that of the previous algorithm without considering the feedback of $\underline{V}(t)$.

Example 3: Building Equipped With Sliding Base Isolation System and Actuator

Instead of using a rubber-bearing base isolation system, a frictional-type sliding base isolation system, as shown schematically in Fig. 3.2(b), is considered for the same eight-story bilinear elasto-plastic building described in Example 1. This type of isolators allows greater resistance to damage by permitting the structure to slide on its foundation during severe earthquakes. This isolation system decouples the structure from its foundation with nearly frictionless teflon on stainless steel sliding plates that have very low frictional resistance.

When the sliding system slides, the frictional force, F_{sb} , developed in the sliding system is given by

$$F_{sb} = \mu \bar{m} g \operatorname{sgn}(\dot{x}) \quad (3.5)$$

in which $\bar{m}g = w$ is the weight of the structural system above the sliding bearings and μ

TABLE 3.2: Maximum Response Quantities of Building Equipped with Base Isolation System and Actuator (Limited No. of Sensors) : x_{mi} =maximum deformation of i th story unit; a_i =maximum absolute acceleration of i th floor; U_m =maximum active control force

FLOOR	Yield Displ	without control		with BIS		BIS & AF ¹		BIS & AF ²	
		x_{mi} (cm)	a_i (cm/s ²)	x_{mi} (cm)	a_i (cm/s ²)	x_{mi} (cm)	a_i (cm/s ²)	x_{mi} (cm)	a_i (cm/s ²)
B	-	-	-	42.70	158	26.11	117	25.83	116
1	2.4	3.05	486	1.31	155	0.86	118	0.85	116
2	2.3	2.80	456	1.25	152	0.82	123	0.81	121
3	2.2	3.14	571	1.28	157	0.83	122	0.82	120
4	2.1	2.95	529	1.17	164	0.74	116	0.72	114
5	2.0	2.70	558	1.07	177	0.66	125	0.65	123
6	1.9	2.91	720	0.97	185	0.58	117	0.57	115
7	1.7	2.90	580	0.82	198	0.48	131	0.47	129
8	1.5	2.08	617	0.52	206	0.33	129	0.32	127

BIS = Base Isolation System; AF¹ = Active Force without Y feedback

AF² = Active Force with Y feedback

is the coefficient of friction. When the sliding system sticks, the frictional force F_{sb} is smaller than the one given by Eq. (3.5). In the dynamic analysis and active control of the sliding system, the highly nonlinear frictional force is represented in this report by the following analytical function

$$F_{sb} = \mu \bar{m} g v_b \quad (3.6)$$

in which v_b is a nondimensional hysteretic quantity described by Eq. (2.4) with $i=b$. It is mentioned that during the sliding phase, v_b takes a value of either 1 or -1. During the sticking phase, the absolute value of v_b is less than unity, i.e., $|v_b| \leq 1$. The conditions of sticking and sliding are accounted for by Eq. (2.4) automatically. The parameters governing the scale and general shape of the hysteresis loop of the sliding system are $A_b=1.0$, $\beta_b=0.5$, $n_b=2$, $\gamma_b=0.5$ and $D_{yb}=0.012\text{cm}$. The hysteresis loop of the hysteretic component of such a sliding system is schematically shown in Fig. 3.3(b). The mass of the sliding system is $m_b=450$ metric tons and the coefficient of friction is $\mu=10\%$. The response vector is given by $\underline{X}=[x_b, x_1, \dots, x_8]'$.

Time histories of all the response quantities were computed. The time history, $x_1(t)$, of the first story deformation and that of the sliding system, $x_b(t)$, were presented in Ref. 29, where $x_b(t)$ denotes the relative displacement of the teflon and the stainless steel plate. Further, the hysteresis loops for the shear force of the sliding system, the first, fourth, and eighth story units were also given in Ref. 29. The maximum response quantities of the structure within 30 seconds of the earthquake episode are shown in Table 3.3 in the columns designated as "With SIS". As observed from Table 3.3, the interstory deformations and floor accelerations are drastically reduced using a sliding type base isolation system. However, the deformation of the eighth story unit is still in the inelastic range. The time history of the deformation of the first story unit, $x_1(t)$, without the base sliding system is shown in Fig. 3.4(a). The corresponding result when the building is equipped with a base sliding system alone is presented in Fig. 3.4(b).

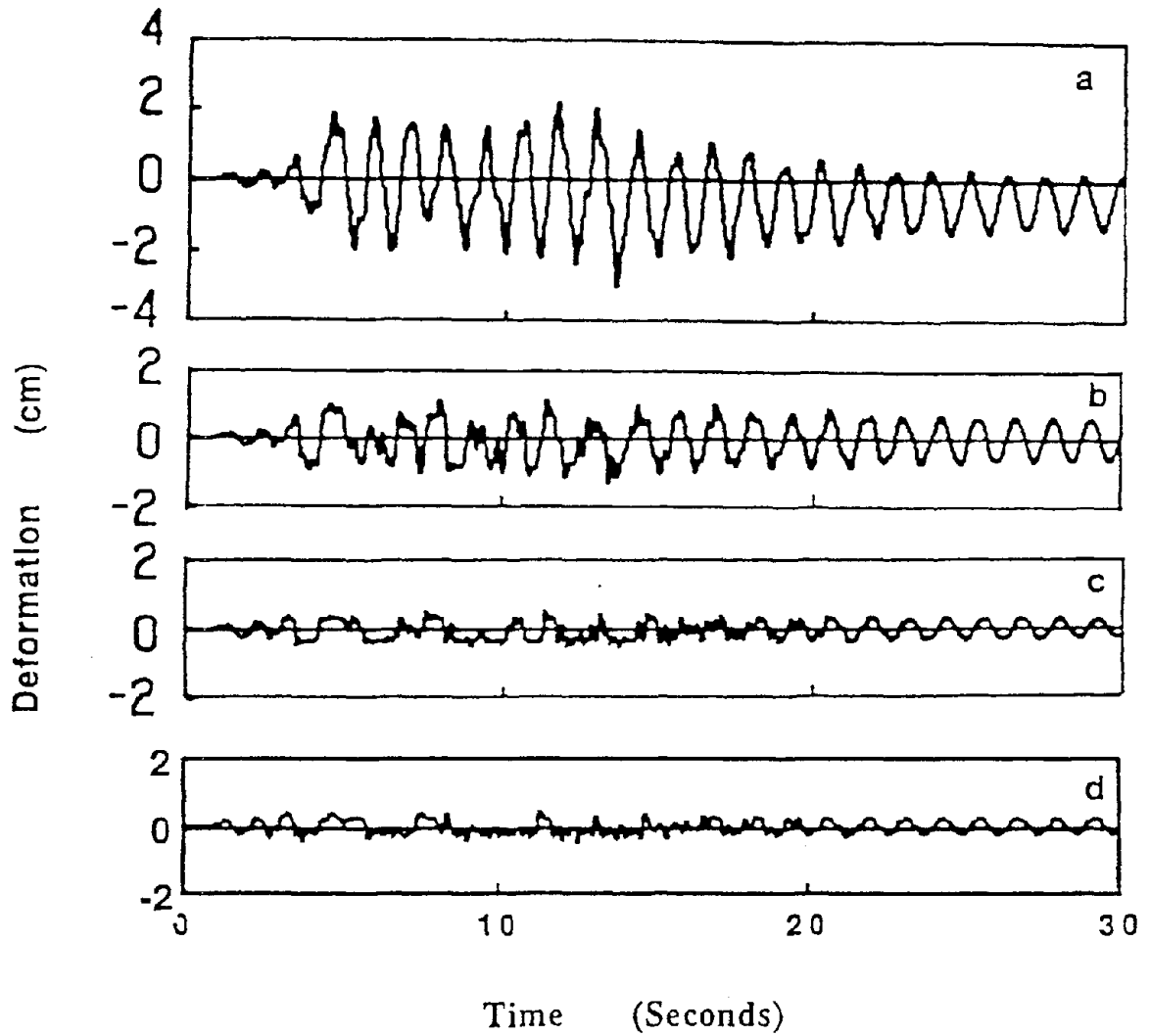


FIGURE 3.4 : Deformation of First-Story Unit : (a) Without Control; (b) With Sliding Isolation System; (c) With Sliding Isolation System and Actuator without \underline{V} feedback; (d) With Sliding Isolation System and Actuator with \underline{V} feedback

TABLE 3.3 : Maximum Response Quantities of Building Equipped with Sliding Isolation System and Actuator (SIS & AF) : x_{mi} =maximum deformation of i th story unit; a_i =maximum absolute acceleration of i th floor; U_m =maximum active control force

FLOOR	Yield Displ D_{yi} (cm)	without control		with SIS		(A) $U_m=3074.7\text{kN}$		(B) $U_m=2321.3\text{kN}$	
		x_{mi} (cm)	a_i (cm/s^2)	x_{mi} (cm)	a_i (cm/s^2)	x_{mi} (cm)	a_i (cm/s^2)	x_{mi} (cm)	a_i (cm/s^2)
B	-	-	-	11.54	658	18.13	688	44.86	380.
1	2.4	3.05	486	1.30	370	0.56	325	0.50	214
2	2.3	2.80	456	1.23	547	0.76	342	0.50	239
3	2.2	3.14	571	1.38	531	0.91	379	0.56	230
4	2.1	2.95	529	1.40	404	0.83	300	0.68	217
5	2.0	2.70	558	1.50	424	0.89	379	0.78	242
6	1.9	2.91	720	1.72	462	1.00	412	0.74	298
7	1.7	2.90	580	1.82	541	1.09	341	0.93	218
8	1.5	2.08	617	1.64	601	0.99	391	0.87	344

(A) = without V feedback; (B) = with V feedback

To further reduce the structural response and to bring the deformation of the 8th story unit into the elastic range, an actuator is connected to the sliding system as shown in Fig. 3.2(b). The actuator will apply the active control force directly on the sliding system. The basic idea of the active force, in this case, is to counteract the frictional force in order to maintain the system in the sliding condition as much as possible, so that the transmission of the earthquake ground motion to the building can be kept to a minimum.

With the active control force, the structural response depends on the weighting matrices \underline{R} and \underline{Q} . Again, the weighting matrix \underline{R} consists of only one element, denoted by R_0 , whereas the dimension of the \underline{Q} matrix is (27x27). R_0 is chosen to be 10^{-3} for simplicity and the \underline{Q} matrix is partitioned as shown in Eq. (3.2), where \underline{Q}_{21} , \underline{Q}_{22} and \underline{Q}_{23} are (9x9) matrices and \underline{Q} is a (18x9) zero matrix.

First, consider the case in which the hysteretic component vector \underline{V} is not a feedback quantity for the determination of the control vector $\underline{U}(t)$. In this case, all the elements of the \underline{Q}_{22} matrix are zero, i.e., $\underline{Q}_{22} = \underline{0}$. Note that the deformation of the building is in-phase with the frictional force and the velocity of the building is out of phase of the frictional force. As a result, we set $\underline{Q}_{23} = \underline{0}$. As described in Part I, for the base-isolated building connected to an actuator, the control force $\underline{U}(t)$ depends on the difference between the first two rows of the \underline{Q}_{21} and \underline{Q}_{22} matrices, i.e., $Q_{21}(1,j) - Q_{21}(2,j)$ and $Q_{22}(1,j) - Q_{22}(2,j)$. For simplicity, elements of $Q_{21}(2,j)$ and $Q_{22}(2,j)$ rows will be assigned to be zero. The elements of $Q_{21}(1,j)$ are assigned in the following for illustrative purposes:

$$Q_{21}(1,j) = [0, -30000, -3000, -300, -30, -3, -0.3, -0.03, -0.003] \quad (3.7)$$

All other elements of the \underline{Q}_{21} matrix are set to be zero.

Time histories of all the structural response quantities were computed for $\alpha/R_0 = 2.25 \times 10^8$ and $\Delta t = 0.03 \times 10^{-2}$ sec. Time histories of the deformations of the sliding system and the first story unit as well as that of the required active control force were shown in Ref. 29. Hysteresis loops for the sliding system were also plotted in Ref. 29. Within 30 seconds of the earthquake episode, the maximum interstory deformations,

Within 30 seconds of the earthquake episode, the maximum interstory deformations, $x_{mi}(i=b,1,2,\dots,8)$, the maximum floor acceleration, a_i , and the maximum active control force, U_m , are summarized in the column (A) of Table 3.3. The time history of the deformation of the first story unit, $x_1(t)$, is shown in Fig. 3.4(c).

Secondly, the hysteretic component vector \underline{V} is used for the feedback to determine the control vector $\underline{U}(t)$ and hence $\underline{Q}_{22} \neq \underline{0}$. Recall that the basic idea of installing an actuator is to overcome the frictional force in the sliding system in order to minimize the sticking phase of the motion during earthquakes. In other words, the active control force is intended to keep the sliding phase of the motion as much as possible. It is observed from Eq. (3.6) that the frictional force is proportional to v_b of the sliding system. Hence, a feedback of v_b will be sufficient to reduce the frictional force. Consequently, all elements of the \underline{Q}_{21} and \underline{Q}_{23} matrices are set to be zero. Further, since v_b of the sliding system is reflected only by the element $Q_{22}(1,1)$, all elements of the \underline{Q}_{22} matrix are also set to be zero except $Q_{22}(1,1)$ that is chosen to be -10.258, i.e. $Q_{22}(1,1) = -10.258$.

Within 30 seconds of the earthquake episode, the maximum response quantities for $\alpha/R_0=3.39 \times 10^9$ and $\Delta t=0.03 \times 10^{-2}$ sec. are summarized in the columns (B) of Table 3.3 for comparison. The time history of the deformation of the first story unit, $x_1(t)$, is presented in Fig. 3.4(d). It is observed from Table 3.3 and Fig. 3.4 that (i) the performance of the present optimal algorithm with \underline{V} feedback is superior to that of the optimal algorithm without considering \underline{V} feedback, and (ii) the hybrid control system consisting of a frictional-type sliding system and actuators is quite effective, although the required maximum active control force is large.

SECTION 4

CONCLUSIONS

Optimal control for nonlinear and inelastic structural systems has been formulated incorporating the specific hysteretic model of the system. This is accomplished by including the hysteretic components of the structural system in the equations of motion which serve as constraints in the optimization process. The resulting control vector is obtained as a function of the deformations, velocities and hysteretic components of the structural system. The hysteretic components of the structural response can be estimated easily from a simple observer using the measured structural response quantities.

In this report, the optimal control vector has been shown to satisfy not only the necessary conditions but also the sufficient condition of optimality. Specific applications of the optimal algorithm to two types of aseismic hybrid control systems have been demonstrated. These include (i) a lead-core rubber bearing isolation system connected to either an actuator or an active mass damper, and (ii) a frictional-type base sliding isolation system connected to an actuator. Numerical results indicate that (i) the performance of the present optimal algorithm is better than that of the algorithm without considering the feedback of hysteretic components of the structural response, (ii) the present optimal algorithm is simple for on-line operations and practical applications, (iii) the two types of aseismic hybrid control systems considered are effective for practical applications, and (iv) for active control of base-isolated buildings, the installation of sensors on the building is not necessary.

SECTION 5

REFERENCES

1. Baber, T.T., and Wen, Y.K. (1981), "Random Vibration of Hysteretic Degrading Systems", Journal of Engineering Mechanics Division, ASCE, Vol. 107, No. EM6, pp. 1069-1987.
2. Bouc, R. (1967), "Forced Vibration of Mechanical Systems With Hysteresis, abstract", Proceedings of 4th Conference on Nonlinear Oscillation, Prague, Czechoslovakia.
3. Chong, K.P., Liu, S.C., and Li, J.C., Editors, Intelligent Structures (1990). Elsevier Applied Science, London and New York.
4. Constantinou, M.C., and Papageorgiou, A.S. (1990), "Stochastic Response of Practical Sliding Isolation System", Probabilistic Engineering Mechanics, Vol. 5, No. 1, pp. 27-34.
5. Contantinou, M.C., Mokha, A., and Reinhorn, A. (1990), "Teflon Bearings in Base Isolation. II: Modeling", Journal of Structural Engineering, ASCE, Vol. 116, No. 2, February, pp. 455-474.
6. Constantinou, M.C., and Tadjbakhsh, I.G. (1984), "Response of a Sliding Structures to Filtered Random Excitation", Journal of Structural Mechanics, Vol. 12, pp. 401-418.
7. Fan, F.G., Ahmadi, G., and Tadjbakhsh, I.G. (1988), "Base Isolation of a Multi-Story Building Under a Harmonic Ground Motion - A Comparison of Performances of Various Systems", National Center for Earthquake Engineering Research, Technical Report NCEER-88-0010, SUNY, Buffalo.
8. Gueraud, R., Noel-Leroux, J.P., Livolant, M., and Michalopoulos, A.P.(1985), "Seismic Isolation Using Sliding-Elastomer Bearing Pads", Nuclear Engineering and Design, Vol 84. pp. 363-377.
9. Housner, G.W. and Masri, S. (1990), Editors, Proceedings of U.S. National Workshop on Structural Control Research, October, USC publication no. CE-9013.
10. Kelly, J.M., and Beuckle, K.E. (1983), "A Friction Damped Base Isolation System with Failsafe Characteristics", Earthquake Engineering and Structural Dynamics, Vol. 11, pp. 33-56.

11. Li, Z., Katukura, H., and Izumi, M. (1991), "Synthesis and Extension of One-Dimensional Nonlinear Hysteretic Models", J. Engineering Mechanics, ASCE, Vol 117, No. 1, pp. 100-109.
12. Mokha, A., Constantinou, M., and Reinhorn, A. (1990), "Teflon Bearings in Base Isolation. I: Testing", Journal of Structural Engineering, ASCE, Vol. 116, No. 2, February, pp. 438-454.
13. Mokha, A., Constantinou, M., and Reinhorn, A. (1988), "Teflon Bearings in Aseismic Base Isolation: Experimental Studies and Mathematical Modeling", Technical Report NCEER-88-0038, SUNY, Buffalo, NY.
14. Mostaghel, N. and Khoaversian, M. (1987), "Dynamics of Resilient-Friction Base Isolator (R-FBI)", Earthquake Engineering and Structural Dynamics, Vol. 15, pp. 379-390.
15. Park, Y.J., Wen, Y.K., and Ang, A.H-S. (1986), "Two Dimensional Random Vibration of Hysteretic Structures", Journal of Earthquake Engineering and Structural Dynamics, Vol. 14, pp. 543-557.
16. Soong, T.T. (1990), Active Structural Control: Theory and Practice, Longman Scientific and Technical, New York.
17. Su, L., Ahmadi, G., and Tadjbakhsh, I.G. (1987), "A Comparative Study of Performance of Various Base Isolation Systems Part I: Shear Beam Structures", Report No. MIE-153, Clarkson University, October.
18. Wen, Y.K. (1989), "Methods of Random Vibration for Inelastic Structures", Journal of Applied Mechanics Reviews, Vol. 42, No. 2, February, pp. 39-52.
19. Yang, J.N., Akbarpour, A., and Ghaemmaghami, P. (1987) "New Optimal Control Algorithms for Structural Control", Journal of Engineering Mechanics, ASCE, Vol. 113, No. 9, June, pp. 1369-1386.
20. Yang, J.N., Akbarpour, A., and Ghaemmaghami, P. (1987) "Instantaneous Optimal Control Laws For Building Structures Under Earthquake Excitations", National Center for Earthquake Engineering Research, Technical Report NCEER-TR-87-0007, SUNY, Buffalo.
21. Yang, J.N., Long, F.X., and Wong, D. (1988) "Optimal Control of Nonlinear Structures", Journal of Applied Mechanics, ASME, Vol. 55, December, pp. 931-938.

22. Yang, J.N., and Soong, T.T. (1988) "Recent Advancement in Active Control of Civil Engineering Structures", Journal of Probabilistic Engineering Mechanics, Vol. 3, No. 4, December, pp. 179-188.
23. Yang, J.N., Danielians, A. and Liu, S.C. (1990) "Aseismic Hybrid Control Systems For Building Structures Under Strong Earthquakes", Intelligent Structures, edited by K.P. Chong, S.C. Liu and J.C. Li, Elsevier Applied Science, pp. 179-195, Proceedings of International Workshop on Intelligent Structures, July 23-26, Taipei, Taiwan.
24. Yang, J.N., Danielians, A., and Liu, S.C. (1991), "Aseismic Hybrid Control Systems for Building Structures", Journal of Engineering Mechanics, ASCE, Vol. 117, No. 4, April, pp. 836-853.
25. Yang, J.N., and Li, Z. (1990) "Instantaneous Optimal Control With Acceleration and Velocity Feedback", National Center for Earthquake Engineering Research, NCEER, Technical Report, NCEER-90-0016, SUNY, Buffalo.
26. Yang, J.N., Li, Z., and Liu, S.C. (1990) "Instantaneous Optimal Control With Acceleration and Velocity Feedback", Proceedings of the 2nd International Conference on Stochastic Structural Dynamics, May 7-9, Boca Raton, FL.
27. Yang, J.N., Li, Z., and Liu, S.C. (1991) "Instantaneous Optimal Control With Acceleration and Velocity Feedback", paper accepted for publication in Journal of Probabilistic Engineering Mechanics.
28. Yang, J.N., Li, Z., Danielians, A., and Liu, S.C., "Optimal Control of Nonlinear Hybrid Structural Systems," paper presented at the Eighth VPI&SU Symposium on Dynamics and Control of Large Structures, May 6-8, 1991, Blacksburg, VA; to appear in the Conference Proceedings.
29. Yang, J.N., Li, Z., and Danielians, A. (1991), "Hybrid Control of Seismic-Excited Nonlinear and Inelastic Structural Systems Part I", technical report, NCEER-91-0020.
30. Yang, J.N., Li, Z., Danielians, A., and Liu, S.C., "Hybrid Control of Nonlinear Inelastic Structures Under Strong Earthquakes", paper to be presented at the IUTAM Symposium on Nonlinear Stochastic Mechanics to be held on July 1-5, 1991, in Trino, Italy.
31. Papalambros, P.Y. and Wilde, D.J., Principles of Optimal Design, Chapter 3, Cambridge University Press, Cambridge, 1988.

**NATIONAL CENTER FOR EARTHQUAKE ENGINEERING RESEARCH
LIST OF TECHNICAL REPORTS**

The National Center for Earthquake Engineering Research (NCEER) publishes technical reports on a variety of subjects related to earthquake engineering written by authors funded through NCEER. These reports are available from both NCEER's Publications Department and the National Technical Information Service (NTIS). Requests for reports should be directed to the Publications Department, National Center for Earthquake Engineering Research, State University of New York at Buffalo, Red Jacket Quadrangle, Buffalo, New York 14261. Reports can also be requested through NTIS, 5285 Port Royal Road, Springfield, Virginia 22161. NTIS accession numbers are shown in parenthesis, if available.

- NCEER-87-0001 "First-Year Program in Research, Education and Technology Transfer," 3/5/87, (PB88-134275/AS).
- NCEER-87-0002 "Experimental Evaluation of Instantaneous Optimal Algorithms for Structural Control," by R.C. Lin, T.T. Soong and A.M. Reinhorn, 4/20/87, (PB88-134341/AS).
- NCEER-87-0003 "Experimentation Using the Earthquake Simulation Facilities at University at Buffalo," by A.M. Reinhorn and R.L. Ketter, to be published.
- NCEER-87-0004 "The System Characteristics and Performance of a Shaking Table," by J.S. Hwang, K.C. Chang and G.C. Lee, 6/1/87, (PB88-134259/AS). This report is available only through NTIS (see address given above).
- NCEER-87-0005 "A Finite Element Formulation for Nonlinear Viscoplastic Material Using a Q Model," by O. Gycbi and G. Dasgupta, 11/2/87, (PB88-213764/AS).
- NCEER-87-0006 "Symbolic Manipulation Program (SMP) - Algebraic Codes for Two and Three Dimensional Finite Element Formulations," by X. Lee and G. Dasgupta, 11/9/87, (PB88-219522/AS).
- NCEER-87-0007 "Instantaneous Optimal Control Laws for Tall Buildings Under Seismic Excitations," by J.N. Yang, A. Akbarpour and P. Ghaemmaghami, 6/10/87, (PB88-134333/AS).
- NCEER-87-0008 "IDARC: Inelastic Damage Analysis of Reinforced Concrete Frame - Shear-Wall Structures," by Y.J. Park, A.M. Reinhorn and S.K. Kunnath, 7/20/87, (PB88-134325/AS).
- NCEER-87-0009 "Liquefaction Potential for New York State: A Preliminary Report on Sites in Manhattan and Buffalo," by M. Budhu, V. Vijayakumar, R.F. Giese and L. Baumgras, 8/31/87, (PB88-163704/AS). This report is available only through NTIS (see address given above).
- NCEER-87-0010 "Vertical and Torsional Vibration of Foundations in Inhomogeneous Media," by A.S. Veletsos and K.W. Dotson, 6/1/87, (PB88-134291/AS).
- NCEER-87-0011 "Seismic Probabilistic Risk Assessment and Seismic Margins Studies for Nuclear Power Plants," by Howard H.M. Hwang, 6/15/87, (PB88-134267/AS).
- NCEER-87-0012 "Parametric Studies of Frequency Response of Secondary Systems Under Ground-Acceleration Excitations," by Y. Yong and Y.K. Lin, 6/10/87, (PB88-134309/AS).
- NCEER-87-0013 "Frequency Response of Secondary Systems Under Seismic Excitation," by J.A. HoLung, J. Cai and Y.K. Lin, 7/31/87, (PB88-134317/AS).
- NCEER-87-0014 "Modelling Earthquake Ground Motions in Seismically Active Regions Using Parametric Time Series Methods," by G.W. Ellis and A.S. Cakmak, 8/25/87, (PB88-134283/AS).
- NCEER-87-0015 "Detection and Assessment of Seismic Structural Damage," by E. DiPasquale and A.S. Cakmak, 8/25/87, (PB88-163712/AS).
- NCEER-87-0016 "Pipeline Experiment at Parkfield, California," by J. Isenberg and E. Richardson, 9/15/87, (PB88-163720/AS). This report is available only through NTIS (see address given above).

- NCEER-87-0017 "Digital Simulation of Seismic Ground Motion," by M. Shinozuka, G. Deodatis and T. Harada, 8/31/87, (PB88-155197/AS). This report is available only through NTIS (see address given above).
- NCEER-87-0018 "Practical Considerations for Structural Control: System Uncertainty, System Time Delay and Truncation of Small Control Forces," J.N. Yang and A. Akbarpour, 8/10/87, (PB88-163738/AS).
- NCEER-87-0019 "Modal Analysis of Nonclassically Damped Structural Systems Using Canonical Transformation," by J.N. Yang, S. Sarkani and F.X. Long, 9/27/87, (PB88-187851/AS).
- NCEER-87-0020 "A Nonstationary Solution in Random Vibration Theory," by J.R. Red-Horse and P.D. Spanos, 11/3/87, (PB88-163746/AS).
- NCEER-87-0021 "Horizontal Impedances for Radially Inhomogeneous Viscoelastic Soil Layers," by A.S. Veletsos and K.W. Dotson, 10/15/87, (PB88-150859/AS).
- NCEER-87-0022 "Seismic Damage Assessment of Reinforced Concrete Members," by Y.S. Chung, C. Meyer and M. Shinozuka, 10/9/87, (PB88-150867/AS). This report is available only through NTIS (see address given above).
- NCEER-87-0023 "Active Structural Control in Civil Engineering," by T.T. Soong, 11/11/87, (PB88-187778/AS).
- NCEER-87-0024 "Vertical and Torsional Impedances for Radially Inhomogeneous Viscoelastic Soil Layers," by K.W. Dotson and A.S. Veletsos, 12/87, (PB88-187786/AS).
- NCEER-87-0025 "Proceedings from the Symposium on Seismic Hazards, Ground Motions, Soil-Liquefaction and Engineering Practice in Eastern North America," October 20-22, 1987, edited by K.H. Jacob, 12/87, (PB88-188115/AS).
- NCEER-87-0026 "Report on the Whittier-Narrows, California, Earthquake of October 1, 1987," by J. Pantelic and A. Reinhorn, 11/87, (PB88-187752/AS). This report is available only through NTIS (see address given above).
- NCEER-87-0027 "Design of a Modular Program for Transient Nonlinear Analysis of Large 3-D Building Structures," by S. Srivastav and J.F. Abel, 12/30/87, (PB88-187950/AS).
- NCEER-87-0028 "Second-Year Program in Research, Education and Technology Transfer," 3/8/88, (PB88-219480/AS).
- NCEER-88-0001 "Workshop on Seismic Computer Analysis and Design of Buildings With Interactive Graphics," by W. McGuire, J.F. Abel and C.H. Conley, 1/18/88, (PB88-187760/AS).
- NCEER-88-0002 "Optimal Control of Nonlinear Flexible Structures," by J.N. Yang, F.X. Long and D. Wong, 1/22/88, (PB88-213772/AS).
- NCEER-88-0003 "Substructuring Techniques in the Time Domain for Primary-Secondary Structural Systems," by G.D. Manolis and G. Juhn, 2/10/88, (PB88-213780/AS).
- NCEER-88-0004 "Iterative Seismic Analysis of Primary-Secondary Systems," by A. Singhal, L.D. Lutes and P.D. Spanos, 2/23/88, (PB88-213798/AS).
- NCEER-88-0005 "Stochastic Finite Element Expansion for Random Media," by P.D. Spanos and R. Ghanem, 3/14/88, (PB88-213806/AS).
- NCEER-88-0006 "Combining Structural Optimization and Structural Control," by F.Y. Cheng and C.P. Pantelides, 1/10/88, (PB88-213814/AS).
- NCEER-88-0007 "Seismic Performance Assessment of Code-Designed Structures," by H.H-M. Hwang, J-W. Jaw and H-J. Shau, 3/20/88, (PB88-219423/AS).

- NCEER-88-0008 "Reliability Analysis of Code-Designed Structures Under Natural Hazards," by H.H-M. Hwang, H. Ushiba and M. Shinozuka, 2/29/88, (PB88-229471/AS).
- NCEER-88-0009 "Seismic Fragility Analysis of Shear Wall Structures," by J-W Jaw and H.H-M. Hwang, 4/30/88, (PB89-102867/AS).
- NCEER-88-0010 "Base Isolation of a Multi-Story Building Under a Harmonic Ground Motion - A Comparison of Performances of Various Systems," by F-G Fan, G. Ahmadi and I.G. Tadjbakhsh, 5/18/88, (PB89-122238/AS).
- NCEER-88-0011 "Seismic Floor Response Spectra for a Combined System by Green's Functions," by F.M. Lavelle, L.A. Bergman and P.D. Spanos, 5/1/88, (PB89-102875/AS).
- NCEER-88-0012 "A New Solution Technique for Randomly Excited Hysteretic Structures," by G.Q. Cai and Y.K. Lin, 5/16/88, (PB89-102883/AS).
- NCEER-88-0013 "A Study of Radiation Damping and Soil-Structure Interaction Effects in the Centrifuge," by K. Weissman, supervised by J.H. Prevost, 5/24/88, (PB89-144703/AS).
- NCEER-88-0014 "Parameter Identification and Implementation of a Kinematic Plasticity Model for Frictional Soils," by J.H. Prevost and D.V. Griffiths, to be published.
- NCEER-88-0015 "Two- and Three- Dimensional Dynamic Finite Element Analyses of the Long Valley Dam," by D.V. Griffiths and J.H. Prevost, 6/17/88, (PB89-144711/AS).
- NCEER-88-0016 "Damage Assessment of Reinforced Concrete Structures in Eastern United States," by A.M. Reinhorn, M.J. Seidel, S.K. Kunnath and Y.J. Park, 6/15/88, (PB89-122220/AS).
- NCEER-88-0017 "Dynamic Compliance of Vertically Loaded Strip Foundations in Multilayered Viscoelastic Soils," by S. Ahmad and A.S.M. Israil, 6/17/88, (PB89-102891/AS).
- NCEER-88-0018 "An Experimental Study of Seismic Structural Response With Added Viscoelastic Dampers," by R.C. Lin, Z. Liang, T.T. Soong and R.H. Zhang, 6/30/88, (PB89-122212/AS).
- NCEER-88-0019 "Experimental Investigation of Primary - Secondary System Interaction," by G.D. Manolis, G. Juhn and A.M. Reinhorn, 5/27/88, (PB89-122204/AS).
- NCEER-88-0020 "A Response Spectrum Approach For Analysis of Nonclassically Damped Structures," by J.N. Yang, S. Sarkani and F.X. Long, 4/22/88, (PB89-102909/AS).
- NCEER-88-0021 "Seismic Interaction of Structures and Soils: Stochastic Approach," by A.S. Veletsos and A.M. Prasad, 7/21/88, (PB89-122196/AS).
- NCEER-88-0022 "Identification of the Serviceability Limit State and Detection of Seismic Structural Damage," by E. DiPasquale and A.S. Cakmak, 6/15/88, (PB89-122188/AS).
- NCEER-88-0023 "Multi-Hazard Risk Analysis: Case of a Simple Offshore Structure," by B.K. Bhartia and E.H. Vanmarcke, 7/21/88, (PB89-145213/AS).
- NCEER-88-0024 "Automated Seismic Design of Reinforced Concrete Buildings," by Y.S. Chung, C. Meyer and M. Shinozuka, 7/5/88, (PB89-122170/AS).
- NCEER-88-0025 "Experimental Study of Active Control of MDOF Structures Under Seismic Excitations," by L.L. Chung, R.C. Lin, T.T. Soong and A.M. Reinhorn, 7/10/88, (PB89-122600/AS).
- NCEER-88-0026 "Earthquake Simulation Tests of a Low-Rise Metal Structure," by J.S. Hwang, K.C. Chang, G.C. Lee and R.L. Ketter, 8/1/88, (PB89-102917/AS).
- NCEER-88-0027 "Systems Study of Urban Response and Reconstruction Due to Catastrophic Earthquakes," by F. Kozin and H.K. Zhou, 9/22/88, (PB90-162348/AS).

- NCEER-88-0028 "Seismic Fragility Analysis of Plane Frame Structures," by H.H.-M. Hwang and Y.K. Low, 7/31/88, (PB89-131445/AS).
- NCEER-88-0029 "Response Analysis of Stochastic Structures," by A. Kardara, C. Bucher and M. Shinozuka, 9/22/88, (PB89-174429/AS).
- NCEER-88-0030 "Nonnormal Accelerations Due to Yielding in a Primary Structure," by D.C.K. Chen and L.D. Lutes, 9/19/88, (PB89-131437/AS).
- NCEER-88-0031 "Design Approaches for Soil-Structure Interaction," by A.S. Veletsos, A.M. Prasad and Y. Tang, 12/30/88, (PB89-174437/AS).
- NCEER-88-0032 "A Re-evaluation of Design Spectra for Seismic Damage Control," by C.J. Turkstra and A.G. Tallin, 11/7/88, (PB89-145221/AS).
- NCEER-88-0033 "The Behavior and Design of Noncontact Lap Splices Subjected to Repeated Inelastic Tensile Loading," by V.E. Sagan, P. Gergely and R.N. White, 12/8/88, (PB89-163737/AS).
- NCEER-88-0034 "Seismic Response of Pile Foundations," by S.M. Mamoon, P.K. Banerjee and S. Ahmad, 11/1/88, (PB89-145239/AS).
- NCEER-88-0035 "Modeling of R/C Building Structures With Flexible Floor Diaphragms (IDARC2)," by A.M. Reinhorn, S.K. Kunnath and N. Panahshahi, 9/7/88, (PB89-207153/AS).
- NCEER-88-0036 "Solution of the Dam-Reservoir Interaction Problem Using a Combination of FEM, BEM with Particular Integrals, Modal Analysis, and Substructuring," by C.-S. Tsai, G.C. Lee and R.L. Ketter, 12/31/88, (PB89-207146/AS).
- NCEER-88-0037 "Optimal Placement of Actuators for Structural Control," by F.Y. Cheng and C.P. Pantelides, 8/15/88, (PB89-162846/AS).
- NCEER-88-0038 "Teflon Bearings in Aseismic Base Isolation: Experimental Studies and Mathematical Modeling," by A. Mokha, M.C. Constantinou and A.M. Reinhorn, 12/5/88, (PB89-218457/AS).
- NCEER-88-0039 "Seismic Behavior of Flat Slab High-Rise Buildings in the New York City Area," by P. Weidlinger and M. Ettouney, 10/15/88, (PB90-145681/AS).
- NCEER-88-0040 "Evaluation of the Earthquake Resistance of Existing Buildings in New York City," by P. Weidlinger and M. Ettouney, 10/15/88, to be published.
- NCEER-88-0041 "Small-Scale Modeling Techniques for Reinforced Concrete Structures Subjected to Seismic Loads," by W. Kim, A. El-Attar and R.N. White, 11/22/88, (PB89-189625/AS).
- NCEER-88-0042 "Modeling Strong Ground Motion from Multiple Event Earthquakes," by G.W. Ellis and A.S. Cakmak, 10/15/88, (PB89-174445/AS).
- NCEER-88-0043 "Nonstationary Models of Seismic Ground Acceleration," by M. Grigoriu, S.E. Ruiz and E. Rosenblueth, 7/15/88, (PB89-189617/AS).
- NCEER-88-0044 "SARCF User's Guide: Seismic Analysis of Reinforced Concrete Frames," by Y.S. Chung, C. Meyer and M. Shinozuka, 11/9/88, (PB89-174452/AS).
- NCEER-88-0045 "First Expert Panel Meeting on Disaster Research and Planning," edited by J. Pantelic and J. Stoyke, 9/15/88, (PB89-174460/AS).
- NCEER-88-0046 "Preliminary Studies of the Effect of Degrading Infill Walls on the Nonlinear Seismic Response of Steel Frames," by C.Z. Chrysostomou, P. Gergely and J.F. Abel, 12/19/88, (PB89-208383/AS).

- NCEER-88-0047 "Reinforced Concrete Frame Component Testing Facility - Design, Construction, Instrumentation and Operation," by S.P. Pessiki, C. Conley, T. Bond, P. Gergely and R.N. White, 12/16/88, (PB89-174478/AS).
- NCEER-89-0001 "Effects of Protective Cushion and Soil Compliancy on the Response of Equipment Within a Seismically Excited Building," by J.A. HoLung, 2/16/89, (PB89-207179/AS).
- NCEER-89-0002 "Statistical Evaluation of Response Modification Factors for Reinforced Concrete Structures," by H.H.-M. Hwang and J.-W. Jaw, 2/17/89, (PB89-207187/AS).
- NCEER-89-0003 "Hysteretic Columns Under Random Excitation," by G.-Q. Cai and Y.K. Lin, 1/9/89, (PB89-196513/AS).
- NCEER-89-0004 "Experimental Study of 'Elephant Foot Bulge' Instability of Thin-Walled Metal Tanks," by Z.-H. Jia and R.L. Ketter, 2/22/89, (PB89-207195/AS).
- NCEER-89-0005 "Experiment on Performance of Buried Pipelines Across San Andreas Fault," by J. Isenberg, E. Richardson and T.D. O'Rourke, 3/10/89, (PB89-218440/AS).
- NCEER-89-0006 "A Knowledge-Based Approach to Structural Design of Earthquake-Resistant Buildings," by M. Subramani, P. Gergely, C.H. Conley, J.F. Abel and A.H. Zaghaw, 1/15/89, (PB89-218465/AS).
- NCEER-89-0007 "Liquefaction Hazards and Their Effects on Buried Pipelines," by T.D. O'Rourke and P.A. Lane, 2/1/89, (PB89-218481).
- NCEER-89-0008 "Fundamentals of System Identification in Structural Dynamics," by H. Imai, C.-B. Yun, O. Maruyama and M. Shinozuka, 1/26/89, (PB89-207211/AS).
- NCEER-89-0009 "Effects of the 1985 Michoacan Earthquake on Water Systems and Other Buried Lifelines in Mexico," by A.G. Ayala and M.J. O'Rourke, 3/8/89, (PB89-207229/AS).
- NCEER-89-R010 "NCEER Bibliography of Earthquake Education Materials," by K.E.K. Ross, Second Revision, 9/1/89, (PB90-125352/AS).
- NCEER-89-0011 "Inelastic Three-Dimensional Response Analysis of Reinforced Concrete Building Structures (IDARC-3D), Part I - Modeling," by S.K. Kunnath and A.M. Reinhorn, 4/17/89, (PB90-114612/AS).
- NCEER-89-0012 "Recommended Modifications to ATC-14," by C.D. Poland and J.O. Malley, 4/12/89, (PB90-108648/AS).
- NCEER-89-0013 "Repair and Strengthening of Beam-to-Column Connections Subjected to Earthquake Loading," by M. Corazao and A.J. Durrani, 2/28/89, (PB90-109885/AS).
- NCEER-89-0014 "Program EXKAL2 for Identification of Structural Dynamic Systems," by O. Maruyama, C.-B. Yun, M. Hoshiya and M. Shinozuka, 5/19/89, (PB90-109877/AS).
- NCEER-89-0015 "Response of Frames With Bolted Semi-Rigid Connections, Part I - Experimental Study and Analytical Predictions," by P.J. DiCorso, A.M. Reinhorn, J.R. Dickerson, J.B. Radzinski and W.L. Harper, 6/1/89, to be published.
- NCEER-89-0016 "ARMA Monte Carlo Simulation in Probabilistic Structural Analysis," by P.D. Spanos and M.P. Mignolet, 7/10/89, (PB90-109893/AS).
- NCEER-89-P017 "Preliminary Proceedings from the Conference on Disaster Preparedness - The Place of Earthquake Education in Our Schools," Edited by K.E.K. Ross, 6/23/89.
- NCEER-89-0017 "Proceedings from the Conference on Disaster Preparedness - The Place of Earthquake Education in Our Schools," Edited by K.E.K. Ross, 12/31/89, (PB90-207895).

- NCEER-89-0018 "Multidimensional Models of Hysteretic Material Behavior for Vibration Analysis of Shape Memory Energy Absorbing Devices, by E.J. Graesser and F.A. Cozzarelli, 6/7/89, (PB90-164146/AS).
- NCEER-89-0019 "Nonlinear Dynamic Analysis of Three-Dimensional Base Isolated Structures (3D-BASIS)," by S. Nagarajaiah, A.M. Reinhorn and M.C. Constantinou, 8/3/89, (PB90-161936/AS).
- NCEER-89-0020 "Structural Control Considering Time-Rate of Control Forces and Control Rate Constraints," by F.Y. Cheng and C.P. Pantelides, 8/3/89, (PB90-120445/AS).
- NCEER-89-0021 "Subsurface Conditions of Memphis and Shelby County," by K.W. Ng, T-S. Chang and H-H.M. Hwang, 7/26/89, (PB90-120437/AS).
- NCEER-89-0022 "Seismic Wave Propagation Effects on Straight Jointed Buried Pipelines," by K. Elhmadi and M.J. O'Rourke, 8/24/89, (PB90-162322/AS).
- NCEER-89-0023 "Workshop on Serviceability Analysis of Water Delivery Systems," edited by M. Grigoriu, 3/6/89, (PB90-127424/AS).
- NCEER-89-0024 "Shaking Table Study of a 1/5 Scale Steel Frame Composed of Tapered Members," by K.C. Chang, J.S. Hwang and G.C. Lee, 9/18/89, (PB90-160169/AS).
- NCEER-89-0025 "DYNA1D: A Computer Program for Nonlinear Seismic Site Response Analysis - Technical Documentation," by Jean H. Prevost, 9/14/89, (PB90-161944/AS).
- NCEER-89-0026 "1:4 Scale Model Studies of Active Tendon Systems and Active Mass Dampers for Aseismic Protection," by A.M. Reinhorn, T.T. Soong, R.C. Lin, Y.P. Yang, Y. Fukao, H. Abe and M. Nakai, 9/15/89, (PB90-173246/AS).
- NCEER-89-0027 "Scattering of Waves by Inclusions in a Nonhomogeneous Elastic Half Space Solved by Boundary Element Methods," by P.K. Hadley, A. Askar and A.S. Cakmak, 6/15/89, (PB90-145699/AS).
- NCEER-89-0028 "Statistical Evaluation of Deflection Amplification Factors for Reinforced Concrete Structures," by H.H.M. Hwang, J-W. Jaw and A.L. Ch'ng, 8/31/89, (PB90-164633/AS).
- NCEER-89-0029 "Bedrock Accelerations in Memphis Area Due to Large New Madrid Earthquakes," by H.H.M. Hwang, C.H.S. Chen and G. Yu, 11/7/89, (PB90-162330/AS).
- NCEER-89-0030 "Seismic Behavior and Response Sensitivity of Secondary Structural Systems," by Y.Q. Chen and T.T. Soong, 10/23/89, (PB90-164658/AS).
- NCEER-89-0031 "Random Vibration and Reliability Analysis of Primary-Secondary Structural Systems," by Y. Ibrahim, M. Grigoriu and T.T. Soong, 11/10/89, (PB90-161951/AS).
- NCEER-89-0032 "Proceedings from the Second U.S. - Japan Workshop on Liquefaction, Large Ground Deformation and Their Effects on Lifelines, September 26-29, 1989," Edited by T.D. O'Rourke and M. Hamada, 12/1/89, (PB90-209388/AS).
- NCEER-89-0033 "Deterministic Model for Seismic Damage Evaluation of Reinforced Concrete Structures," by J.M. Bracci, A.M. Reinhorn, J.B. Mander and S.K. Kunnath, 9/27/89.
- NCEER-89-0034 "On the Relation Between Local and Global Damage Indices," by E. DiPasquale and A.S. Cakmak, 8/15/89, (PB90-173865).
- NCEER-89-0035 "Cyclic Undrained Behavior of Nonplastic and Low Plasticity Silts," by A.J. Walker and H.E. Stewart, 7/26/89, (PB90-183518/AS).
- NCEER-89-0036 "Liquefaction Potential of Surficial Deposits in the City of Buffalo, New York," by M. Budhu, R. Giese and L. Baumgrass, 1/17/89, (PB90-208455/AS).

- NCEER-89-0037 "A Deterministic Assessment of Effects of Ground Motion Incoherence," by A.S. Veletsos and Y. Tang, 7/15/89, (PB90-164294/AS).
- NCEER-89-0038 "Workshop on Ground Motion Parameters for Seismic Hazard Mapping," July 17-18, 1989, edited by R.V. Whitman, 12/1/89, (PB90-173923/AS).
- NCEER-89-0039 "Seismic Effects on Elevated Transit Lines of the New York City Transit Authority," by C.J. Costantino, C.A. Miller and E. Heymsfield, 12/26/89, (PB90-207887/AS).
- NCEER-89-0040 "Centrifugal Modeling of Dynamic Soil-Structure Interaction," by K. Weissman, Supervised by J.H. Prevost, 5/10/89, (PB90-207879/AS).
- NCEER-89-0041 "Linearized Identification of Buildings With Cores for Seismic Vulnerability Assessment," by I-K. Ho and A.E. Aktan, 11/1/89, (PB90-251943/AS).
- NCEER-90-0001 "Geotechnical and Lifeline Aspects of the October 17, 1989 Loma Prieta Earthquake in San Francisco," by T.D. O'Rourke, H.E. Stewart, F.T. Blackburn and T.S. Dickerman, 1/90, (PB90-208596/AS).
- NCEER-90-0002 "Nonnormal Secondary Response Due to Yielding in a Primary Structure," by D.C.K. Chen and L.D. Lutes, 2/28/90, (PB90-251976/AS).
- NCEER-90-0003 "Earthquake Education Materials for Grades K-12," by K.E.K. Ross, 4/16/90, (PB91-113415/AS).
- NCEER-90-0004 "Catalog of Strong Motion Stations in Eastern North America," by R.W. Busby, 4/3/90, (PB90-251984/AS).
- NCEER-90-0005 "NCEER Strong-Motion Data Base: A User Manual for the GeoBase Release (Version 1.0 for the Sun3)," by P. Friberg and K. Jacob, 3/31/90 (PB90-258062/AS).
- NCEER-90-0006 "Seismic Hazard Along a Crude Oil Pipeline in the Event of an 1811-1812 Type New Madrid Earthquake," by H.H.M. Hwang and C-H.S. Chen, 4/16/90(PB90-258054).
- NCEER-90-0007 "Site-Specific Response Spectra for Memphis Sheahan Pumping Station," by H.H.M. Hwang and C.S. Lee, 5/15/90, (PB91-108811/AS).
- NCEER-90-0008 "Pilot Study on Seismic Vulnerability of Crude Oil Transmission Systems," by T. Ariman, R. Dobry, M. Grigoriu, F. Kozin, M. O'Rourke, T. O'Rourke and M. Shinozuka, 5/25/90, (PB91-108837/AS).
- NCEER-90-0009 "A Program to Generate Site Dependent Time Histories: EQGEN," by G.W. Ellis, M. Srinivasan and A.S. Cakmak, 1/30/90, (PB91-108829/AS).
- NCEER-90-0010 "Active Isolation for Seismic Protection of Operating Rooms," by M.E. Talbott, Supervised by M. Shinozuka, 6/8/9, (PB91-110205/AS).
- NCEER-90-0011 "Program LINEARID for Identification of Linear Structural Dynamic Systems," by C-B. Yun and M. Shinozuka, 6/25/90, (PB91-110312/AS).
- NCEER-90-0012 "Two-Dimensional Two-Phase Elasto-Plastic Seismic Response of Earth Dams," by A.N. Yiagos, Supervised by J.H. Prevost, 6/20/90, (PB91-110197/AS).
- NCEER-90-0013 "Secondary Systems in Base-Isolated Structures: Experimental Investigation, Stochastic Response and Stochastic Sensitivity," by G.D. Manolis, G. Juhn, M.C. Constantinou and A.M. Reinhorn, 7/1/90, (PB91-110320/AS).
- NCEER-90-0014 "Seismic Behavior of Lightly-Reinforced Concrete Column and Beam-Column Joint Details," by S.P. Pessiki, C.H. Conley, P. Gergely and R.N. White, 8/22/90, (PB91-108795/AS).
- NCEER-90-0015 "Two Hybrid Control Systems for Building Structures Under Strong Earthquakes," by J.N. Yang and A. Danielians, 6/29/90, (PB91-125393/AS).

- NCEER-90-0016 "Instantaneous Optimal Control with Acceleration and Velocity Feedback," by J.N. Yang and Z. Li, 6/29/90, (PB91-125401/AS).
- NCEER-90-0017 "Reconnaissance Report on the Northern Iran Earthquake of June 21, 1990," by M. Mehrain, 10/4/90, (PB91-125377/AS).
- NCEER-90-0018 "Evaluation of Liquefaction Potential in Memphis and Shelby County," by T.S. Chang, P.S. Tang, C.S. Lee and H. Hwang, 8/10/90, (PB91-125427/AS).
- NCEER-90-0019 "Experimental and Analytical Study of a Combined Sliding Disc Bearing and Helical Steel Spring Isolation System," by M.C. Constantinou, A.S. Mokha and A.M. Reinhorn, 10/4/90, (PB91-125385/AS).
- NCEER-90-0020 "Experimental Study and Analytical Prediction of Earthquake Response of a Sliding Isolation System with a Spherical Surface," by A.S. Mokha, M.C. Constantinou and A.M. Reinhorn, 10/11/90, (PB91-125419/AS).
- NCEER-90-0021 "Dynamic Interaction Factors for Floating Pile Groups," by G. Gazetas, K. Fan, A. Kaynia and E. Kausel, 9/10/90, (PB91-170381/AS).
- NCEER-90-0022 "Evaluation of Seismic Damage Indices for Reinforced Concrete Structures," by S. Rodríguez-Gómez and A.S. Cakmak, 9/30/90, PB91-171322/AS).
- NCEER-90-0023 "Study of Site Response at a Selected Memphis Site," by H. Desai, S. Ahmad, E.S. Gazetas and M.R. Oh, 10/11/90, (PB91-196857/AS).
- NCEER-90-0024 "A User's Guide to Strongmo: Version 1.0 of NCEER's Strong-Motion Data Access Tool for PCs and Terminals," by P.A. Friberg and C.A.T. Susch, 11/15/90, (PB91-171272/AS).
- NCEER-90-0025 "A Three-Dimensional Analytical Study of Spatial Variability of Seismic Ground Motions," by L-L. Hong and A.H.-S. Ang, 10/30/90, (PB91-170399/AS).
- NCEER-90-0026 "MUMOID User's Guide - A Program for the Identification of Modal Parameters," by S. Rodríguez-Gómez and E. DiPasquale, 9/30/90, (PB91-171298/AS).
- NCEER-90-0027 "SARCF-II User's Guide - Seismic Analysis of Reinforced Concrete Frames," by S. Rodríguez-Gómez, Y.S. Chung and C. Meyer, 9/30/90, (PB91-171280/AS).
- NCEER-90-0028 "Viscous Dampers: Testing, Modeling and Application in Vibration and Seismic Isolation," by N. Makris and M.C. Constantinou, 12/20/90 (PB91-190561/AS).
- NCEER-90-0029 "Soil Effects on Earthquake Ground Motions in the Memphis Area," by H. Hwang, C.S. Lee, K.W. Ng and T.S. Chang, 8/2/90, (PB91-190751/AS).
- NCEER-91-0001 "Proceedings from the Third Japan-U.S. Workshop on Earthquake Resistant Design of Lifeline Facilities and Countermeasures for Soil Liquefaction, December 17-19, 1990," edited by T.D. O'Rourke and M. Hamada, 2/1/91, (PB91-179259/AS).
- NCEER-91-0002 "Physical Space Solutions of Non-Proportionally Damped Systems," by M. Tong, Z. Liang and G.C. Lee, 1/15/91, (PB91-179242/AS).
- NCEER-91-0003 "Kinematic Seismic Response of Single Piles and Pile Groups," by K. Fan, G. Gazetas, A. Kaynia, E. Kausel and S. Ahmad, 1/10/91, to be published.
- NCEER-91-0004 "Theory of Complex Damping," by Z. Liang and G. Lee, to be published.
- NCEER-91-0005 "3D-BASIS - Nonlinear Dynamic Analysis of Three Dimensional Base Isolated Structures: Part II," by S. Nagarajaiah, A.M. Reinhorn and M.C. Constantinou, 2/28/91, (PB91-190553/AS).

- NCEER-91-0006 "A Multidimensional Hysteretic Model for Plasticity Deforming Metals in Energy Absorbing Devices," by E.J. Graesser and F.A. Cozzarelli, 4/9/91.
- NCEER-91-0007 "A Framework for Customizable Knowledge-Based Expert Systems with an Application to a KBES for Evaluating the Seismic Resistance of Existing Buildings," by E.G. Ibarra-Anaya and S.J. Fenves, 4/9/91, (PB91-210930/AS).
- NCEER-91-0008 "Nonlinear Analysis of Steel Frames with Semi-Rigid Connections Using the Capacity Spectrum Method," by G.G. Deierlein, S-H. Hsieh, Y-J. Shen and J.F. Abel, 7/2/91.
- NCEER-91-0009 "Earthquake Education Materials for Grades K-12," by K.E.K. Ross, 4/30/91, (PB91-212142/AS).
- NCEER-91-0010 "Phase Wave Velocities and Displacement Phase Differences in a Harmonically Oscillating Pile," by N. Makris and G. Gazetas, 7/8/91, (PB92-108356/AS).
- NCEER-91-0011 "Dynamic Characteristics of a Full-Sized Five-Story Steel Structure and a 2/5 Model," by K.C. Chang, G.C. Yao, G.C. Lee, D.S. Hao and Y.C. Yeh," to be published.
- NCEER-91-0012 "Seismic Response of a 2/5 Scale Steel Structure with Added Viscoelastic Dampers," by K.C. Chang, T.T. Soong, S-T. Oh and M.L. Lai, 5/17/91.
- NCEER-91-0013 "Earthquake Response of Retaining Walls; Full-Scale Testing and Computational Modeling," by S. Alampalli and A-W.M. Elgamal, 6/20/91, to be published.
- NCEER-91-0014 "3D-BASIS-M: Nonlinear Dynamic Analysis of Multiple Building Base Isolated Structures," by P.C. Tsopelas, S. Nagarajaiah, M.C. Constantinou and A.M. Reinhorn, 5/28/91.
- NCEER-91-0015 "Evaluation of SEAOC Design Requirements for Sliding Isolated Structures," by D. Theodossiou and M.C. Constantinou, 6/10/91.
- NCEER-91-0016 "Closed-Loop Modal Testing of a 27-Story Reinforced Concrete Flat Plate-Core Building," by H.R. Somaprasad, T. Toksoy, H. Yoshiyuki and A.E. Aktan, 7/15/91.
- NCEER-91-0017 "Shake Table Test of a 1/6 Scale Two-Story Lightly Reinforced Concrete Building," by A.G. El-Attar, R.N. White and P. Gergely, 2/28/91, to be published.
- NCEER-91-0018 "Shake Table Test of a 1/8 Scale Three-Story Lightly Reinforced Concrete Building," by A.G. El-Attar, R.N. White and P. Gergely, 2/28/91, to be published.
- NCEER-91-0019 "Transfer Functions for Rigid Rectangular Foundations," by A.S. Veletsos, A.M. Prasad and W.H. Wu, 7/31/91, to be published.
- NCEER-91-0020 "Hybrid Control of Seismic-Excited Nonlinear and Inelastic Structural Systems," by J.N. Yang, Z. Li and A. Danielians, 8/1/91.

